National Technical University of Athens

Laboratory of Marine Engineering

EFFECT OF VARYING THE OPERATIONAL CHARACTERISTICS OF A 2-STROKE MARINE DIESEL ENGINE DURING ITS PASSAGE OF THE BARRED SPEED RANGE

DIPLOMA THESIS

KOUZOUPIS ANTONIOS

Supervisor: **Professor N. P. Kyrtatos**

Committee Member: **Professor G. K. Politis**

Committee Member: **Assistant Professor G. Papalamprou**

Athens, March 2019

Abstract

This thesis investigates methods for faster acceleration of a large marine two-stroke diesel engine through the Barred Speed Range (BSR). The Barred Speed Range (BSR) is a speed range of engine operation set by classification societies where due to resonance, torsional vibrations in the shaftline are excessively high. Prolonged operation inside the BSR may have a detrimental effect on the fatigue lifetime of the shaftline and even lead to a breakdown.

Before the Energy Efficiency Design Index (EEDI) was introduced, propulsion engines had generally adequate torque margins and the passage through BSR was usually rather swift, and thus there was little issue with torsional fatigue cycle buildup. The introduction of EEDI resulted, in part, to the so called Eco-efficient ships with engines being derated and having reduced power margins. However, this in turn led to potential problems such as a reduced ship acceleration capability, loitering within BSR and possibly also reduced maneuverability under certain conditions, particularly in bad weather conditions.

The use of electronic engines, that permits some variability within limits of their operational characteristics, has provided some flexibility to address this problem. In this thesis, the acceleration capabilities of a marine two-stroke diesel engine were studied under transient loading conditions.

A Ship-Hull model and a Four Quadrant Wageningen B Series Screw Propeller model were developed in order to simulate the coupled hull-engine-propeller system. Simulations using the engine process simulation code MOTHER were performed.

Variability in Fuel Injection Timing, Valve Timing and Compression Ratio was examined by using VIT (Variable Injection Timing), VVT (Variable Valve Timing) and VCR (Variable Compression Ratio) systems. Furthermore, the above methods combined with increased fuel injected or increased air mass flow were also investigated. In particular, the increase in the air mass flow was achieved by intervening in the operation of the Turbocharger. The effect of these parameters during the acceleration of the two stroke diesel engine through its BSR was examined.

In conclusion, earlier injection timing showed a significant increase in the in-cylinder pressures accompanied by significant losses, leading to a small acceleration and power improvement. Increased compression ratio produced slightly increased work with slightly reduced losses, marginally increasing the engine's acceleration and power. Variability in the exhaust valve timing resulted in negligible effects since the little extra or less work produced was balanced by slightly higher or lower losses respectively. Lastly, increased fuel and air mass flow led to a significant improvement of the engine's acceleration and produced increased work with more power directed towards acceleration. The combined cases did not show significant differences in their acceleration and power output compared to simply injecting more fuel or inserting more air.

Conclusively, the most effective method of improving the engine's acceleration and aiding in a quicker passage through the BSR resulted to be increasing the fuel injected or the air mass flow in the cylinders.

Acknowledgements

First and foremost, I would like to thank my supervisor Professor N. P. Kyrtatos who provided me the opportunity to conduct a thesis in the Laboratory of Marine Engineering (LME) at National and Technical University of Athens (NTUA). His valuable support and guidance was of great importance throughout the course of this thesis.

Special thanks need to be given to PhD candidate M. Foteinos for his patience, guidance and outstanding help in progressing the modeling required to complete this thesis but also in understanding the simulation software MOTHER. Moreover, I would like to give my thanks to the graduate student of LME D. Vlon for contributing in the propeller and ship surge modeling, bearing with me, and for providing a pillar of support when the thesis had gotten the best of me.

Furthermore, I would like to thank my family for their support in my whole endeavor. Their patience and devotion was remarkable while always helping me to keep focused and to progress my work. I do not believe I could have reached this point without their constant support.

Lastly, I would like to give my warmest thanks to my girlfriend Erica, all my friends, my band mates and all the people who supported me through the end and who are too numerous to list.

This thesis is dedicated to all the people aforementioned, my sister Natalia, my parents and Odin.

Table of Contents

Chapter 1: Introduction

The marine industry has been in the primary activities of mankind since ancient times being a source of food and a path of communication, transport and trade. It is not surprising that in many cultures the sea has been given divine attributes. Its importance set the foundations for humans to dwell further in naval engineering and throughout the ages they achieved the transition from wind driven sails to electronically operating engines. Nowadays, despite marine engineering having made huge advancements, there are still many challenges to overcome.

1.1 Internal combustion engines: operation and challenges

Internal combustion engines have been constructed to use the internal combustion cycle to propel forth any size of vessel. Their operation is based on utilizing the available air and the fuel injected in order to produce the torque needed for propulsion. The newest designs include systems which replace mechanical parts with electronic functions unlocking further potentials in the engine's operations. However regardless of how advanced the design or the engine is, all marine engines face the same two operating conditions: steady states and transient states.

The first can be described as small changes in the load of the engine or large load changes in a wide time period. Calm sea state and stable vessel speed is a common scenario. Usually, in these cases, there is an ample amount of air supply and thus the torque produced depends mainly on the fuel injected. The latter operating conditions can be described as major fluctuations in the engine load over a short time period. Adverse sea conditions and accelerations or decelerations are a common scenario. Here, lags in the air supply are greater than the ones in the fuel supply. This "air to fuel ratio" fluctuation may drop to such low levels that the engine functions inefficiently and expends the fuel producing less torque and instead more smoke [1].

Throughout the life span of a vessel, the cases where it operates in transient conditions will most certainly be more compared to operating in steady state scenarios. Transient operation is much more complex than the steady one and is of a higher concern due to the emissions produced and the straggle of the engine to adapt to the sudden changes.

1.2 Environmental pollution, considerations and regulations

Nevertheless, the new direction that the field of engineering has adopted, towards the protection of the environment, has set the marine industry under retrospection. The marine industry includes, for a fact, a very widespread spectrum of activities. This can be easily demonstrated by the size of the marine fleets that exist worldwide. Since marine engines are of the largest in terms of power and size, utilize heavy fuels and are in such numbers, they unavoidably contribute to a great extent in the environmental pollution with their emissions and wastes. New regulations have been implemented and have set limits for marine engines in order to make them more efficient and contain the environmental consequences of their operation. On the other hand, most of these regulations do not clearly specify how designs abide to their edicts but instead demand that they fulfill specific requirements or are below certain thresholds. This has led engineers and researchers to come up with new technologies and designs that, despite aiding the vessel to comply with the regulations, sometimes introduce new problems.

The most striking example is the Barred Speed Range. The introduction of the Energy Efficiency Design Index (EEDI) from the International Maritime Organization (IMO) in 2013 [2] had the intention of making marine engines more efficient and reduce their CO_2 emissions. The regulation necessitated that any vessel under consideration needed to have its EEDI below a specific threshold but without providing any specific instructions on how to achieve this.

Furthermore, recent trends in fuel economy have promoted the practice of slow streaming were the vessel reduces its speed in favor of fuel-saving since fuel consumption scales exponentially with the vessel's velocity. Slow steaming means that the vessel reduces its speed and the power output of the engine. Nevertheless, when slow steaming is required for lengthy time periods the drawbacks of temporarily dropping the current operating point of the engine overcome the advantages of fuel economy.

1.3 Derating the engine: EEDI and issues with the Barred Speed Range (BSR)

The most common and efficient practice that designers came up with in order to comply with the EEDI and simultaneously allow an efficient and prolonged slow steaming vessel condition was the derating of the engine.

Derating is a retuning procedure where the engine operates efficiently at less than its maximum rated capability. This enables ship owners to keep their existing engines instead of purchasing new ones, while simultaneously allowing for compliance with the EEDI regulation. The process is quite complex but the mentality behind it is to maintain the same combustion pressure and reduce the mean effective pressure. The first increases the maximum fire pressure to mean effective pressure ratio, thus, improving the engine's efficiency while the latter lowers the engine layout point and, hence, reduces power output and rotational speed. This can be achieved by a plethora of methods which include intervening physically or not to the engine. However, even though derating provides a possible solution for the EEDI, it poses a great threat to the integrity of the engine shaft.

Like all materials and mechanical systems, the engine and particularly its crankshaft have a main critical frequency. During the operation of the engine, forces and moments are produced and become excitation sources, which lead to proportional responses. The vibrations that occur, and especially the torsional ones, are amplified when their frequency lies near the main critical one due to resonance. This has led classification societies to set boundaries in the area were the corresponding torsional stresses and fatigue are dangerous naming this region of engine rotational speeds "Barred Speed Range" (BSR) [3]. Prolonged operation inside the BSR can have a severe effect on the fatigue lifetime of the crankshaft and might even lead to a breakdown.

Under normal conditions and in typical designs the BSR is usually at low percentages of the maximum rotational speed of the engine. Its position is such that the power available at that point is adequate enough in order for the engine to pass through the BSR swiftly. However, a derated engine has its layout point lower in terms of power and speed and, unless specific actions are taken, the torsional characteristics of the engine remain the same. This means that the BSR remains in the same values of rpm while the engine has less available power for acceleration. Consequently, a

derated engine may not be able to accelerate fast enough through the BSR and, as a result, endanger its integrity from a slow and prolonged passage [4, 5].

1.4 Dynamic Limiter Function (DLF)

This problem was in a dire need of an efficient solution. MAN's Dynamic Limiter Function (DLF) [4] was one of the most effective solutions, where an electronic engine can overcome its fuel limiters for short periods of time. This enables the engine to increase its power output during transient conditions so that it may achieve sufficient acceleration. This is based on the theory that during acceleration events the engine operates in a part load condition and, consequently, there is room for it to surpass its fuel operating limits for small periods of time.

This technology is really interesting and its function is based on the operating foundations of an engine. The engine can be seen as a system whose inputs are the fuel injected and the air supply available while its output is the torque produced. By intervening with the input factors there is great potential in increasing the torque and, hence, the power and the engine's acceleration, particularly in transient events where new engines show a weakness in quickly passing the dangerous BSR region.

1.5 Current Thesis

Inspired by the operation and mentality behind the DLF, this thesis aimed to investigate the effects that different parameters may had on an engine's acceleration capabilities in order to help a quick passage through BSR. The parameters of the engine that contributed in such an effort were controlled by a Variable Injection Timing (VIT), a Variable Valve Timing (VVT) and a Variable Compression Ratio (VCR) system. Their effects on the engine operation were monitored in order to determine the most efficient setting. Combined with these systems, the effect of increased fuel injected and air mass flow was also investigated.

This thesis focuses on the operation of a large two stroke marine diesel engine. It must be specified that real time experiments on an existing engine were not feasible and thus engine simulations were utilized. Simulations on a specific engine were executed using the in-house developed engine simulation code MOtor THERmodynamics (MOTHER) [6]. The VIT, VVT and VCR systems were already integrated in this simulation environment.

In order for the simulation to run smoothly the problem at hand needed to be properly described through specific models. This was achieved via a code written in a FORTRAN programming environment.

This code included three models:

1. A Hull Ship model which describes the interaction between the hull, the engine and the propeller using a theoretical vessel and an amalgamation of the methods proposed by Carlton [7] and Holtrop and Mennen [8, 9].
2. A Four Quadrant Wageningen B Series Screw Propeller model [10] which calculates the propeller operating characteristics and in the end computes the torque and thrust produced by a theoretical propeller used in the simulation.

3. A Propeller Inertia model which calculates the inertia characteristics of a theoretical propeller used in the simulation and follows the method that Carlton [7] proposes.

The models and their interaction are explained in depth in their according passages.

Moreover, a speed governor model was implemented in order to conduct the transient simulations since ungoverned diesel engine transient simulations cannot converge unless active control is imposed on the fuel mass injected. The speed governor is responsible for stabilizing the engine speed around a specified speed setpoint in the operation region by controlling the fuel injected. It is the key component in order to run simulations under transient conditions.

Chapter 2: Engine Operation

This thesis mainly focuses on the acceleration capabilities of a vessel, and more specifically, on the acceleration capabilities of its respective engine. In order to determine the aspects that show the most promise in controlling the engine's acceleration, a short description of a marine engine's operation was deemed necessary.

During the two stroke cycle of an engine, many events take place so that an adequate thrust might be produced in order to achieve adequate propulsion of the vessel. To start with, there must be a system, which will enable the cold engine to begin its operation. This external power system's task is to provide sufficient cylinder pressure and temperature in order to achieve a first ignition of the fuel. Once the fuel is ignited, the engine should be able to start and run up to a self-sustaining speed. Although the principles based on which starting systems function differ, all store energy so that they can release it in order to accelerate the engine. The most common starting systems in marine engines are the pneumatic starting systems, which work on pressurized air.

Once the engine runs on its own, its operation is pretty straightforward. The crankshaft revolves clockwise and the piston moves up the cylinder. While the scavenge ports are uncovered, pressurized air is inserted in the cylinder and the moving piston compresses it on its way upwards. Just before the piston reaches the Top Dead Centre (TDC), the fuel is injected into the cylinder by the fuel injectors. The fuel is broken down to very small droplets which mix with the air and produce a combustible mixture. The mixture of a diesel oil fuel self- ignites due to its compression. Due to the expanding gas from the combustion, the piston is forced to move downwards, turning the crankshaft and, as a result produce energy for the engine. During the downward movement of the piston, the exhaust valves open and the hot exhaust gas leaves the cylinder through them. Simultaneously, when the piston uncovers the scavenge ports fresh pressurized air enters the cylinder aiding in the clearance of the exhaust gas, a process known as scavenging. The piston expends its energy as it reaches the Bottom Dead Center (BDC) and then it starts moving upwards, the exhaust valves close and the compression process begins again [11].

Generally, a diesel engine produces an output of Torque by utilizing as inputs Fuel and Combustion Air. The speed of the engine and thus of the vessel will be determined by the balance between the torque produced from the engine and the load torque [1].

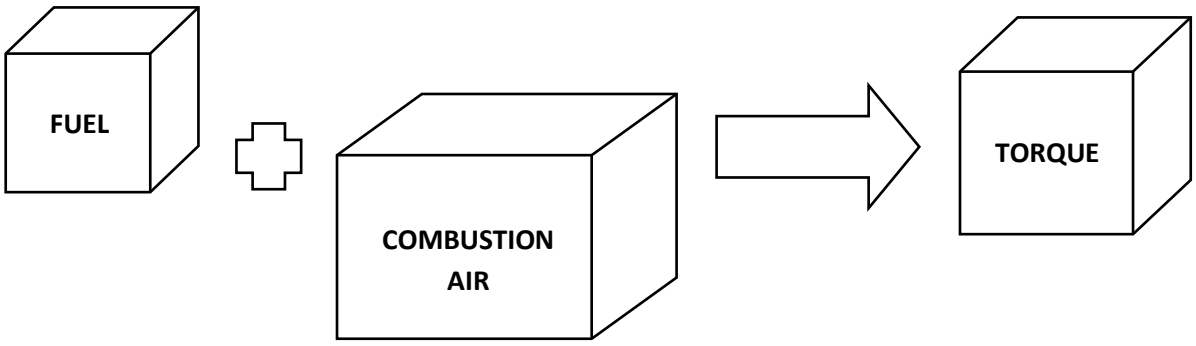

Figure 2.1: Engine Operation Basics

This means that control of the torque and thus the rate of change of the engine speed and thus the acceleration capabilities of the vessel can be achieved by monitoring the air supply and the fuel injected.

A quick review of the notion described above, shows that if one is to study the acceleration and how it can be affected by tweaking systems of the engine then the elements that he should primarily focus on are:

- The control of the fuel injected inside the cylinder.
- The control of the exhaust valves leaving the cylinder.
- The compression of the fuel and air mixture.
- The control of the air inserted in the cylinder during scavenging.

The fuel injected can be controlled by adjusting the parameters of a Variable Injection Timing (VIT) system while the exhaust valves can be affected by modifying the parameters of a Variable Valve Timing (VVT) system. Furthermore, a recent system called Variable Compression Ratio (VCR) can be utilized in order to intervene in the compression of the engine. Lastly, considering the air inserted in the cylinders during the scavenging process, since this is a two stroke marine engine, there are inlet ports instead of inlet valves which makes their control quite complex. An attempt to indirectly tamper with the scavenging could be made by using the VCR system and the crank angle the cylinders uncover/cover the inlet ports.

Taking into consideration the parameters mentioned above, this thesis concentrates in the acceleration capabilities of a specific engine in transient conditions. While most of the research made on internal combustion engines is based on steady state conditions, in reality the majority of the daily operation of an engine involves transient conditions. During transient operation, there are quick changes in the operating conditions, which require an equivalently quick response from the engine. Mechanical systems such as the governor and the fuel pumps need to continuously adapt to the new conditions in order to avoid problematic situations such as over- or under- speeding, overshooting of exhaust gas and excessive fuel consumption [12]. Meanwhile, engine load constantly changes, which affects the engine speed, the injected fuel and the inserted air in the cylinders. In succession, the exhaust gas is affected in terms of their energy and thermal content, which consecutively influences the operation of the Turbocharger. This whole procedure makes transient operation a very demanding state for the engine especially if we take into consideration the fact that an engine of a marine scale requires some time to cope with instant operational changes. For instance, a change in the fuel rack position will be fully implemented only after all the cylinders have completed their cycles [1].

Consequently, transient conditions are a very complicated state where values constantly change making the prediction of the engine's behavior quite difficult. In this thesis, the behavior of a marine engine during transient conditions and the engine's acceleration are studied during a specific load region where torsional vibrations may cause a series of problems due to resonance. This region is known as Barred Speed Range.

Chapter 3: The Barred Speed Range (BSR) & the Energy Efficiency Index (EEDI)

3.1 The Barred Speed Range (BSR)

Vibrations on board ships started to become of interest due to the need of providing comfortable conditions to the passengers and crew. However, recent events and studies have shown that vibrations have the potential to reach levels that might disturb the smooth operation of mechanical and electronic components and even endanger the integrity of the vessel. Such a case is the Barred Speed Range or BSR.

The BSR is a range of shaft speeds where excessive fatigue and torsional vibrations occur due to resonance. In order to better comprehend this phenomenon, a brief passage in vibrations and excitations during the operation of engine is presented.

To start with, an excitation is a force or moment applied to the mass-elastic system, which the ship represents. The excitations occur from different kind of internal or external excitation sources. These sources, in a diesel engine, are cyclic by nature and their influence can be evaluated using the "harmonic analysis" where the excitations are decomposed as a sum of trigonometric functions with different amplitudes, phase angles and periods. These periods are different fractions of the basic excitation's period and determine the so called "order" of each excitation. The order indicates how many times the excitation acts per revolution [13, 14].

Moreover, every solid object can be correlated with a characteristic frequency where, if it is subjected to an impact, it will vibrate freely. This frequency is called "natural frequency" and for a system of solid elements several natural frequencies exist, each corresponding to a certain vibration mode with different nodes.

When the frequency of an excitation matches the one of the natural frequencies then a resonance occurs. This leads to high vibration and stress levels with a response that in some cases is magnified more than 50 times the usual value [14]. The resonance that occurs when the 1^{st} order excitation or else "main harmonic excitation" matches one of the natural frequencies is called the "main critical resonance".

Based on the above, there are two scenarios that exist when someone studies the resonance of an object:

- Overcritical condition: where the frequency of the main harmonic excitation is placed higher, in terms of frequencies, compared to the natural frequency
- Undercritical condition: where the frequency of the main harmonic excitation is placed lower, in terms of frequencies, compared to the natural frequency

In the case of an engine, the natural frequency of the shaft depends on its geometric characteristics and the material from which it is manufactured. This means that by altering the diameter or the material of the shaft, the natural frequency can be adjusted. Furthermore, the classification society's methodologies in designing and determining shaft characteristics usually lead to excessive

dimensioning, torsional vibrations and bearing loads due to their simplicity and lack of accuracy [15]. Nevertheless, they usually permit the increase of the shaft diameter or a reduction accompanied by an improvement in the material used.

Therefore, a shaft can be designed with reduced diameter and crafted from a better material compared to the classification society's proposed one, which places the natural frequency below the normal speed range. This is known as overcritical running. Another proposed countermeasure in order to lower the natural frequency, is introducing a turning wheel. On the other hand, a shaft can be designed with a larger diameter, which increases the frequencies where resonance takes place above the MCR, known as undercritical running. This solution however, might induce a high varying torque on the shaft which might affect the torque produced [13].

In addition, the excitations, which occur during the operation of an engine, can be divided in two major categories; primary excitations and secondary excitations [14]. The first are forces and moments that stem from the combustion pressure and the inertia forces of rotating and reciprocating masses while the second occur due to forced vibratory response from different substructures.

Primary excitation sources are mainly related to the engine pressure, which acts on the crankshaft and the connecting rod mechanism. These can be either external forces and moments which are generated by the inertia forces of unbalanced rotating and reciprocating masses, or internal forces and moments which are linked to the combustion pressure. These forces pass to the hull of the ship through the foundations and the top bracing of the engine. If the engine frame was infinitely stiff, they would not be able to produce excitations to the ship.

Secondary excitation sources are considered the axial and torsional vibrations [13, 14]. Also, within this category fall the propeller excitations due to the non-uniform wake field, which are a complicated subject beyond the interest of this thesis.

The axial vibrations are linked to the radial and tangential forces during combustion and to the mass forces of individual cylinders. These forces apply to the crank pin via the connecting rod mechanism and, thus, the webs of the crank deflect in their axial direction causing axial vibrations. The vibrations may be transferred to the vessel's hull through the thrust bearing. Nonetheless, an axial vibration damper is standard practice in all engines protecting the crankshaft against heavy stresses and controlling the varying forces in the thrust bearing that may excite the hull.

Torsional vibrations are mainly excited by the tangential force applied to the crankshaft and connecting rod mechanism. The varying gas pressure during the operation of the engines leads to a varying toque in the crankshaft, which causes the generation of torsional vibrations on the shaft. These are of the most importance because a resonance of this kind can cause increased additional stresses to the shaft system and consequently might have a severe effect on its operation, by even causing a fracture.

For this reason, classification societies request the calculation of the torsional characteristics of a shaft system and have laid down specific limits in order to protect it from these extra stresses that occur during resonance. Two limits for torsional stress have been devised, τ_1 and τ_2, which refer to a speed range up to 80% of the MCR [3, 14].

The lower limit τ_1 determines a stress level that the engine is permitted to exceed for small amounts of time and not for long periods such as continuous running. For the speed range where the engine exceeds this limit, the Barred Speed Range is introduced, prohibiting continuous operation. The upper limit τ_2 can never be exceeded at all. Above 80% of the MCR, only the limit τ_1 is applicable.

More specifically, these limits can be calculated for each rotational speed using the equations given by GL 2008 Section 16 Torsional Vibrations [3] which dictate that:

$$\tau_1 = \pm C_W \cdot C_K \cdot C_D \cdot (3 - 2 \cdot \lambda^2) \text{ for speed ratio values } \lambda < 0.9 \quad (3.1)$$

$$\tau_1 = \pm C_W \cdot C_K \cdot C_D \cdot 1.38 \text{ for speed ratio values } 0.9 \leq \lambda \leq 1.05 \quad (3.2)$$

$$\tau_2 = \pm 1.7 \cdot 6.0 \cdot \frac{\tau_1}{\sqrt{C_K \cdot C_W}} \text{ depending on the material and design} \quad (3.3)$$

In these equations, C_W is the material factor that equals to $C_W = \frac{R_m + 160}{18}$, C_K is the form factor for intermediate and propeller shafts, C_D is the size factor depending on the shaft diameter and λ is the ratio of the current rotation speed to the nominal rotation speed. R_m is the tensile strength of the shaft depending on its material.

An optical example from an analysis of the torsional vibrations in the intermediate shaft of an example ship derived from YangGon Kim's paper [16] is shown in Figure 3.1. The vibrations produced by different order excitations and the limits explained above are clearly depicted.

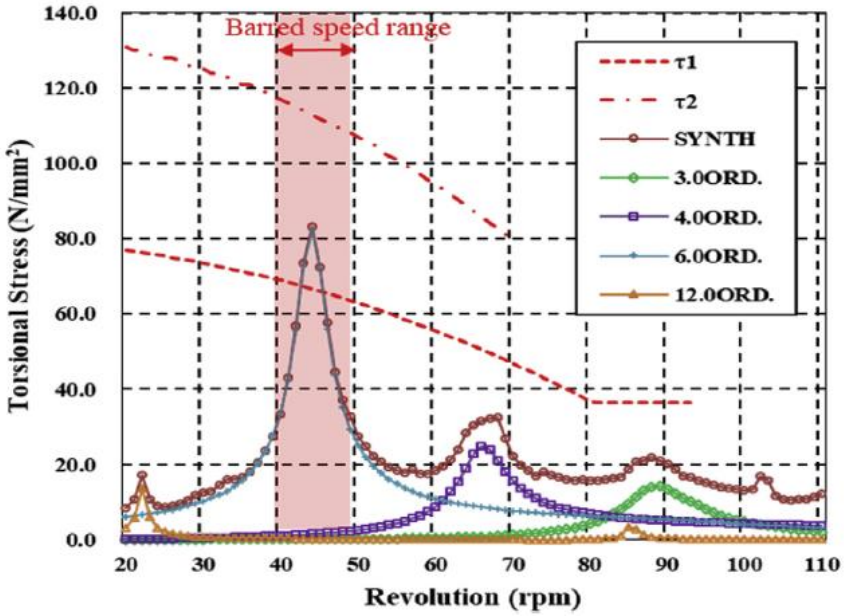

Figure 3.1: Simulation results of torsional vibrations in the intermediate shaft during steady states **[16]**

According to IACS_UR_M68.5 [17] regulations, the BSR can be calculated using the following formula provided that the stresses at the border of the BSR during normal and steady conditions are below the limit τ_1:

$$\frac{16 \cdot n_c}{18 - \lambda_c} \leq n \leq \frac{(18 - \lambda_c) \cdot n_c}{16} \quad (3.4)$$

Where n_c is the resonance rotational speed and λ_c is the ratio of the resonance rotational speed to the nominal rotational speed.

In conclusion, an engine must not operate for long terms inside the BSR. Up until recently, no specific measures were required to be taken, since the vessels had the potential to pass through the BSR quickly. However, the introduction of new regulations in the maritime industry has slowed down the passing of the BSR.

3.2 Energy Efficiency Design Index (EEDI)

Nowadays, in all industrial and scientific fields, researchers strive to find new ways in order to protect the environment and suppress the human imprint on it. Existing technologies are either further evolving or pushed aside for newer and more advanced ones. In addition, the growing human needs for transport of goods and services have led to the construction of even larger and more powerful engines, whose emissions and operation pose a further substantial threat to the ecosystem. As a result, world-influencing organizations have been setting regulations in order to reduce the impact existing and future engines have on nature and make them more "eco-friendly".

Undoubtedly, the biggest and most powerful engines that exist are used in power plants and in the marine industry. Especially the latter, operate in a very fragile environment making them a prime target for devising regulations that restrict their effect. These regulations usually impose limits and instruct vessels to reduce their emissions, which is usually accompanied by lowering the power output of the engine, changing the type of fuel used or installing expensive additions that tweak with the engine's functions.

These limitations however, frequently create challenges. One such case is one of the most recent regulations imposed by the International Maritime Organization (IMO) called the Energy Efficiency Design Index (EEDI) [2]. The EEDI was made mandatory in July 2011 for all new ships and was an effort to enhance fuel economy and to promote more energy efficient engines and equipment. It is a technical measure which is calculated in grams of CO_2 per tone-mile from the following simplified equation:

$$EEDI = \frac{P_{ME} \cdot CF_{ME} \cdot SFC_{ME}}{Capacity \cdot V_{ref}} \tag{3.5}$$

Where P_{ME} is the engine power at 75% of the Maximum Continuous Rating in KW, CF_{ME} is a conversion factor which relates the tones of CO_2 emitted to the tones of fuel consumed, SFC_{ME} is the engine's specific fuel consumption in grams of fuel per KWh, $Capacity$ is the ship's capacity measured in tones and V_{ref} is the ship's velocity at 75% engine load in ideal sea trial conditions measured in knots (miles per hour). According to this rule, the lower the Energy Efficiency Design Index of a vessel is, the more efficient it is perceived.

Despite the fact that the regulations are obligatory, they do not define how the ship should comply with them and are merely thought to be met as long as the EEDI is below a specific threshold, depending on the ship's size and type. In the beginning, the threshold was set so that a 10% CO_2 reduction level (grams per tone-mile) was imposed and is tightening every 5 years until the year period 2025-2030 when it will have become a 30% reduction [18].

This mentality, however, leaves a designer or a shipbuilder with many options and lets them choose the most cost-efficient method for their ship. By examining equation (3.5) and bearing in mind that power is proportional to the 3rd power of the vessel's speed ($P_{ME} \propto V_{ref}^3$), the most obvious way to abide with the regulations would be to tamper with the fuel, reduce the power of the engine or the reference speed of the ship or reduce its capacity. However, for a given ship the capacity and fuel type would be pretty much standard, which means that the EEDI is mainly related to the main engine power, specific fuel consumption and the ship's reference speed. Thus, if we want to keep the EEDI below a threshold the base options would be either to reduce the vessel's speed or its installed power or lower its engine's specific fuel consumption.

Lowering the vessel's speed may be easy for high speed vessels such as containerships but is troublesome for already slow moving vessels such as bulk carriers and tankers. Moreover, some specific shipyards have tried to reduce the lightweight of vessels and thus increase their deadweight/capacity and lower their EEDI. Other options could be the application of an Energy Saving Device (such as Air Lubrication of the hull) or a better hull or propeller design which could lead to a more energy efficient vessel [19].

However, serious concerns raised by the implementation of the EEDI were mentioned in the presentation of P. Zachariadis in SNAME 2011 Athens [19]:

- EEDI leads to underpowered ships that lack safety and maneuverability
- CO2 reductions are negligible or negative when it comes to small ships operating in real weather conditions
- EEDI promotes the plain reduction of speed instead of new, better and cost effective hulls, propellers or engines
- EEDI creates the drive for lighter ships which lack structural safety

Whatever the case, the most widespread tactic which usually does not include tampering physically with the engine or the ship would be applying slow steaming, which according to *Wärtsila Encyclopedia* [20], is "The operation of a ship at a lower speed than normal one in order to save fuel on ballast voyage or when fuel is expensive". Another very popular trend would be reducing the installed power by derating the engine which, nonetheless, causes a series of difficulties. These difficulties have a direct impact to the Barred Speed Range.

Chapter 4: Derated Engines

An engine is optimized to operate at a specific maximum vessel speed. The engine is designed in that way so that maximum cylinder pressure is achieved at its continuous service rating. This means that for any other operational speed or load rather than the optimized, the engine under-functions. With the introduction of the EEDI regulation and the slow steaming trend, it became a necessity for vessels to use engines which are more efficient and that need to be efficient even in circumstances where a reduced operational speed is required.

One of the EEDI's demands would be to lower specific fuel consumption or power which gives the designers two engine options; either use smaller engines that work at their maximum continuous ratings or use derated but yet powerful ones [5].

The first option means that the engine runs at high speed and high power and has high fuel consumption thus high operational emissions. However, their designed emissions are low since their output power is low and since an engine operates most effectively at its MCR. This means that the difference between operational and designed emissions depends on how heavily the engine is loaded. An important drawback would be that since the engine will be working at its MCR, there will be a large need for lubrication and cooling of the main propulsion and auxiliaries meaning a high Brake Mean Effective Pressure (BMEP) demand for long periods.

The second option, which is more favored and is most commonly referred to by the term "derated engine", means that the engine will be tweaked not to run at its maximum continuous rating but rather at a lower point. During this type of operation, the engine can maintain the same ship speed, while operating at a lower load, thus reducing specific fuel consumption. Although lower specific fuel consumption translates to lower operational emissions, design emissions will still be high since the output power is of a higher value compared to the smaller engines. Therefore, the difference between operational and designed emissions depends on how the output power is applied in the EEDI equation.

In theory, a derated engine is an engine that operates at less than its maximum rated capability. In practice, a derated engine operates at a lower than designed (BMEP) and shaft speed while keeping Maximum Pressure (P_{max}) constant. Hence, the $\frac{P_{max}}{BMEP}$ is increased which in succession increases the efficiency of the engine. This, means that a reduction in the specific fuel consumption is achieved and, therefore, a reduction in emissions [5].

Derating offers the engine the possibility to be optimized by lowering its specified MCR so that it can operate efficiently at another designed load point. A deration of an engine actually reduces the specific fuel consumption of the engine by improving the match between its operational point and its optimal working point. Moreover, sometimes a derated engine is accompanied by a new propeller, optimized for the new load point which further improves the overall propulsion efficiency. More specifically, according to MAN [21] a reduction of up to 10-12% may be achieved.

There are a handful of ways, both permanent and not, to derate an engine. Some of those include physical tampering of the engine, such as installing shims between the piston rod and the crosshead to reduce the stroke length, deactivating current parts such as a cylinder or a turbocharger, adding

another cylinder or utilizing different tuning methods. The method to be chosen is up to the ship owner or designer and differs in terms of cost and complexity. According to MAN [21], the cost of derating an engine accompanied with new optimized parts may fluctuate between 0.9-3.0 million Euros depending on the engine type.

All things considered, the deration of engines has nowadays become a very common practice in order to abide with the latest regulations and to make the operation of ships as efficient as possible. Nevertheless, this trend is responsible for the aggravation of a very serious problem associated with the passage of the Barred Speed Range.

4.1 Derated effect on BSR

Until recently, the passage of the BSR was always quick since it was placed in the lower region of the RPM range, where the propeller power was low. In that region, the engine power available was more than sufficient so there was a fast translation through the BSR.

The most common practice would be to firstly set the rpm setting just below the BSR. Next, the vessel is awaited to accelerate to a speed corresponding to the above speed setting. In succession, the rpm setting is increased to a value above the BSR. When this procedure was followed correctly, the engine almost always passed the BSR quickly. Nevertheless, in some cases such as maneuvering or during adverse sea conditions there is no time to follow this procedure or the vessel's resistance is too high in order for it to achieve a speed corresponding to the set rpm setting [4]. This makes the above mentioned procedure ineffective. Such cases may also require the engine to pass the BSR at low or zero vessel speed.

In the case where the ship has zero speed, the propeller operates at the Bollard Pull Curve. This means that higher power is required compared to light running, hence longer time to pass the BSR.

Moreover, with the introduction of the EEDI regulation, all designs focus on fuel economy and efficiency. When choosing to derate the engine, the BSR is placed in a higher region relative to the MCR [4].

When the engine is derated, the engine layout point (MCR point) is moved down in terms of power and speed along a propeller curve and the BSR is moved upwards. This is clearly explained in the example below.

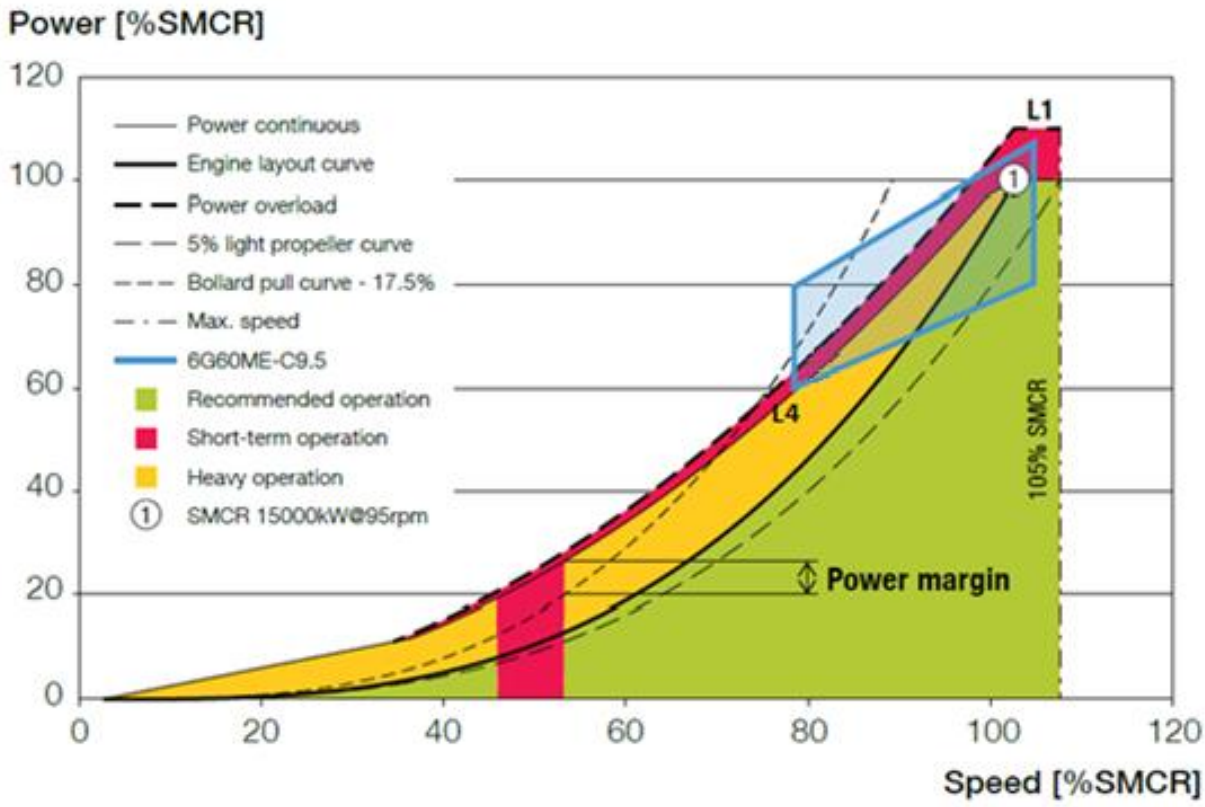

Figure 4.1: Load Diagram - Un-derated Engine **[4]**

Figure 4.1 shows the load diagram of an engine before it is derated. For instance, this engine operates at point L1 (15000kW and 95 rpm) inside the layout diagram (blue envelope) on a propeller curve. In this state, the BSR is located approximately at 50% of the maximum speed at the MCR, marked as the red area. In this diagram there is also the bollard pull curve which is equal to the pulling (or towing) power of the vessel and is considered equal to 17.5% heavy running relative to the light propeller curve. The distance between the bollard pull curve and the continuous power curve is a design index explained later on and is called the Barred Speed Range Power Margin. This margin represents the engine's available power in the BSR region which can be used in order to accelerate and quickly pass this dangerous area. If this margin is sufficient then a quick passage can be achieved.

However, when an engine is derated, its power output is reduced and instead it operates at point L4 as shown in Figure 4.2. The new MCR would be in this example at approximately 9000kW and 75 rpm. Since the engine is the same, this means that the operating point is moved from L1 to L4 along a propeller curve, still in the same layout diagram (blue envelope).

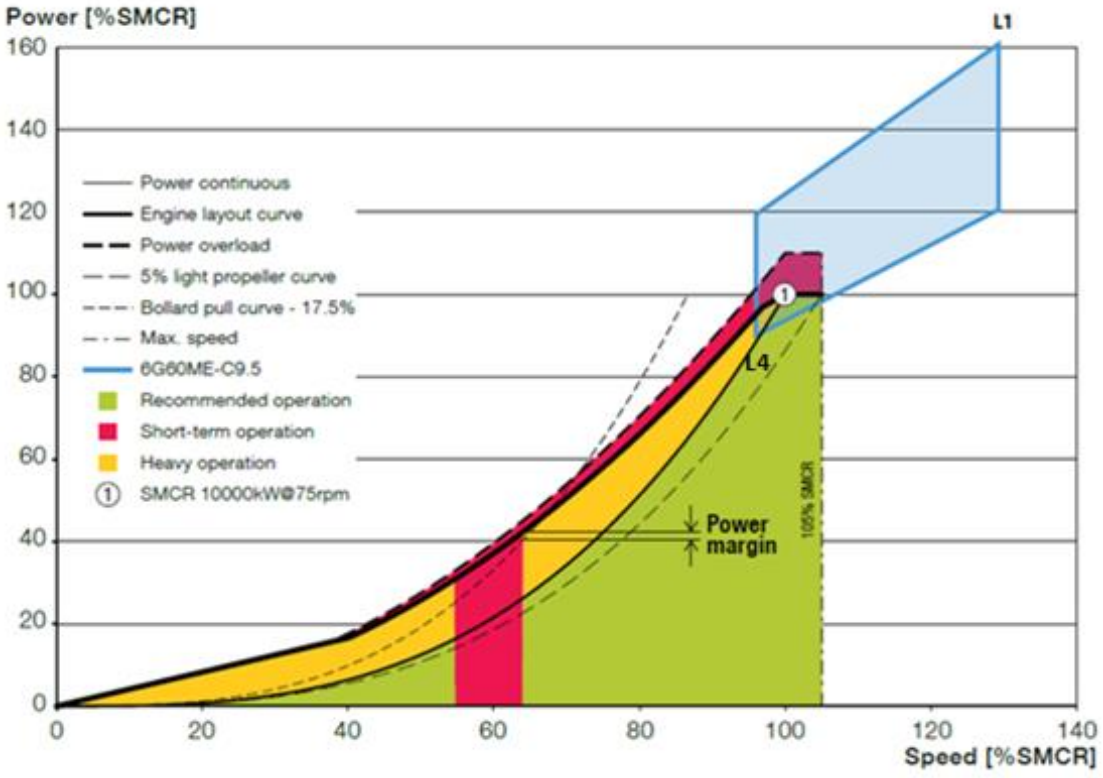

Figure 4.2: Load Diagram – Derated Engine **[4]**

At the same time, the basic engine, the shaft and the propeller design are not usually significantly changed, unless an action is taken, which means that their torsional vibration characteristics remain the same. This leaves the BSR which depends on the torsional characteristics of the system in the same region of absolute values of rotational speed. Nevertheless, the operating point (L4) is placed lower in comparison to the un-derated engine (L1) which means that the engine now operates at a lower power output and a lower speed. In conclusion, the BSR moves up as a percentage relative to the new MCR, from 50% of the speed in L1 operation point to approximately 63% of the speed in L4 operation point. This is accompanied, as clearly shown in Figure 4.2, with a decrease in the power margin thus a decrease in the power available for acceleration in the BSR region and hence a slower passage.

Conclusively, derating an engine is important in order to make it more efficient and it is an option for ships to abide to the new EEDI rules. However, it is also responsible for a delayed passage in the BSR which may have negative consequences at the shaft lifetime and ship maneuvering. Designers and manufacturers have tried to devise ways to counter the drawbacks that occur from derating. Some of the most acknowledged work would be the introduction of MAN's DLF and Barred Speed Range Power Margin [4].

4.2 The Dynamic Limiter Function & the BSR Power Margin Index

The problems that have occurred due to the slow passage of the BSR, were in dire need of a solution. A survey carried on by MAN [4] indicated that there were two points that needed to be addressed in order to effectively overcome this issue. Firstly, there was a need for a simple design rule, which would avoid acceleration difficulties of the vessel as early as the ship design stage. Secondly, there was a need for a method which would increase the available power during the acceleration of the vessel so that the previous task would impose as few as possible constraints on the ship design.

Considering the first task, the Barred Speed Range Power Margin was introduced. This is a simple design value that is capable of predicting whether the vessel will pass the BSR quickly or not.

This value is calculated using the following equation (4.1):

$$BSR_{PM} = \frac{P_L - P_P}{P_P} \cdot 100\% \tag{4.1}$$

Where P_L is the power limit for the continuous power curve of the engine while P_P is the required power at the upper end of the BSR during the Bollard Pull condition. Thus, $P_L - P_P$ is indicative of the power surplus for propeller acceleration. These are depicted in Figure 4.3 below which shows an engine load diagram as an example. The highlighted red area is the Barred Speed Range of the specific engine.

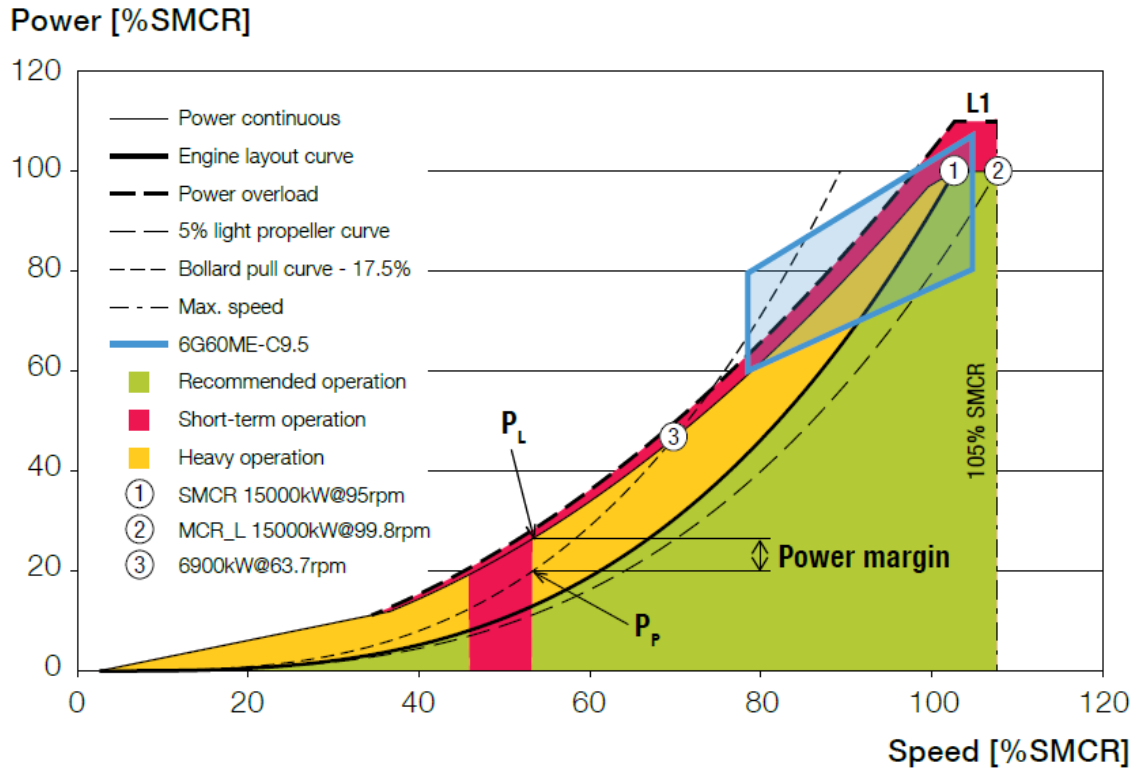

Figure 4.3: Barred Speed Range Power Margin **[4]**

For high values of the BSR_{PM} the passing of the BSR is quick while for $BSR_{PM} < 10\%$ the time required increases rapidly. This can be clearly seen from the following Figure 4.4 depicting the time required for an engine to pass the BSR as a function of the BSR_{PM}.

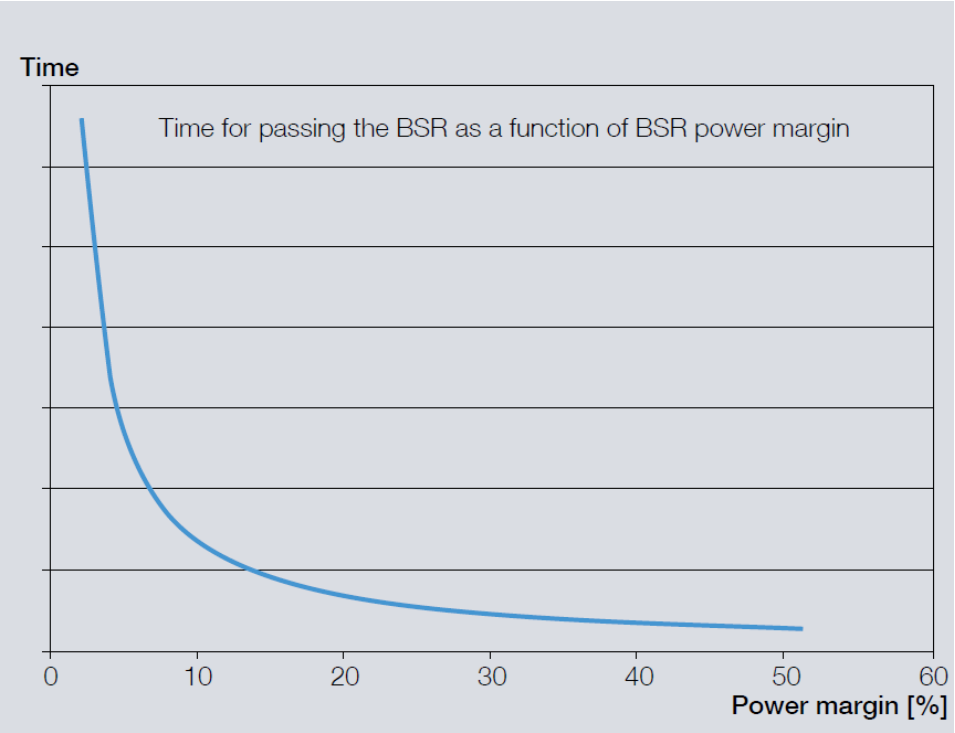

Figure 4.4: Time required for passing the BSR as a function of the $\boldsymbol{BSR_{PM}}$ **[4]**

This means that if during the design phase of the vessel this index is marginally above 10%, then even the slightest error, such as small deviations in calculations or measurements, may result into a very lengthy passage. Such errors can be, for example, the propeller light running turning out lower than expected or the bollard pull heavy running turning out to be higher than predicted due to the hull – propeller combination.

Therefore, a conservatively large BSR_{PM} is recommended in cases where there is uncertainty about sufficient acceleration performance during the design phase.

Considering the second task, MAN developed a new engine control system whose purpose is to improve the acceleration of the engine and consequently the acceleration of the vessel. This technology is known as Dynamic Limiter Function (DLF) [4].

An engine's capacity for fuel injection is mainly restricted by two limits. Firstly, thermal and mechanical overload should be avoided and secondly emission of excessive black smoke is undesirable. The engine's parameters are set so that it operates under these restrictions for long periods of time without risking a breakdown.

However, the engine must also be able to cope with accelerations. Accelerations are short events that take place when then engine functions at a lesser point than its maximum power and speed output. Thus, it is possible to enable the engine to exceed the above mentioned limitations for short periods of time and have it generate higher torque and thus more power.

The DLF adjusts the fuel parameters and limiters so that a maximum output of torque can be produced for a maximum duration of 30 minutes. If it is applied for a longer period the engine might be in jeopardy. After that, the limiters gradually return to their normal values and several hours are needed in order for the system to cool down and be ready for another use. Moreover, in ME-C engines it is possible to increase the amount of air available for combustion while accelerating, thus avoid generating excessive black smoke.

In practice, the DLF calculates the air available inside the cylinder before its combustion takes place. This is achieved via extensive CFD analysis and experimental validation. In succession, it estimates the amount of fuel that can be injected until either the maximum allowable torque at this specific rotational speed is achieved (torque limiter) or the minimum acceptable air-fuel ratio is reached (lamda limiter). The results of these calculations are an increased torque and power output during accelerations [4].

The tests MAN conducted indicated that the torsional vibrations developed with the application of the DLF were significantly lower, despite the fact that the DLF increases the torque produced by the engine. This reduction can be attributed to the fact that with the application of the DLF, the engine achieves a quicker passage through the BSR meaning that the engine stays for a shorter period of time at a shaft speed near the resonance frequency and, hence the resonance cannot develop to the same extent. Furthermore, during the faster accelerations with the DLF, the propeller is loaded more heavily, which increases propeller damping while the application of the DLF also alters the cylinder pressure excitation.

It must be mentioned that the above functions can be achieved via the engine's electronic control of the fuel injection and exhaust valve timing.

MAN has defined two levels of DLF application [4], the DLF "Standard" and the DLF "Full". Their difference concerns the torsional vibration stress levels. DLF "Standard" applies the measures that are known not to increase the torsional vibration stress levels. This means that, when it is retrofitted on a vessel, the ship needs not to renew its torsional vibration level measurements for the correspondent classification society. On the other hand, when further acceleration is required, a "Full" DLF system may be applied that adjusts the DLF parameters in order to further increase the produced torque. An example would be earlier exhaust valve closure. However, this may or may not increase torsional vibration stresses and thus a renewal of its torsional vibration level measurements for the correspondent classification society is required.

To sum up, the DLF is a viable solution which, by pushing the engine over its limits and tampering with the fuel indexes during acceleration events, is able to ensure a quick passage of the BSR. Nonetheless, the DLF can function for a limited amount of time and needs to cool off before being able to operate again. This means that in order to achieve sufficient power for long lasting heavy conditions, a sufficient power margin must also be considered.

Chapter 5: The VIT, VVT and VCR systems

The VIT, VVT and VCR systems where used in order to examine their effect on the acceleration capabilities of a specific engine. Therefore, it was deemed necessary to introduce how these systems operate. For each system, the general theory behind its function is described while also a note on how it should affect the engine's operation is presented.

5.1 Variable Injection Timing (VIT)

Every engine has a system which transfers the fuel from the fuel tanks via the fuel lines to the injector nozzles so that it can be injected inside the cylinders. Fuel pumps pressurize it while also mechanically control the amount of fuel inserted in the injectors by utilizing a rack. This rack rotates the plunger inside the barrel of the pump, thus moving a notch carved on the plunger which consequently controls the amount of pressurized fuel stored in it. This fuel will be sent at the injector nozzles when the injection time is at hand.

Considering the fuel injection timing, the injection commences during compression, just before the piston reaches the TDC. It is pivotal that fuel injection takes place in the right moment, otherwise severe problems might occur. In the case of an early injection, it might result in high peak pressures which might lead to the application of unsafe stresses on the engine caused by a tendency of the pressure to reverse the rotation of the crankshaft. In the case of a delayed injection, this might lead to incomplete combustion causing low power output and overheating of the engine.

In summary [22], an early injection:

- Increases the maximum pressure at low loads.
- Increases the fuel efficiency since it reduces the specific fuel consumption.
- Improves thermal efficiency and, thus, decreases the exhaust gas temperature.
- May lead to unsafe stresses.

On the other hand, a delayed injection may:

- Result in decreased maximum pressure.
- Result in extreme-dangerous exhaust temperatures.
- Reduce thermal efficiency.
- Lead to incomplete combustion and thus increased corrosion.

Traditionally, the fuel pump was designed in order to inject fuel at the same time irrespective of the load or the demand of the engine. In order to control the fuel injection timing, the Variable Injection Timing system is applied. In addition to the normal rack, which exists to regulate the amount of fuel injected, the fuel pump is fitted with an adjustable barrel, which is threaded at the bottom and rotated by a second rack. A sleeve rotates the barrel moving it up and down altering the position of the spill ports relative to the plunger, thus varying the start of injection [23]. Despite the fact that it is a complex design, a VIT system may prove very useful in operating at low loads, in reducing the fuel consumption and increasing the in-cylinder pressures [24].

Below in Figure 5.1, a mechanical VIT system is depicted. Nowadays, electronic control has prevailed over mechanical control.

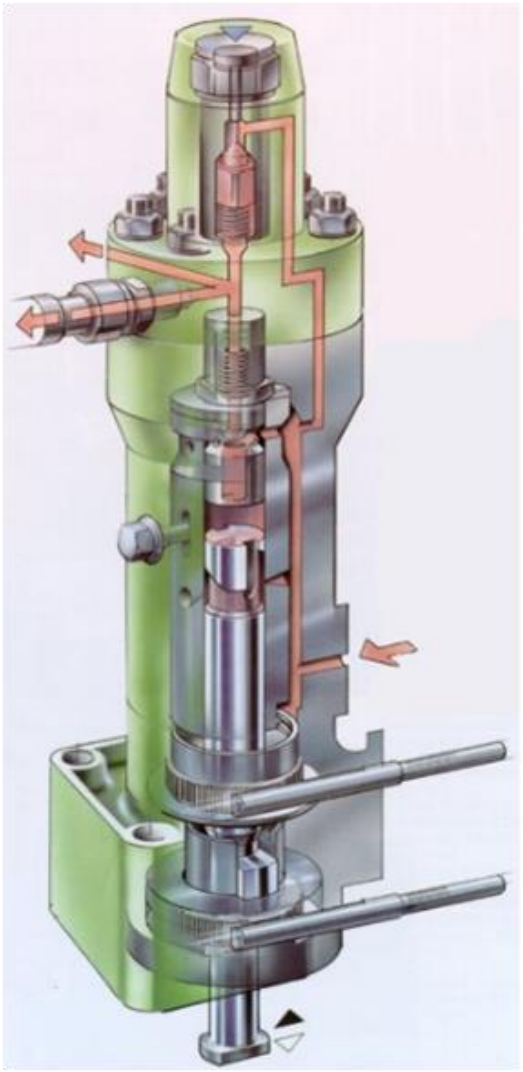

Figure 5.1: VIT System **[23]**

In this thesis, where transient conditions are studied, a VIT system is used in order to investigate the impact that a change in the fueling process might have on the acceleration capabilities of the engine. By advancing the commencement of the fuel injection, the maximum combustion pressure at MCR can be maintained at loads below 100% (as low as 70% [22]) which helps in reducing specific fuel consumption [24, 25]. Higher combustion pressure in low loads improves the engine's efficiency and the torque produced and, as a result, aids the engine's acceleration.

For most applications, the VIT system is adjusted so that in low loads, the start of injection is constant while for loads above 40% it steadily advances until it reaches a peak at almost 85% load. After this threshold it starts to reduce in order to avoid excessive firing pressures [26]. This can be observed in the Figure 5.2 below.

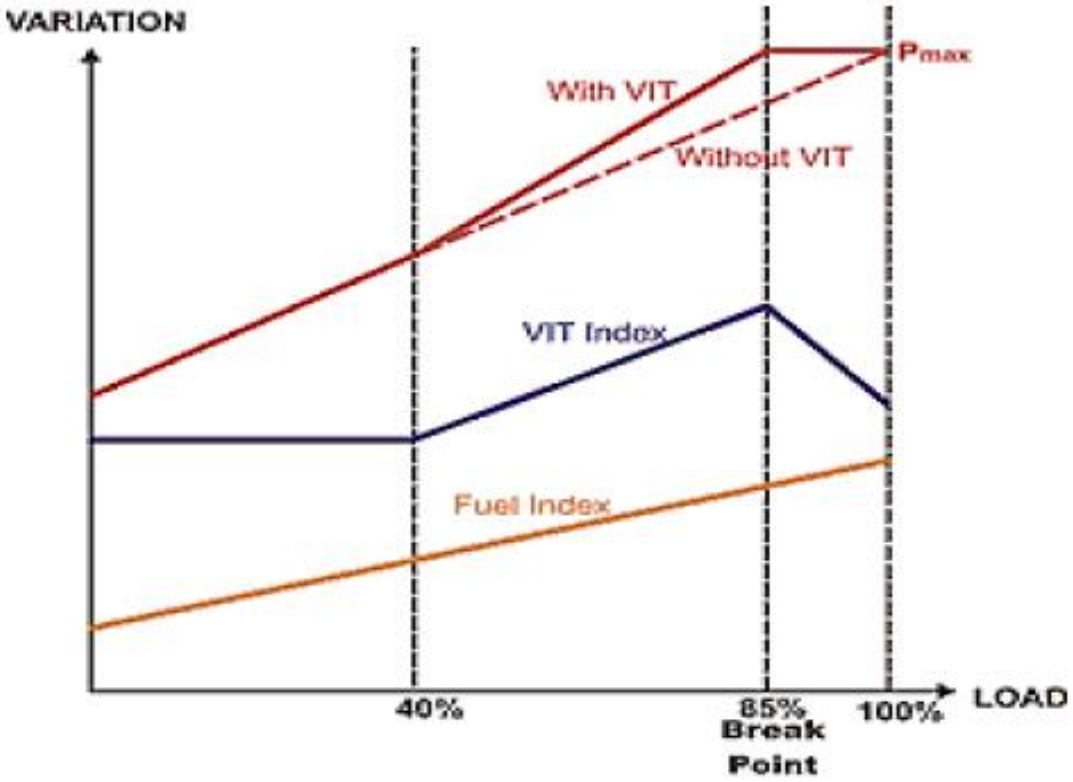

Figure 5.2: VIT operation **[26]**

In the available bibliography [26] a research for the effect of a VIT system on the operation of a two stroke marine diesel engine and its NOx emissions was conducted and confirmed the increase of the maximum pressure in low loads and the decrease in the specific fuel consumption.

In the simulations which were conducted, the VIT system was parameterized via a VIT index which was controlled by the Fuel Injection Index. In addition, the VIT index controlled the crank angle at which the start of the injection took place.

5.2 Variable Valve Timing (VVT)

In the end of the combustion, the gas produced has a very high temperature and needs to be removed from the cylinder so that new fresh air can be inserted and mixed with the newly injected fuel. For this reason, the exhaust valves exist. The exhaust valves open inwards into the cylinder so that the gas pressure produced will ensure that the valves will be pushed upwards to close. Moreover, this also helps in cleansing the valve seat of carbon or other metal deposits which build up from the combustion.

The exhaust valves have to face the highest temperatures compared to all the other engine's parts due to the exhaust gas that flows from them. These gasses are extremely hot and corrosive, and as a result Lead and Nickel are the most commonly used materials for making their steel alloys. Although these materials possess very good anti-corrosive and very high strength properties, they do have an increased cost [27].

Usually, in two stroke engines, a single or two exhaust valves are placed on the center of the cylinder head. In older designs, their opening and closing is controlled by a cam mounted on a camshaft. When this cam rotates, it lifts a push rod which is connected to a rocker arm that opens the valve. When the cam lowers the push rod, springs which are located around the valve rod force the valve to close. This system, since it utilizes rotating mechanical parts, has the disadvantage of the engine needing to overcome their inertia while operating. Furthermore, there is the possibility of wear damage. The wear damage might lead to exhaust gas leakage inside the valve mechanism, which might overheat its parts and accelerate the wear. The exhaust gas may also weaken the springs leading to further problems.

To compensate these disadvantages, newer designs utilize hydraulically operated air spring exhaust valves that function on hydraulic pumps instead of a push rod. The exhaust valve opens with the aid of a piston which is operated by displaced oil from the hydraulic pumps. In addition, the mechanical spring is replaced by an air spring. Air is led to the underside of the piston and gets compressed during the process of the opening of the valve. When the hydraulic pressure is relieved, as this portion of air expands, it aids in the closing of the valve. Along with the air inserted, a small quantity of lubrication oil is also injected so that the whole mechanism is well lubricated and cooled, thus preventing the leakage of exhaust gas. In the case of an oil excess, the surplus is drained to a collection tank [28]. Latest designs include electronic or cam-less systems.

Most of the large marine engines' exhaust valves have fitted on their spindles a winged valve rotator. This mechanical part slightly rotates the valve during its operation and in succession the impact produced by its closing ensures that the damage on the valve is uniform. Moreover, this event aids further in reducing the metal deposits at the valve seat prolonging the valves' life. The presence of these deposits is related mainly to the Vanadium and Sodium and limits the functionality and effectiveness of the valves' operation.

In Figure 5.3 a typical exhaust valve operating with an air spring is displayed.

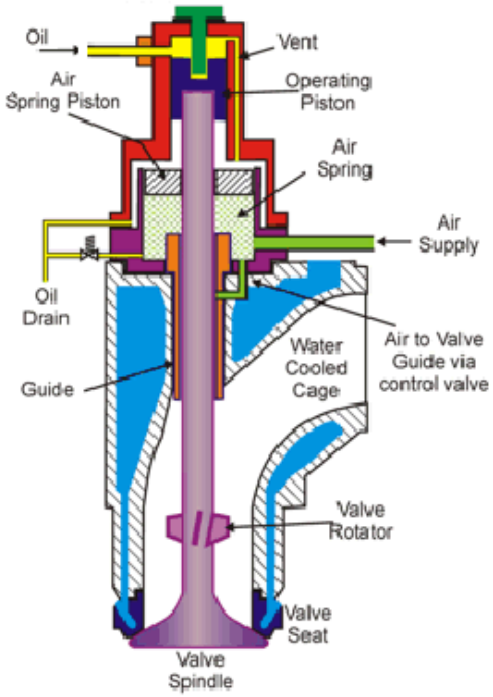

Figure 5.3: Exhaust Valve with Air spring **[28]**

The most commonly used valve timing can be seen in Figure 5.4. This figure, illustrates a two stroke engine operation cycle where the six basic phases can be seen clearly. More specifically, the phases of compression, fuel injection, power production, exhaust blowdown, scavenging and post scavenging are shown.

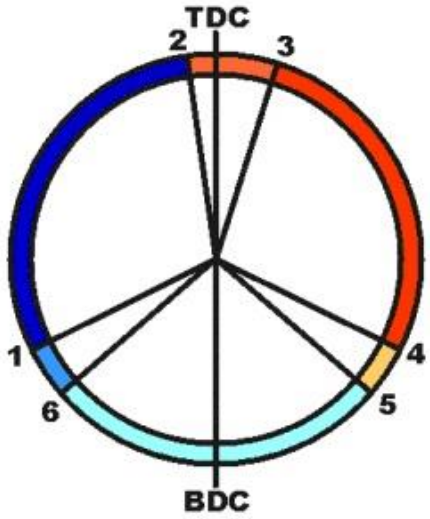

Figure 5.4: Exhaust Valve Timing **[29]**

Phase 1-2, occurs approximately 110° before TDC and is the compression where the piston is moving upwards. During phase 2-3, the fuel injection starts approximately 10° before TDC. In succession, phase 3-4 describes the power production which takes place approximately 12° after the TDC. The exhaust blowdown is next which corresponds to phase 4-5 and begins at approximately 110° after TDC. It is at this point where the exhaust valves open. In addition, at phase 5-6, is the scavenging

where the inlet ports are revealed, approximately at 140^{o} after TDC. Finally, phase 6-1 is the post scavenging taking place approximately 140^{o} before TDC, from the moment the inlet ports are covered until the moment when the exhaust valve closes [29].

By studying the above figure it is obvious that there are four applicable scenarios [30] in a Variable Valve Timing system:

- Open the exhaust valve earlier.
- Open the exhaust valve later.
- Close the exhaust valve earlier.
- Close the exhaust valve later.

By opening the exhaust valve earlier, the exhaust gas has a higher temperature when it exits the cylinder, since its energy content is not yet "used", leading to a more efficient Turbocharger operation. Moreover, more exhaust gas is removed from the cylinder, thus succeeding a better scavenging and consequently ensuring that more air can be inserted inside the cylinder. However, this scenario means that the power production phase is shorter since there is a reduced displacement volume thus losing work.

On the other hand, retarded opening of the exhaust valve means that the scavenging of the cylinder might not be as efficient and the exhaust gas has a lower temperature. Hence, when removed, they will have expended their energy content and as a result might reduce the effectiveness of an installed Turbocharger. However, there is a small gain from the slightly increased work produced due to the longer expansion of the exhaust gas.

Advancing the exhaust valve closing is associated with more exhaust gas trapped inside the cylinder, which increases fuel efficiency especially in part loads, and also leads to a longer compression phase, which increases the work and, hence the exhaust gas temperature. However, the scavenging phase is not efficient since the maximum volume of fresh air is not allowed to enter the cylinder.

On the fourth and last scenario, there is a more efficient scavenging of the cylinder with more available air which enables further fuel injection which may lead to increased produced power. Still, the compression phase of the fuel and air mixture is shorter which leads to lower exhaust gas temperatures and produced work.

In conclusion, all scenarios have their benefits and disadvantages making them all worthwhile investigating in this thesis. The VVT seems to be a practical method to affect exhaust gas temperatures in different engine speeds and loading cases. Nevertheless, it also affects volumetric efficiency, the heat capacity of the exhaust gas and fuel consumption. High exhaust gas temperatures are linked to low volumetric efficiency, while high volumetric efficiency is linked to low exhaust gas temperatures [31].

In the simulations which were conducted, the VVT system was parameterized via the crank angles at which the valves opened and closed. Since this engine possessed inlet ports and exhaust valves, what could be controlled via the VVT system were the exhaust valves and, thus, theirs and not the inlet ports' effect on the engine was investigated.

5.3 Variable Compression Ratio (VCR)

Another very important parameter which determines the operation characteristics of an engine is its compression ratio. The compression ratio equals to the volume of the cylinder when the piston is at the BDC divided by the volume of the cylinder when the piston is at the TDC. It can be expressed through the following equation:

$$\varepsilon = \frac{V_d + V_c}{V_c} \tag{5.1}$$

In equation (5.1), ε is the compression ratio, V_d is the displacement volume i.e. the volume from the beginning of the compression stroke until its end and V_c is the clearance volume i.e. the volume remaining at the end of the compression stroke. Increased compression ratio means increased thermal efficiency due to the fact that the same combustion temperature can be reached with less fuel, while also giving a longer expansion cycle. However, the optimum compression ratio depends on the output power of the engine, and more specifically, on its operating conditions.

In particular, the compression ratio is restricted at high power output due to the design limit of the maximum firing pressure. On the other hand, when the engine operates in low power outputs, the maximum pressure is lower compared to high power outputs meaning that the compression ratio can be increased in partial loads in order to improve thermal efficiency [32].

Moreover, the engine's design stipulates the position and height of the inlet ports in order to ensure adequate amount of air trapped during scavenging in high power outputs. This restricts the effective expansion ratio since the expansion stroke is limited by the opening of the inlet ports, which are uncovered by the piston passing. Furthermore, in high outputs a large amount of air is required, in contrast to low outputs where a lesser amount of air is needed. Consequently, at low power outputs, by altering the compression ratio and, consequently, the piston passing and the opening of the scavenging ports, the amount of air entering the cylinder during scavenging could be reduced, thus increasing the effective expansion ratio.

Nevertheless, equation (5.1) clearly indicates that the compression ratio depends on the geometric characteristics of the cylinder such as the cylinder bore, the piston length etc. Since these units are almost constant, the compression ratio is also almost constant. The term "almost" is used because with the passage of time the engine parts are subjected to wear damage, which alters slightly their characteristics. This used to be the case until recently when a Variable Compression Ratio system was developed for crosshead type engines that enables the compression ratio to be changed while the engine operates.

The principle behind the VCR system is very simple. By increasing the length of the piston rod at the TDC, the clearance volume V_c of the combustion chamber is reduced and, therefore the compression ratio is increased. The mechanical procedure to accomplish the desirable increase of the piston rod is based on the application of hydraulic oil between the crosshead pin and the piston rod. In this way the combination of the hydraulic oil, the piston rod and the crosshead pin acts as a hydraulic cylinder. Research [32] has showed that with this technique the length between the piston crown and the crosshead pin in a two stroke 6-cylindered engine can be increased up to 100mm, which caused an increase up to 50% of the compression ratio.

Figure 5.5 illustrates how the VCR system operates.

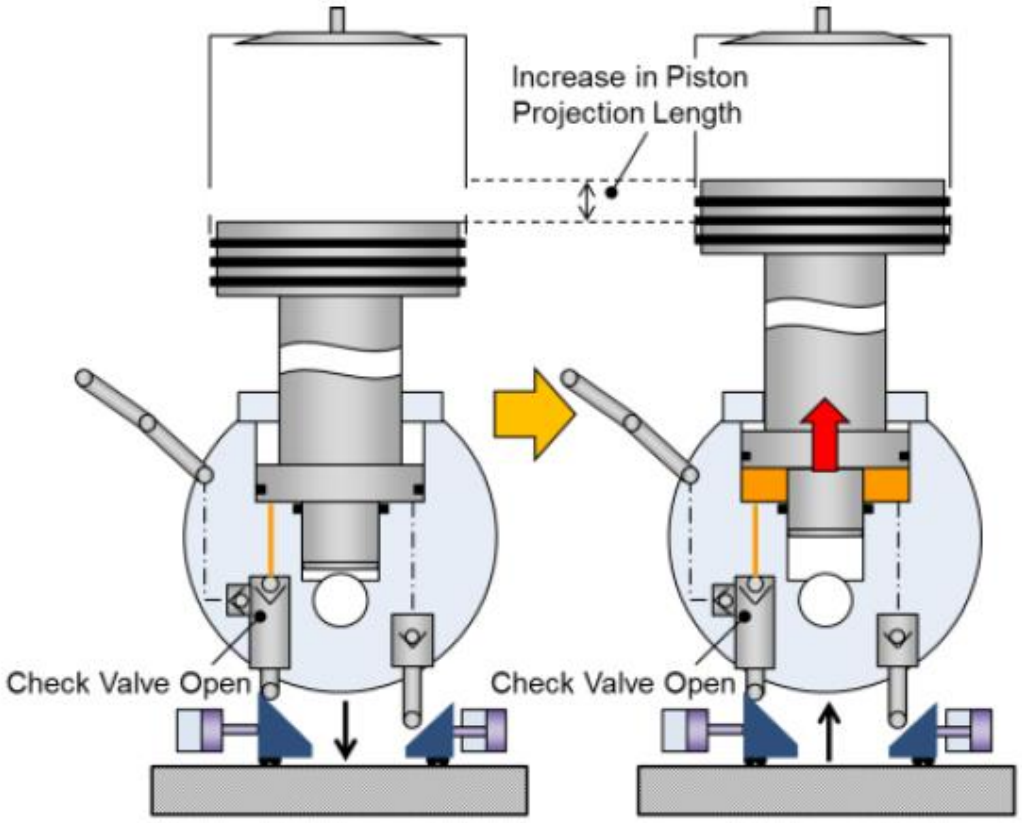

Figure 5.5: VCR system **[32]**

The oil is supplied via a pump through the swing lever which already exists for the purpose of piston cooling and, as a result, no additional piping is required. When there is the need for decreasing the projection length of the piston rod, the oil is depressurized by a relief valve.

The pressure required for the projection of the piston rod is produced from the physical contact of the pump with the cam plate. Since this contact occurs near the BDC, the pressures applied to the piston top are minimal and, thus, only a small hydraulic pressure is necessary for the projection.

All things considered, the VCR system provides this thesis with another option; by altering the compression ratio and increasing thermal efficiency, it is possible to test its effects on the power output of the engine and its ability to accelerate at different loads. Also, the possibility of delaying the revealing of the scavenge ports and, thus, the amount of air inserted during scavenging, could also provide some interesting results but was not investigated further in this thesis.

Chapter 6: MOtor THERmodynamics & the Models Used

For the purposes of this thesis, since experiments on a real engine were not possible, engine simulations were required via engine modeling. The proper modeling of the engine is of vital importance since it can effectively describe the operation and performance of the engine while avoiding the increased cost and time that accompany actual experiments. In our case, the in-house developed engine simulation tool MOtor THERmodynamics (MOTHER) was used.

6.1 MOTHER

MOTHER [6] is a comprehensive thermodynamic engine performance prediction code, which falls under the category of "zero-dimensional" or "control volume" simulation models. In it, the engine is considered as a series of volumes which are interconnected via valves or ports. In each control volume and at any given computational time step, spatial uniformity of fluid properties and constant rate of change of parameters ("quasi-steady") is assumed. Also, work, heat and mass transfer are presumed to take place across the boundaries of each control volume.

This program has been under development in the Laboratory of Marine Engineering (LME) of the National Technical University of Athens (NTUA), and is capable of predicting the performance of an engine under both steady state and transient conditions.

The following four governing equations are applied in any control volume:

$$\dot{T} = f(\dot{U}, \dot{H}, \dot{\varphi}, \dot{Q}, \dot{W}) \tag{6.1}$$

$$\dot{m} = f(P, T, g, R, A_{flow}, C_d) \tag{6.2}$$

$$\dot{m} = \sum \dot{m}_j \tag{6.3}$$

$$P = f(m, R, T, V) \tag{6.4}$$

Equation (6.1) describes the non-steady flow of energy inside the control volume, manipulated so as to express the rate of change of temperature $\dot{T}$, in terms of other parameters. The rate of change of the internal energy $\dot{U}$ and enthalpy $\dot{H}$ of the working fluid is obtained by reference to thermodynamic property data for air/fuel mixtures. The rate of change of equivalence ratio $\dot{\varphi}$, is obtained by summing the air and fuel exchanges. The rate of change of heat $\dot{Q}$, depends on the heat released by combustion and the heat lost due to heat transfer. The rate of change of work $\dot{W}$, depends on the rate of change of the control volume based on the engine geometry, as well as the instantaneous pressure.

Equation (6.2) models the unsteady mass flow between interconnected volumes via valves and ports as a quasi-steady flow. This depends on the instantaneous pressure P, temperature T and mixture properties in each volume, as well as the geometry dependent flow area A_{flow} and discharge coefficient C_d of the restrictions between the volumes (valves, ports etc.).

At the end of each computational step, a summation of mass exchanges is made for each control volume, given by equation (6.3).

Lastly, the instantaneous pressure P is determined by the use of equation (6.4) which is based on the actual volume V, mass m, temperature T and fluid properties.

For all the control volumes of the system, the resulting sets of coupled differential equations are solved numerically using a typical resolution of one degree crank angle or smaller (for more precision). Various sub-models are included for the different processes inside the engine's cylinders as well as a series of subsystems that affect the engine thermodynamics. Typical examples of sub-models are a combustion model, a heat transfer model, a friction model etc. while typical subsystems are the turbochargers, power turbines etc.

The philosophy behind the MOTHER code design is based on the concept of Basic Engineering Elements (BEE) which allows complex configurations, such as a diesel engine, to be represented by using a limited number of simple elements. MOTHER offers different kinds of BEE, such as thermodynamic elements, which are divided into Flow Receivers (cylinders, plenums, etc.) and Flow Controllers (valves, compressors, turbines etc.). Furthermore, mechanical elements (crankshaft, shaft loads etc.) and controller elements (speed governor, PID controllers) are also available for the mechanical connections of the systems.

In Table 6.1 are presented the entire available BEE which MOTHER provides for the modelling of various configurations. Detailed information about each one and their operation can be found in [6].

Table 6.1: BEE available in MOTHER

Thermodynamic Elements		**Mechanical Elements**	**Control Elements**
Flow Receivers	**Flow Controllers**		
Cylinder	Valve	Crank Shaft	Speed Governor
Plenum	Heat Exchanger	Shaft	PID Controller
Fixed Fluid	Compressor	Shaft Load	
	Turbine	Clutch	
		Gear Box	

6.2 Models

Different models were used during the simulations. These included thermal and heat transfer models, friction models and models which described how a vessel and its propeller would co-act with their respectful engine.

The ones which had to do with the in-cylinder procedures (such as the thermal, friction, combustion etc.) were already integrated in the simulation program while the ship surge model, the propeller model and the propeller's inertia calculation were written in a Fortran Code and added to the simulation as subroutine programs.

Lastly, a governor was set up since it is necessary in order to conduct transient simulations.

Each of these models is explained below on its according passage.

6.2.1 In-Cylinder Models

In MOTHER, considering the engine modeling, the three basic engineering components from which the engine constitutes are: the cylinder units, the turbochargers and the different scavenge and exhaust manifolds and plenums.

Regarding the in-cylinder models, each cylinder unit consists of the cylinder itself, its inlet ports and its exhaust valves. The most important models which were integrated in MOTHER so that they could describe the performance and operation of a single cylinder unit were the three following:

- Combustion Model
- Friction Model
- Heat Transfer Model

For each of these categories of models, MOTHER gives the user the option to choose a specific one from a provided list. The parameters that describe each of these models are subject to changes if the user decides. Nonetheless, the same models and parameters were used for all the cylinders.

Considering the outside environment, it is regarded as a fixed fluid element, with constant pressure, temperature and chemical composition. The working mixture consists of 11 gas species plus the fuel. These are O_2, N_2, H_2O, H, H_2, N, NO, O, OH and CO.

Combustion Model: Woschni – Anisits

The combustion model used was the Woschni – Anisits, a phenomenological model, used for combustion simulations of direct injection engines. It is based on the (single) S-curve equation that calculates the fraction of the mass of the burnt fuel m_b [kg] and the total mass of fuel injected in the cylinder m_{tot} [kg].

This fraction, symbolized as x_b, is calculated as follows:

$$x_b = \frac{m_b}{m_{tot}} = 1 - e^{-a\cdot\left(\frac{\theta-\theta_0}{\Delta\theta_b}\right)^{m+1}} \tag{6.5}$$

Where θ [deg] is the crank shaft angle, θ_0 [deg] is the crank shaft angle at the start of combustion, $\Delta\theta_b$ [deg] the total combustion duration and a and m are adjustable parameters that fix the shape of the S-curve. The principle behind the model's function is to assume that the different constants of the S-curve are known at a specific "reference" point and, based on that point, calculate the constants at any other condition. It is noted that regarding the calculation of θ_0, the ignition delay is also taken into consideration. Detailed information for the calculation of each combustion parameter can be found in [6].

Friction Model: Mc Auly et al.

The model of Mc Auly et al. was used as a friction model which assumes that the total friction losses vary linearly depending on the piston speed and the peak pressure. According to this model, the friction mean effective pressure ($fmep$) can be calculated using the following equation:

$$fmep = k_1 + k_2 \cdot P_{max} + k_3 \cdot V_P \tag{6.6}$$

Where P_{max} [Pa] is the peak pressure inside the cylinder and V_P [m/s] is the piston's mean speed. The constants k_1, k_2 and k_3 are used in order to determine the effect of each of the parameters above.

Heat Transfer Model: Woschni

In general, the instantaneous heat fluxes q [kW] from the gas to the cylinder walls (cylinder head, piston crown, upper and lower part of the liner) are calculated at each step of the simulation with the following relation:

$$q = h \cdot A \cdot \left(T_{gas} - T_{wall}\right) \tag{6.7}$$

Where h [kW/m^{2}K] is the gas-cylinder instantaneous spatial average heat transfer coefficient, A [m^2] is the respective cylinder part wall gas side area, $\mathrm{T_{gas}}$ [K] the instantaneous cylinder gas temperature and $\mathrm{T_{wall}}$ [K] the respective cylinder part wall surface temperature.

The heat transfer coefficient h is calculated by utilizing the Woschni equation:

$$h = 0.00326 \cdot B^{-0.2} \cdot P^{0.8} \cdot T_{gas}^{-0.55} \cdot w^{0.8} \tag{6.8}$$

Where B [m] is the cycle bore, P [Pa] the cylinder gas pressure and w [m/s] the average cylinder gas velocity.

6.2.2 Ship Surge Model

In this thesis, it was necessary to derive a way in order to estimate the acceleration of the vessel during transient conditions. The model used to solve this problem was an amalgamation of empirical methods and theoretical equations produced and used by well acknowledged researchers throughout the years.

The key to calculating the ship's acceleration was to study Newton's second law of motion which states that for any object; mass times acceleration equals the summation of forces applied on the object.

$$\sum F = M \times a \tag{6.9}$$

This means that for any ship, according to Newton's second law of motion, its total mass multiplied by its acceleration equals to the thrust generated by the propeller reduced by its total resistance. Keeping in mind that the total resistance needs to take also into account the thrust deduction factor, the above leads to the linear momentum equation:

$$\dot{V}_{SHIP} \cdot (M_{SHIP} + M_{ADDED}) = T_{pr} - {}^{R_{tot}}/_{(1-t)} \tag{6.10}$$

On the above equation $\dot{V}_{SHIP}$ [m/s^2] is the acceleration of the vessel, M_{SHIP} [kg] is the displacement of the ship, M_{ADDED} [kg] is the added mass of the ship, t is the thrust deduction factor, T_{pr} [N] is the thrust generated by the propeller and R_{tot} [N] is the total resistance of the ship.

The thrust deduction factor is indicative of the fact that the flow over the hull surface is accelerated due to the presence of the propeller in the ship's wake which leads to a reduction of the local pressure field over the aft part of the hull surface [7]. This pressure drop increases the total resistance of the vessel when compared to its towing state or alternatively, reduces the propeller's effective thrust.

Once everything is calculated, equation (6.10) can be used in order to estimate the vessel's acceleration. Next, by determining a time period dt, the new velocity of the vessel can be calculated at any point using the equation below:

$$V_{SHIP\_NEW} = V_{SHIP\_OLD} + dt \cdot \dot{V}_{SHIP} \tag{6.11}$$

Moreover, a method was needed in order to produce a value for the thrust of the propeller T_{pr}, the thrust deduction factor t and the total resistance of the ship R_{tot}. The first is analyzed in the chapter "Propeller Model" while the other two are discussed below.

All the necessary data needed to run the corresponding calculations and equations were taken from the sea trials of a known ship or were estimated using already confirmed methods by previous researchers [33, 34, 35, 36].

Total Mass of Ship M_{SHIP} and M_{ADDED}

As far as the total mass of the ship is considered, as seen in equation (6.10), it can be fragmented into M_{SHIP} and M_{ADDED}. The first equals to the displacement of the ship taken into account from the ship's particulars while the second is a very complicated hydrodynamics problem attributed to the water deflected by the hull and thus was taken as a fraction of the ship's total mass. More specifically, M_{ADDED} was considered equal to 10% of M_{SHIP}.

Thrust Deduction Factor *t*

This coefficient expresses the increase of the ship's total resistance due to the presence of the propeller in the wake field. On the terms of producing a value for the thrust deduction factor there has been a lot of work by many researchers which have come up with empirical methods that gave good approximations. In this thesis, the method of Holtrop and Mennen [9] was chosen since it was considered the most accurate for single-screw ships. Another vital selection could be the method of Harvald [37] which utilizes diagrams based on hull form parameters but since there was a lack of data about the ship geometry it was decided unreliable.

According to Holtrop and Mennen [9], the thrust deduction factor can be determined by a function which uses as arguments the geometry of the ship. More specifically the function used was:

$$t = \frac{0.25014 \cdot (B/L_{WL})^{0.28956} \cdot (\sqrt{B \cdot T}/D)^{0.2624}}{(1 - c_P + 0.0225 \cdot lcb)^{0.01762}} + 0.0015 \cdot C_{STERN} \qquad (6.12)$$

Where B [m] is the breadth of the ship, L_{WL} [m] the length of ship along the waterline [34], D [m] the depth of the ship, T [m] the draught of the ship, C_P the prismatic coefficient, C_{STERN} a constant depending on the shape of the sections and lcb the longitudinal center of buoyancy calculated from mid ship and written as a percentage of L_{WL}.

We need to point out that while Carlton, in his book "Marine Propellers and Propulsion" [7], is more updated in his work he has an error on equation (6.12) so it was taken into account from the book of Holtrop, "A Statistical Re-Analysis of Resistance and Propulsion Data" [8].

Total Resistance of Ship R_{tot}

One of the most complicated problems in solving equation (6.10) was the estimation of the total resistance of the ship. The most accurate way would be to conduct an experiment using an appropriate model of the ship this thesis is based on. By following the procedure described in countless manuals, research papers and trials methods [38] one could calculate the resistance of the model and then relate it to the actual resistance of the ship by applying specific correlation factors. However, due to lack of data considering the accurate geometry of the ship it was decided that the resistance could only be computed by using a numerical method.

Among the methods proposed by researchers such as Taylor [39], Ayre [40], Auf'm Keller [41] and Lap [42], Harvald [37] and many others, the most reliable was decided the one proposed by Holtrop

and Mennen [8, 9]. Holtrop developed a power prediction method which was based on the regression analysis of random full-scale and model test data. More precisely, his results can be analyzed on the basis of the ship's resistance equation:

$$R_{tot} = (1 + k_1) \cdot R_F + R_{APP} + R_W + R_B + R_{TR} + R_A \tag{6.13}$$

The form factor of the hull $(1 + k_1)$ has been estimated according to Holtrop and Mennen [9]:

$$(1 + k_1) = C_{13} \cdot \left\{0.93 + C_{12} \cdot \left(\frac{B}{L_R}\right)^{0.92497} \cdot (0.95 - C_P)^{-0.521448} \cdot (1 - C_P + 0.0225 \cdot lcb)^{0.6906}\right\} \tag{6.14}$$

Where C_{12} , C_{13} and L_R are coefficients calculated clearly in [9].

Equation (6.13) fragments the total resistance into six different components. These are the frictional resistance R_F, the resistance due to the appendages of the ship R_{APP}, the wave making and wave breaking resistance R_W, the additional resistance due to the presence of a bulbous bow near the surface R_B, the additional pressure resistance due to the immersed transom R_{TR} and lastly the R_A which is the model – ship correlation resistance.

The frictional resistance R_F can be calculated according to the ITTC-1957 [43] friction formulation which states that the friction resistance coefficient C_F is equal to:

$$C_F = \frac{0.075}{(log_{10}Re - 2)^2} \tag{6.15}$$

In succession, the frictional resistance equals to:

$$R_F = \frac{1}{2} \cdot \rho \cdot C_F \cdot S \cdot {V_{SHIP}}^2 \tag{6.16}$$

Where ρ [kg/m^3] is the density of the water and S [m^2] is the total wetted surface of the vessel.

Considering the resistance due to the appendages of the ship, Carlton [7] suggests the following equation to be used:

$$R_{APP} = \frac{1}{2} \cdot \rho \cdot {V_{SHIP}}^2 \cdot C_F \cdot (1 + k_2)_{eq} \cdot S_{APP} + R_{BT} \tag{6.17}$$

In equation (6.17), S_{APP} [m^2] is the total wetted area of the appendages while $(1 + k_2)_{eq}$ is a coefficient which takes into account the contribution of each appendage separately multiplied by its wetted area and finally divided by S_{APP} as seen in equation (6.18).The term R_{BT} refers to the resistance attributed to the bow thrusters. For more details, one can refer to the works of Carlton, Holtrop or Mennen [7, 8, 9].

$$(1 + k_2)_{eq} = \frac{\sum_j (1 + k_2)_j S_{APPj}}{S_{APP}} \tag{6.18}$$

In this thesis, since data about the appendages was scarce, $(1 + k_2)_{eq}$ and S_{APP} were speculated in relation to another ship's for which the method was already applied. Furthermore, since there was no data about the bow thrusters, R_{BT} was considered null.

In addition, R_W is the wave making and wave breaking resistance of the ship. According to Holtrop, if the researcher wants to be precise, this resistance must be calculated differently depending on the Froude Number of the ship. More specifically, Holtrop in [8] suggests utilizing the equation:

$$R_{W-B} = C_{17} \cdot C_2 \cdot C_5 \cdot \nabla \cdot \rho \cdot g \cdot \exp\{m_3 \cdot {F_n}^d + m_4 \cdot cos(\lambda \cdot {F_n}^{-2})\} \quad (6.19)$$

And

$$R_{W-A} = C_1 \cdot C_2 \cdot C_5 \cdot \nabla \cdot \rho \cdot g \cdot \exp\{m_1 \cdot {F_n}^d + m_4 \cdot cos(\lambda \cdot {F_n}^{-2})\} \quad (6.20)$$

On the above equations $C_1,\ C_2,\ C_5,\ C_{17},\ m_1\ , m_3\ , m_4\ , \lambda\ and\ d$ are coefficients described clearly in [8] and F_n is the Froude number. Equation (6.19) is used if F_n>0.55 while equation (6.20) is used when F_n<0.40. If F_n is between 0.40 and 0.55 then Holtrop suggests implementing equation (6.21):

$$R_W = R_{W-A\ 0.4} + (10 \cdot F_n - 4) \cdot \frac{(R_{W-B\ 0.55} - R_{W-A\ 0.4})}{1.5} \quad (6.21)$$

Where $R_{W-A\ 0.4}$ and $R_{W-B\ 0.55}$ are the results of equations (6.19) and (6.20) for F_n=0.40 and F_n=0.55 respectively.

Moreover, R_B is the additional resistance due to the presence of a bulbous bow near the surface and R_{TR} is the additional pressure resistance due to the immersed transom. These two resistances can be calculated with the equations provided by Holtrop and Mennen in [9] where:

$$R_B = 0.11 \cdot \exp(-3 \cdot {P_B}^{-2}) \cdot {F_{ni}}^3 \cdot {A_{BT}}^{1.5} \cdot \rho \cdot \frac{g}{(1 + {F_{ni}}^2)} \quad (6.22)$$

And

$$R_{TR} = \frac{1}{2} \cdot \rho \cdot {V_{SHIP}}^2 \cdot A_T \cdot C_6 \quad (6.23)$$

Where A_{BT} [m^2] and A_T [m^2] are the transverse area of the bulb above the keel line and the immersed transom area at zero velocity respectively. Furthermore, the coefficient P_B is the measure for the emergence of the bow, F_{ni} is the Froude number based on the immersion and C_6 is a coefficient, all of them calculated in [9].

Lastly, R_A is the model – ship correlation resistance. In order to estimate it, the general resistance equation can be used:

$$R_A = \frac{1}{2} \cdot \rho \cdot C_A \cdot S \cdot {V_{SHIP}}^2 \quad (6.24)$$

The only factor in need of calculation is the model – ship correlation resistance coefficient C_A. We need to point out that while Carlton, in his book "Marine Propellers and Propulsion" [7], is more updated in his work he has an error on the calculation of C_A so it was taken into account from the book of Holtrop and Mennen [9]. More specifically, Holtrop suggests utilizing the following equation:

$$C_A = 0.006 \cdot (L_{WL} + 100)^{-0.16} - 0.00205 + 0.003 \cdot \sqrt{{L_{WL}}/{7.5}} \cdot C_B^4 \cdot C_2 \cdot (0.04 - C_4) \quad (6.25)$$

The estimation of coefficients C_2 and C_4 is described clearly in [9]. Moreover, there is a correction for C_A in case of roughness values higher than the standard figure of 150μm. However, in this thesis, it was omitted.

In conclusion, by utilizing all of the above equations and carefully applying them to the data that was available, an accurate model of the total ship's resistance and velocity was achieved.

All equations used and all methods for calculating the needed coefficients and quantities have been summed up in the end of the thesis in the "APPENDIX A': Equations Used" chapter for the comfort of the reader. Moreover, the particulars of the vessel, the propeller and the engine used for the simulation are summed up in the chapter "Simulation Specifics".

6.2.3 Propeller Model

In this thesis, a propeller model was used in order to calculate the thrust and torque produced by the propeller. More specifically, these were needed in order to estimate the acceleration of the ship using the ship model analyzed in the previous chapter "Ship Surge Model". Moreover, since this thesis researches transient events, it was not possible for this analysis to use a constant torque associated with the propeller. The velocity of the ship constantly changes during transient events due to the variation of fuel and air to the engine which in succession leads to a variable torque delivered to the propeller thus a different load to the engine. This variation in the load is depicted as variations in the thrust and torque of the propeller.

The distinctive trait which makes the analysis of a propeller troublesome to begin with, is the presence of the "wake". The wake is practically the water behind the vessel which is disturbed by its passage and more specifically by the rotation of the propeller. Due to many hydrodynamic events taking place, the velocity of the water in the wake of the ship is different than the actual velocity of the ship itself. This is mainly attributed to the fact that part of the flow to the propeller is obstructed by the presence of the ship's boundary layer around the hull resulting in an inhomogeneous velocity field [38]. Thus, the propeller encounters an effective wake velocity V_A [m/s^2] which is also called the advance speed. Therefore, the advance speed aft of the ship equals to a fraction of the velocity of the ship:

$$V_A = (1 - w) \cdot V_{SHIP} \tag{6.26}$$

In equation (6.26) w is the infamous wake factor [7]. Its calculation has interested many researchers. Among others, some of the most popular methods are Van Lammeren's [44] curves which were based in the vertical prismatic coefficient, the equation of Schoenherr [45] based on the ship's and the propeller's characteristics, Harvald's curves [37] which were also based on the ship's geometric characteristics and the hull form, the simple formula of Taylor [39] based on the block coefficient of the vessel and Holtrop and Mennen's equation [8, 9] for single or twin-screw vessels derived from a series of tests over a wide range of hull forms. From the ones mentioned, the last one was considered the most precise and updated and thus used in this thesis. Holtrop and Mennen suggested for a single screw vessel the following equation for the estimation of the wake factor:

$$w = C_9 \cdot (1 + 0.015 \cdot C_{STERN}) \cdot [(1 + k) \cdot C_F + C_A] \cdot \frac{L_{WL}}{T_A}$$
$$\cdot \left\{0.050776 + 0.93405 \cdot C_{11} \cdot \frac{(1 + k) \cdot C_F + C_A}{1.315 - 1.45 \cdot C_P + 0.0225 \cdot lcb}\right\} + 0.27915$$
$$\cdot (1 + 0.015 \cdot C_{STERN}) \cdot \sqrt{\frac{B}{L_{WL} \cdot (1.315 - 1.45 \cdot C_P + 0.0225 \cdot lcb)}} + C_{19}$$
$$\cdot (1 + 0.015 \cdot C_{STERN}) \quad (6.27)$$

In this equation, C_9 , C_{11} and C_{19} are coefficients which are calculated according to Holtrop and Mennen [8, 9], C_{STERN} is a constant depending on the shape of the sections and lcb the longitudinal center of buoyancy calculated from mid ship and written as a percentage of L_{WL}. In addition, L_{WL} [m], B [m] and T_A [m] refer to the length along the waterline, the breadth and the aft draught of the ship respectively. Furthermore, C_P is the prismatic coefficient and $(1 + k)$ is the hull form factor of the vessel. Finally, C_F and C_A are resistance coefficients related to friction and model – ship correlation accordingly.

All the necessary data needed to run the corresponding calculations and equations were taken from the particulars of the propeller at hand, the sea trials of the vessel or were estimated by using already confirmed methods and results by previous researchers [33, 34, 35, 36].

At this point we must indicate the fact that the most preferably used propeller model in the bibliography is the four quadrant propeller model. This model takes into account that a propeller does not only operates with positive rotational speed and inflow velocity. It might also need to produce thrust in the reverse direction in order to propel the ship astern or decelerate it. This means that a negative rotational speed and inflow velocity must also be taken into account. When studying the response of the propeller during transient conditions, all of the possible operating conditions need to be considered.

The key to enable the distinction and mathematization of the different possible combinations is the advance angle β. The advance angle β is estimated at 70% of the propeller radius and for a fixed propeller can be calculated via equation (6.28):

$$\beta = \arctan\left(\frac{V_A}{0.7 \cdot \pi \cdot n \cdot D_P}\right) \quad (6.28)$$

Where n [rps] is the rotational speed of the propeller and D_P [m] is its diameter.

Another viable option which has been frequently used in previous conventional propeller performance models would be basing the model on the advance coefficient J described in equation (6.29). However, when the advance angle is equal to 90° or 270° (meaning that the rotational speed equals to zero), the advance coefficient J takes an infinite value thus making it problematic in its utility.

$$J = \frac{V_A}{n \cdot D_P} \quad (6.29)$$

On the contrary, advance angle β can efficiently describe all four propeller operation cases by relating them to the four quadrants as seen on the table (6.2) below:

Table 6.2: Four quadrants operation

Quadrant	Rotational Speed	Advance Speed	Advance Angle
1st	Ahead/Positive	Ahead/Positive	$0° \leq \beta \leq 90°$
2nd	Astern/Negative	Ahead/Positive	$90° \leq \beta \leq 180°$
3rd	Astern/Negative	Astern/Negative	$180° \leq \beta \leq 270°$
4th	Ahead/Positive	Astern/Negative	$270° \leq \beta \leq 360°$

This table shows the possible combinations of the propeller's rotational speed and advance speed. The first quadrant represents a ship which is moving ahead and its propeller is rotating positively. The second quadrant represents the case where the ship while moving ahead needs to decelerate so the propeller rotates in the opposite direction. The third quadrant refers to the case where the ship is moving astern thus the propeller is rotating negatively producing negative thrust. Finally, in the last quadrant, the fourth, while the ship moves astern the propeller rotates positively thus producing positive thrust. All of the above are better depicted in Figure 6.1 below:

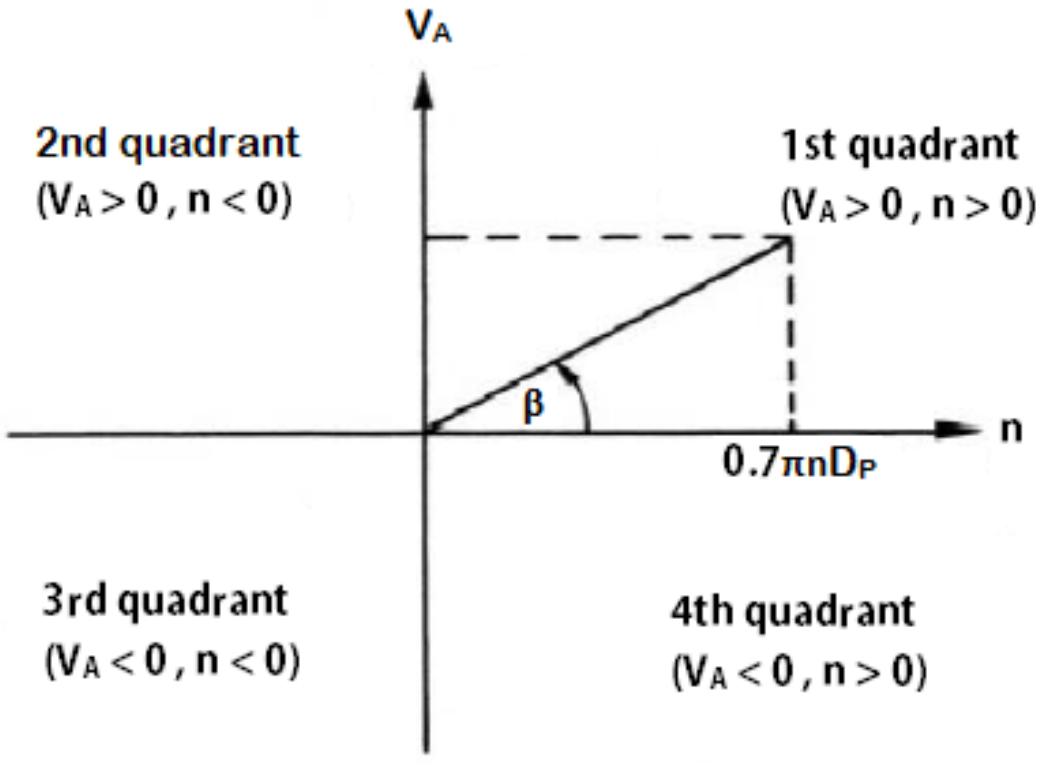

Figure 6.1: Four quadrant figure **[7]**

The use of the advance angle as the base of our chosen model provides us however with another great advantage.

In order to achieve our final goal, which is none other than estimate the thrust and the torque produced by the propeller, we need to use the following basic thrust and torque equations [10]:

$$T_{pr} = \frac{1}{2} \cdot \rho \cdot C_T^* \cdot {V_r}^2 \cdot A_0 \tag{6.30}$$

$$Q_{pr} = \frac{1}{2} \cdot \rho \cdot C_Q^* \cdot {V_r}^2 \cdot A_0 \cdot D_P \tag{6.31}$$

Considering the fact that relative advance velocity V_r equals to:

$${V_r}^2 = {V_A}^2 + (0.7 \cdot \pi \cdot n \cdot D_P)^2 \tag{6.32}$$

And that the propeller area A_0 equals to:

$$A_0 = \frac{\pi}{4} \cdot {D_P}^2 \tag{6.33}$$

Then equations (6.30) and (6.31) can be rewritten in:

$$T_{pr} = \frac{\pi}{8} \cdot \rho \cdot C_T^* \cdot \left({V_A}^2 + (0.7 \cdot \pi \cdot n \cdot D_P)^2\right) \cdot {D_P}^2 \tag{6.34}$$

And

$$Q_{pr} = \frac{\pi}{8} \cdot \rho \cdot C_Q^* \cdot \left({V_A}^2 + (0.7 \cdot \pi \cdot n \cdot D_P)^2\right) \cdot {D_P}^3 \tag{6.35}$$

Now the only real unknown factors to be calculated are the non-dimensional thrust and torque propeller coefficients C_T^* and C_Q^*. Here is where the great advantage of using the advance angle is revealed.

In the known literature, there have been a handful of ways to calculate these factors with the most common one to be to read them from diagrams such as the one shown in Figure 6.2:

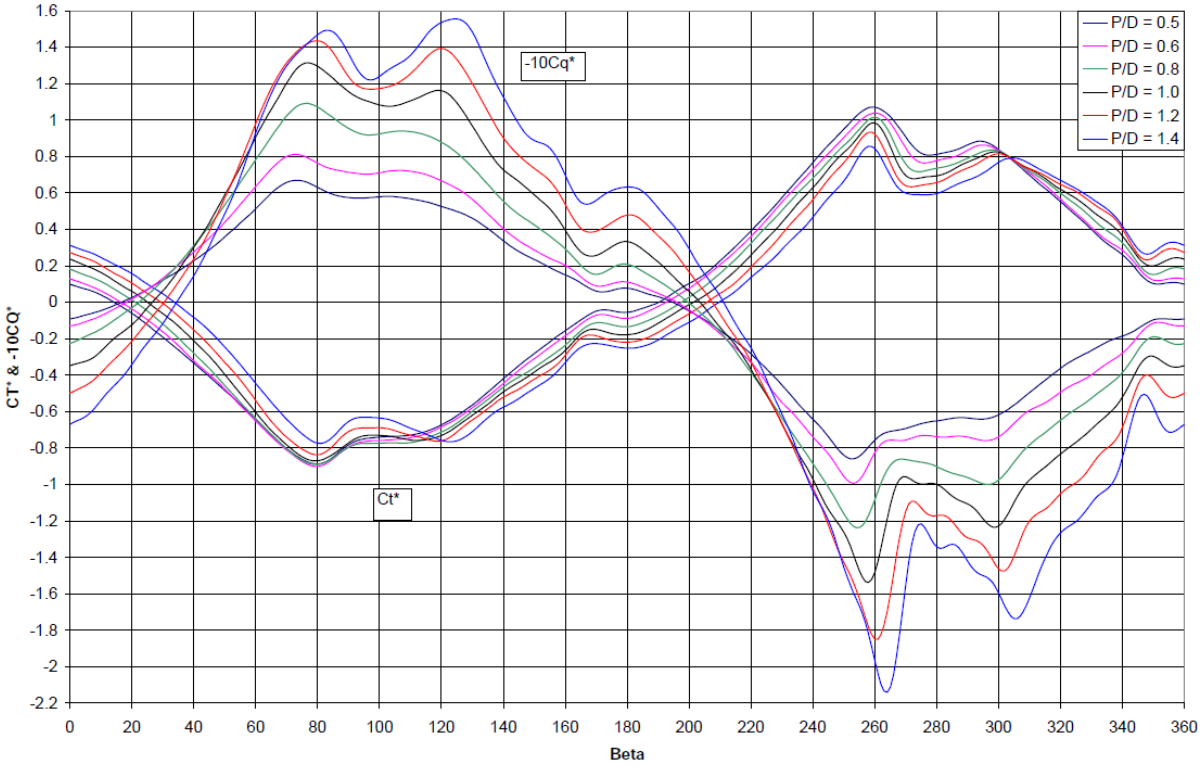

Figure 6.2: B4-70 Series 4-Quadrant Results **[10]**

These figures provide the reader with a value for the thrust and torque propeller coefficients for different advance angles (β) and for different propeller pitches to propeller diameter ratios (P/D_P). Moreover, this kind of diagrams exists for propellers with different blade number and expanded area ratio. However, these diagrams are also difficult to find for all designs of propellers and it was deemed unorthodox to optically estimate the values we needed from these diagrams. Furthermore, the only way to accurately reproduce them for a random propeller would be through modeling and experimentation.

For this reason, the propeller thrust and torque coefficients were seen as periodic functions over the range of $0^o \leq \beta \leq 360^o$ and were calculated using a Fourier type representation shown below:

$$C_T^* = \frac{1}{100} \cdot \sum_{k=1}^{N} \{A_k \cdot \cos(k \cdot \beta) + B_k \cdot \sin(k \cdot \beta)\} \tag{6.36}$$

$$C_Q^* = -\frac{1}{1000} \cdot \sum_{k=1}^{N} \{A_k \cdot \cos(k \cdot \beta) + B_k \cdot \sin(k \cdot \beta)\} \tag{6.37}$$

A note must be made that in equations (6.36) and (6.37) β is calculated in radians.

The A_k and B_k Fourier coefficients were retrieved from the work of Robert F. Roddy [10] who has researched them for a handful of specific propeller designs and has calculated them for N=30. Unfortunately, research in this specific field is not yet complete or rather might be classified and these coefficients are not published for many propeller designs.

Nevertheless, by integrating the known Fourier coefficients to a simple handmade computing code it was possible to calculate the thrust and torque propeller coefficients for any given advance angle β for the specific propeller and thus (from equation (6.28)) any given pair of rotational speed n and advance velocity V_A and in succession (from equation (6.26)) any given pair of rotational speed n and ship velocity V_{SHIP}. The propeller coefficients were plotted in a computer environment and verified with the ones shown in the given figures.

A note needs to be made that since the propeller used in this thesis was not completely covered in any figure in terms of pitch to propeller diameter ratio (P/D_P), two curves for each of the coefficients C_T^* and C_Q^* were calculated, one for the pitch to propeller diameter ratio (P/D_P) which was next largest to the one used and one for the previous smallest. The requested C_T^* and C_Q^* values were gained via interpolation.

Finally, by implementing the known C_T^* and C_Q^* to equations (6.34) and (6.35) the calculation of the thrust and torque produced by the propeller could be completed.

We need to point out that figures such as Figure 6.2 and a method of calculating the propeller thrust and torque coefficients based on the advance coefficient J do exist. More specifically, there is a polynomial method from the works of Oosterveld and Oossanen [46] which utilizes the geometric characteristics of the propeller and the advance coefficient J for the indirect calculation of these coefficients but it was rejected as not safe due to its infinite value problem.

All equations used and all methods for calculating the needed coefficients and quantities have been summed up in the end of the thesis in the "APPENDIX A': Equations Used" chapter for the comfort of the reader. Moreover, the particulars of the vessel, the propeller and the engine used in the simulation are summed up in the chapter "Simulation Specifics".

6.2.4 Propeller Inertia

A vital aspect of this thesis involved calculating the polar mass moment of inertia of the propeller which was chosen for the simulations. This was of great importance since it is used in order to estimate the engine's rotational acceleration.

The polar mass moment of inertia of a rotating object is the sum of all element masses multiplied by the square of their distance from a reference axis. For the propeller, it can be broken down into the "dry propeller" inertia I_{dry} referring to the object rotating in plain air and the "added propeller" or "entrained water" inertia I_E referring to the object immersed and rotating in water taking into consideration the effects of the water's interaction on its inertial characteristics.

The simplest way in order to estimate the propeller's inertia would be to import the characteristics of the propeller to an appropriate program and use the results from its calculations. However, for research purposes and for future references it was decided that a more detailed and "clear" method should be applied.

All the necessary data needed to run the corresponding calculations and equations were taken from the particulars of the propeller or were estimated by using already confirmed methods and results by previous researchers [33, 34, 35, 36].

Dry propeller inertia

For the dry propeller inertia, the method suggested by Carlton [7] and also used by Mournianakis [47] was implemented. This method included a series of Simpson integrations and some Steiner axis transfers. The procedure can be applied to any propeller with the restriction that the researcher has into his possession information about the blade sections.

To start with, drawings of the blade sections were acquired and thickness measurements were made according to Figure 6.3 below.

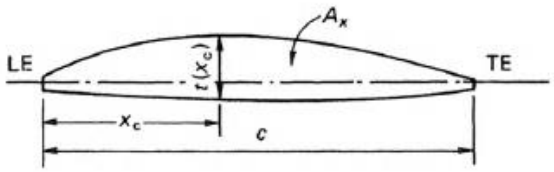

x_c	$t(x_c)$	Simp. mult. (SM)	SM × $t(x_c)$
0.0	t_{LE}	1/2	$t_{LE}/2$
0.1	$t_{0.1c}$	2	$2t_{0.1c}$
0.2	$t_{0.2c}$	1	$t_{0.2c}$
0.3	$t_{0.3c}$	2	$2t_{0.3c}$
•	•	•	•
•	•	•	•
0.9	$t_{0.9c}$	2	$2t_{0.9c}$
1.0	t_{TE}	1/2	$t_{TE/2}$
		Σ_0	

Figure 6.3: Blade thickness measurements **[7]**

Each blade is divided in an odd number of blade sections, given as a percentage of the propeller's radius. For this thesis, the data required the blades to be divided in 9 sections ranging from 0.2 to 1 ($x = r/R$) since the first 20% of the propeller radius is practically occupied by the hub and dealt with as a separate component. Each blade section is then divided in 11 vertical sections x_c (intervals of 0.1· c) and for each vertical section the thickness $t(x_c)$ is measured. In addition, each thickness is multiplied by the Simpson multiplier and then the sum Σ_0 is calculated. For each blade section with a cord length c, the total area A_x is calculated according to Simpson from equation (6.38):

$$A_x = \frac{0.2 \cdot c \cdot \Sigma_0}{3} \tag{6.38}$$

Consequently, when a total area A_x is calculated for all the blade sections, the Simpson integration is applied according to the table in Figure 6.4 below:

x=r/R	A_x	Simpson Multipliers	$A_x \cdot SM$	1st moment arm	$A_x \cdot SM \cdot$ 1st MA	2st moment arm	$A_x \cdot SM \cdot$ 1st MA $\cdot$ 2nd MA
[1]	[2]	[3]	[4] =[2]·[3]	[5]	[6] =[5]·[4]	[7]	[8] =[7]·[6]
1.0	A_{x1}	0.5	$0.5 \cdot A_{x1}$	0	0	0	0
x_2	A_{x2}	2	$2 \cdot A_{x2}$	1	$2 \cdot A_{x2}$	1	$2 \cdot A_{x2}$
x_3	A_{x3}	1	A_{x3}	2	$2 \cdot A_{x3}$	2	$4 \cdot A_{x3}$
x_4	A_{x4}	2	$2 \cdot A_{x4}$	3	$6 \cdot A_{x4}$	3	$18 \cdot A_{x4}$
x_5	A_{x5}	1	A_{x5}	4	$4 \cdot A_{x5}$	4	$16 \cdot A_{x5}$
x_6	A_{x6}	2	$2 \cdot A_{x6}$	5	$10 \cdot A_{x6}$	5	$50 \cdot A_{x6}$
x_7	A_{x7}	1	A_{x7}	6	$6 \cdot A_{x7}$	6	$36 \cdot A_{x7}$
x_8	A_{x8}	2	$2 \cdot A_{x8}$	7	$14 \cdot A_{x8}$	7	$98 \cdot A_{x8}$
x_9	A_{x9}	0.5	$0.5 \cdot A_{x9}$	8	$4 \cdot A_{x9}$	8	$32 \cdot A_{x9}$
			Σ_1		Σ_2		Σ_3

Figure 6.4: Simpson Integration **[7]**

More specifically, this integration produces three sums, Σ_1 , Σ_2 , Σ_3 which are used in the following equations, derived from Carlton [7] and modified for this thesis's needs:

$$l_{ct_{tip}} = \frac{\Sigma_2}{\Sigma_1} \cdot \frac{D_P/_2 - r_h}{8} \tag{6.39}$$

$$l_{ct_{shaft}} = D_P/_2 - l_{ct_{tip}} \tag{6.40}$$

Equation (6.39) calculates the distance of the centroid of the blade from the tip of the blade while equation (6.40) calculates the distance of the centroid of the blade from the shaft. In these equations, D_P [m] stands for the propeller diameter while r_h [m] stands for the radius of the propeller hub at its middle.

In succession, the volume inertia of each propeller blade can be estimated about the propeller tip through equation (6.41):

$$I_{tip} = \frac{2}{3} \cdot \left(\frac{D_P/_2 - r_h}{8} \right)^3 \cdot \Sigma_3 \tag{6.41}$$

This volume inertia of the blade is estimated about the propeller tip so two Steiner theorems are necessary in order to transfer the calculated inertia, first to the centroid of the blade and then to the shaft. Equation (6.42) shows the mathematical procedure:

$$I_{blade} = \rho_P \cdot \left\{ I_{tip} - {l_{ct_{tip}}}^2 \cdot \left(\frac{D_P/_2 - r_h}{8} \cdot \frac{2}{3} \cdot \Sigma_1 \right) + {l_{ct_{shaft}}}^2 \cdot \left(\frac{D_P/_2 - r_h}{8} \cdot \frac{2}{3} \cdot \Sigma_1 \right) \right\} \tag{6.42}$$

This equation can be rewritten as below:

$$I_{blade} = \rho_P \cdot \left\{ I_{tip} - \left(\frac{D_P/_2 - r_h}{8} \cdot \frac{2}{3} \cdot \Sigma_1 \right) \cdot ({l_{ct_{tip}}}^2 - {l_{ct_{shaft}}}^2) \right\} \tag{6.43}$$

At this point we must mention that Carlton [7] has an error in his respective equations by forgetting the denominator "8" or in his case the denominator "10". This denominator in equation (6.39), (6.41) , (6.42) and (6.43) derives from the fact that each blade is divided in 9 sections and thus 8 intervals. Moreover, ρ_P [kg/m^3] refers to the density of the material of the propeller and is used in order to segue from volume inertia units [m^5] to mass inertia units [kg·m^2].

Lastly, we must take into consideration the inertia of the hub. According to literature [48] the hub of the propeller chosen has at its middle a diameter equal to $0.167 \cdot D_P$. Taking into consideration the fact that the hub is a truncated cone then the polar mass moment of inertia of the hub is equal to:

$$I_{hub} = \frac{3}{10} \cdot \frac{{r_{h1}}^5 - {r_{h2}}^5}{{r_{h1}}^3 - {r_{h2}}^3} \cdot V_{hub} \cdot \rho_P \tag{6.44}$$

Where:

$$V_{hub} = \frac{\pi}{3} \cdot ({r_{h1}}^2 + {r_{h2}}^2 + r_{h1} \cdot r_{h2}) \cdot l_{hub} \tag{6.45}$$

On the above equations, V_{hub} [m^3] refers to the volume of the truncated cone, l_{hub} [m] refers to its height, r_{h1} [m] is the radius of the base of the truncated cone and r_{h2} [m] is the radius of its peak. These were estimated by using as a reference the radius of the cone in its middle r_h.

In conclusion, the dry polar moment of inertia of the propeller is equal to:

$$I_{dry} = I_{hub} + Z \cdot I_{blade} \tag{6.46}$$

Where Z is the number of blades of the propeller.

Water Entrained Propeller Inertia

As mentioned above, when the propeller is rotating in water instead of plain air, its inertial characteristics are affected. More specifically, the total polar mass moment of inertia is increased. However, in contrast to the dry propeller inertia which can be calculated with mathematical precision, the added propeller inertia is a more complicated hydrodynamic problem.

The most efficient way to estimate the added propeller inertia would be using empirical equations. Burrill, Parson and Schwanecke [49] have each produced such equations but in this thesis, Schwanecke's equation was deemed more precise. More specifically, according to Schwanecke:

$$I_E = C_{IE} \cdot \rho \cdot {D_P}^5 \tag{6.47}$$

Where ρ [kg/m^3] is the sea water density and C_{IE} is a coefficient equal to:

$$C_{IE} = \frac{0.0703 \cdot \left({P}/{D_P}\right) \cdot EAR^2}{\pi \cdot Z} \tag{6.48}$$

In equation (6.48), (P/D_P) is the pitch to propeller diameter ratio and EAR is the expanded area ratio of the propeller.

Total Inertia of Propeller

In conclusion, having calculated the dry and the added propeller inertia, the total inertia of the propeller is:

$$I_{propeller} = I_{dry} + I_E \tag{6.49}$$

This method of calculating a propeller's inertia was tested on an existent propeller whose inertia characteristics were known in order to validate its effectiveness. The results derived were very satisfying since they were really close to the real values proving that this method can be safely applied to the problem researched by this thesis.

All equations used and all methods for calculating the needed coefficients and quantities have been summed up in the end of the thesis in the "APPENDIX A': Equations Used" chapter for the comfort of the reader. Moreover, the particulars of the vessel, the propeller and the engine used for the simulation are summed up in the chapter "Simulation Specifics".

6.2.5 Shaft-Propeller Dynamics

A crucial part of this thesis necessitates computing the acceleration of the engine's rotational speed. More specifically, for any rotating object, its angular acceleration can be estimated by applying the momentum equation:

$$\frac{d\omega}{dt} = \frac{\sum Q_i}{I_{total}} \tag{6.50}$$

At the numerator is the total summation of the torque values produced and absorbed due to the engine's operation while at the denominator is the total inertia taking into account every attached mass. In our case, the combustion in the cylinders which are mechanically connected to the crankshaft produces torque while the propeller which is also mechanically connected to the crankshaft absorbs torque. Moreover, the total inertia consists of the inertia of the engine (which includes the crankshaft and the cylinders) and the inertia of the propeller. The inertia and torque which pertain to the engine are calculated in MOTHER [6] while the ones which have to do with the propeller need to be mathematically computed.

Taking into consideration the fact that the angular velocity ω equals to $\omega = 2 \cdot \pi \cdot \frac{n}{60}$ where n is the engine rotational speed in rounds per minute [rpm] then equation (6.50) can be rewritten as follows:

$$\dot{n} = \frac{dn}{dt} = \frac{30 \cdot \sum Q_i}{\pi \cdot I_{total}} \tag{6.51}$$

The new rotational speed n_{new} of the engine after a time period dt can be calculated using equation (6.52):

$$n_{new} = n_{old} + \dot{n} \cdot dt \tag{6.52}$$

This calculation is automatically executed by the Speed Governor.

6.2.6 Speed Governor

The speed governor is a device which is used to maintain the engine speed steady around a specific speed setpoint in the operation region. More specifically, its function does not include increasing or decreasing the engine speed (which is achieved via the fuel injection system) but instead, once the desired speed is achieved, keep it stabilized despite the changes in the engine load.

This operation is of great importance especially in transient conditions or heavy weather conditions where, if the engine speed is not steady, damage to the propeller might occur. For instance due to propeller emergence. Moreover, in the absence of a speed governor the engine speed would increase or decrease uncontrollably causing a series of problems.

In the case of our engine, a hydraulic governor [50] was used and is explained in order to gain a basic understanding of its operation. A typical hydraulic speed governor from a simplistic view is composed by a “ballhead spring”, a set of flyweights and an oil supply system as shown in Figure 6.5 below.

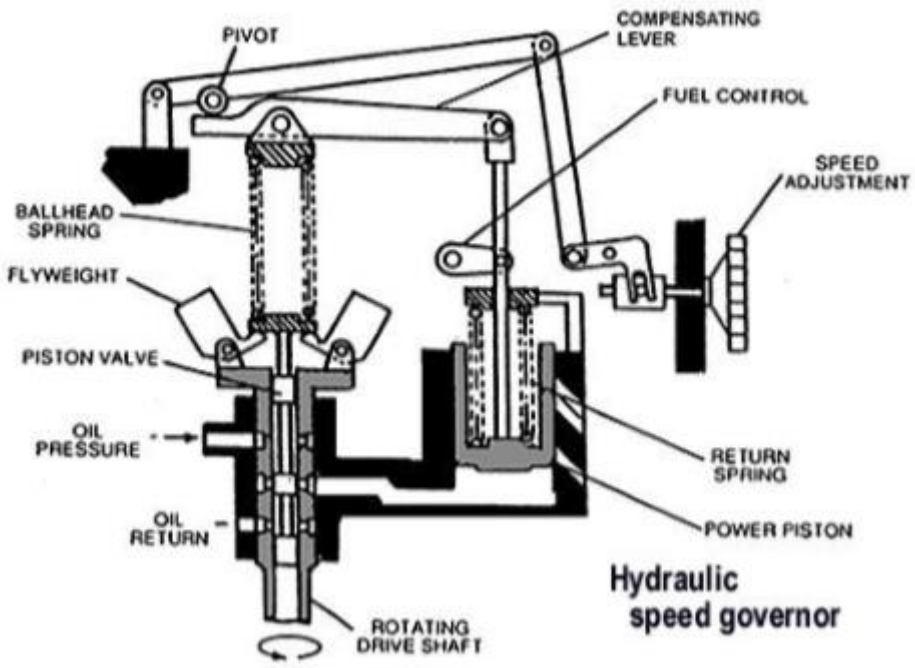

Figure 6.5: Hydraulic Governor **[50]**

Its operation is based on centrifugal forces acting on rotating bodies which in turn control the flow of an amount of pressurized oil. The engine drives the governor.

Under normal conditions, the forces produced from the rotating flyweights are balanced by the vertical force from the ballhead spring and thus the piston valve remains stationary. In case of an increase in the engine load and thus a decrease in the speed, the flyweights tend to move inwards and the ballhead spring tends to move the piston valve downwards. This enables pressurized oil to

be admitted under a power piston which is pushed upwards and in succession moves the fuel control towards more fuel. The movement of the piston also compresses the return spring and a compensating lever which will decrease the force on the ballhead spring and move the piston valve back to its neutral position. In case of a decrease in the engine load and thus an increase in the engine's rotating speed, the flyweights move outwards due to the centrifugal forces, the spring is compressed and the power piston will move downwards moving the fuel control to less fuel. The normal operating speed of the engine can be manually adjusted on the speed adjustment wheel.

Other types of governors also exist and are very popular such as the pneumatic governor which functions on the vacuum created by moving air and the electronic governor which completes the whole process electronically by monitoring electric signals.

In our case where transient conditions are to be studied the speed governor is an essential part of the simulations. Transient conditions with an ungoverned diesel engine cannot converge unless active control is imposed on the fuel mass injected in the cylinders per cycle. This active control is achieved via the speed governor which stabilizes the engine speed around a speed setpoint specified by the user. Consequently, the modeling of a speed governor is vital in order to conduct transient simulations.

The major principle behind its function would be the negative feedback from the engine crankshaft speed or the propeller shaft speed. This method improves the robustness of the system and its performance insensitivity to parameter variations. Moreover, it improves the system's stability and allows for a set of specifications to be met. A simple figure is shown below describing the aforementioned principle.

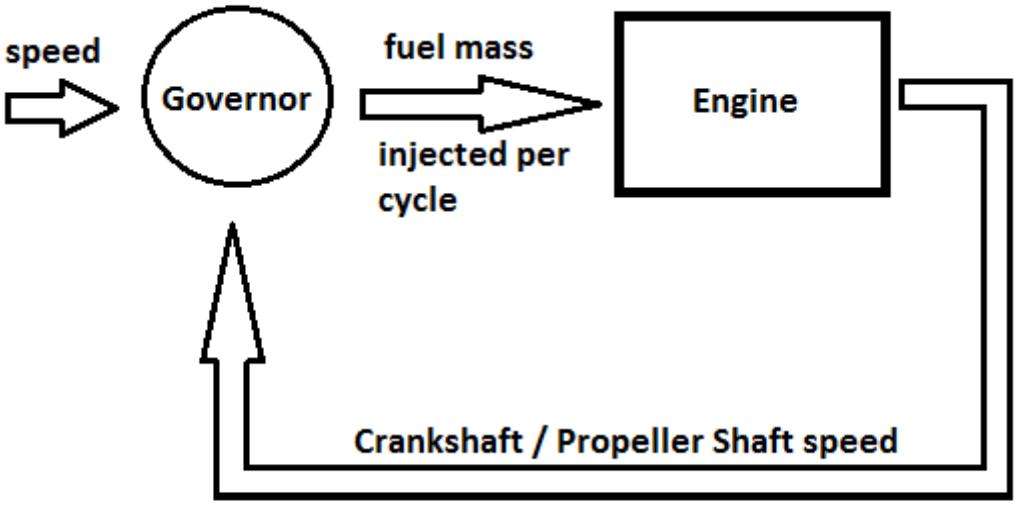

Figure 6.6: Governor Figure

In the engine simulation program MOTHER, the governor includes a PID controller whose output is the fuel index position. The fuel index position directly affects the fuel mass injected in the cylinders per cycle. The relation between the fuel index and the fuel mass injected is accomplished through control laws for each cylinder which are defined by the user.

The output of the PID controller is given by the following Laplace equations in the space domain (s) and in the time domain (t):

In s-domain: $$x(s) = K \cdot \{K_P \cdot e(s) + {K_I}/{s} \cdot e(s) + K_D \cdot s \cdot e(s)\} \quad (6.53)$$

In t-domain: $$x(t) = K \cdot \{K_P \cdot e(t) + K_I \cdot \int_{t_0}^{t} e(\chi) \cdot d\chi + K_D \cdot \frac{d}{dt} e(t)\} \quad (6.54)$$

In these equations e is the speed error defined as:

$$e(t) = N_{ord}(t) - N(t) \quad (6.55)$$

Where $N_{ord}(t)$ is the speed setpoint and $N(t)$ is the actual engine speed.

Furthermore, x is the fuel index position which takes values between 0 and 1. In addition, the parameters K, K_P, K_I and K_D are used for the tuning of the PID controller and can be generated by control laws parameterized by the speed setpoint value. There is the option for all constants (K, K_P, K_I and K_D) to have different values for decreasing or increasing speed error in order to reduce oscillation around the speed setpoint.

Moreover, MOTHER allows the user to set limiters for the governor. In particular, limiters are a set of values provided by the engine manufacturers for the fuel index position, usually parameterized as a function of one or more engine operating variables such as the scavenging pressure, the crankshaft speed, the engine torque etc. MOTHER provides the user with the option to use up to three different limiters with lower and upper limits which can be regulated by a control law. It is obvious that if the lower/upper limit of one limiter is higher/lower compared to the upper/lower limit of the next limiter in sequence then the first is deactivated. Considering the limiters used, two different limiters were available for this engine and applied in all the simulations. The first limiter was one that restricted the scavenger air pressure while the second was a torque limiter.

Finally, the governor was required to pass a tuning phase where trials were made in order to find the correct values for the constants K, K_P, K_I and $K_D$and the other parameters required by MOTHER. These values ensured that the simulations run smoothly and gave logical results.

The tuning procedure involved a series of trial runs where random initial constants were set. By using a trial and error method, these constants converged to values which gave smooth transitions and lacked sudden and intense behavior of the rotational speed.

6.3 Interaction of Models

Having fully described the models in their structure separately, it is of equal importance that we describe their interaction. More specifically, we need to establish how the models interact with each other so that a result is produced representing the acceleration capabilities of the engine.

It must be noted that most of the models described in the previous passage have been written in a FORTRAN code. This code is next fed in the engine simulation program MOTHER which executes the engine thermodynamic calculations.

Wherever an initial value for the ship's velocity or the engine's rotational speed was required it was calculated by using the Propeller Law. According to it, the power output of an engine is proportional to the third power of its rotational speed while the engine's speed itself is relative to the ship's velocity. The following equations depict the above:

$$P = k1 \cdot n^3 \tag{6.56}$$

$$V_{SHIP} = k2 \cdot n \tag{6.57}$$

In these equations, P [kW] is the power output of the engine, n [rpm] is the engine's rotational speed, V_{SHIP} [m/s] is the ship's velocity and $k1$ and $k2$ are the constants/coefficients that connect the values with each other.

To start with, in order for the propeller and ship surge model to interact, an ambient sea water temperature is defined. This is needed in order to produce the viscosity value used in the calculation of the Reynolds number. In succession, by feeding the initial ship's velocity and instantaneous rotational speed through the propeller model, the wake factor w and the advance velocity V_A are calculated and then by computing the advance angle β and calculating and utilizing the propeller coefficients C_T^* and C_Q^*, the propeller thrust T_{pr} and torque Q_{pr} are calculated. Next, through the ship surge model, by utilizing the thrust produced from above and by estimating the different resistances, the thrust deduction factor t and the displacement of the ship, we are able to calculate the acceleration of the ship $\dot{V}_{SHIP}$. Lastly, a crank angle step (CAS) is determined which is used in order to produce a time step dt with the following equation (6.58):

$$dt = \frac{CAS \cdot 60}{n \cdot 360} \tag{6.58}$$

Where n is the rotational speed of the crankshaft in rounds per minute and is constantly calculated by MOTHER.

Finally, from the ship surge model and propeller model produce a new vessel's velocity V_{SHIP_NEW} is produced for the above time step. The new velocity and the instantaneous rotational speed are used as inputs in the code and then the whole procedure is repeated for the next time period (dt).

Nevertheless, the instantaneous rotational speed of the engine, and thus its acceleration, is controlled by the Speed Governor. An initial rotational speed for the engine is set which is fed at the start of the code and corresponds to a desired load. In every cycle of the simulation the Governor takes into account the current rotational speed and torque and calculates the necessary change in its actuator's rack so that the appropriate fuel can be injected into the cylinders in order to ensure

the increase or decrease of the engine's speed. More specifically, the actuator's rack position controls the fuel index which in succession regulates the amount of the fuel injected and the crank angle at which the fuel injection takes place. In the end, the engine accelerates or decelerates producing a new engine speed which is fed in the simulation code and subjected to the aforementioned governor's processing. The whole procedure repeats itself until the desired rotational speed is succeeded.

At this point it is important to note that the inertia of the propeller is calculated in the section "Propeller Inertia" and on a separate FORTRAN code. After the execution of the equations, the inertia is inserted as an input in the engine simulation program MOTHER.

Having computed the inertia of the propeller, MOTHER estimates the rotational acceleration $\dot{n}$ as described in the section "Shaft- Propeller Dynamics". This calculates the new instantaneous rotational speed and shows how the engine's rotational speed changes during the examined time frame.

A record of the total distance [m] travelled by the vessel during the simulation is kept by using equation (6.59):

$$distance = distance_{last} + dt \cdot \frac{(V_{new} + V_{old})}{2} \tag{6.59}$$

Where $distance_{last}$ is the distance travelled during the previous time step, V_{old} is the vessel's velocity at the beginning of the time step dt and V_{new} is the vessel's velocity at the end of the time step dt.

In conclusion, the layout of the engine and the way its different components act together with the speed governor and the models is shown in the following diagram:

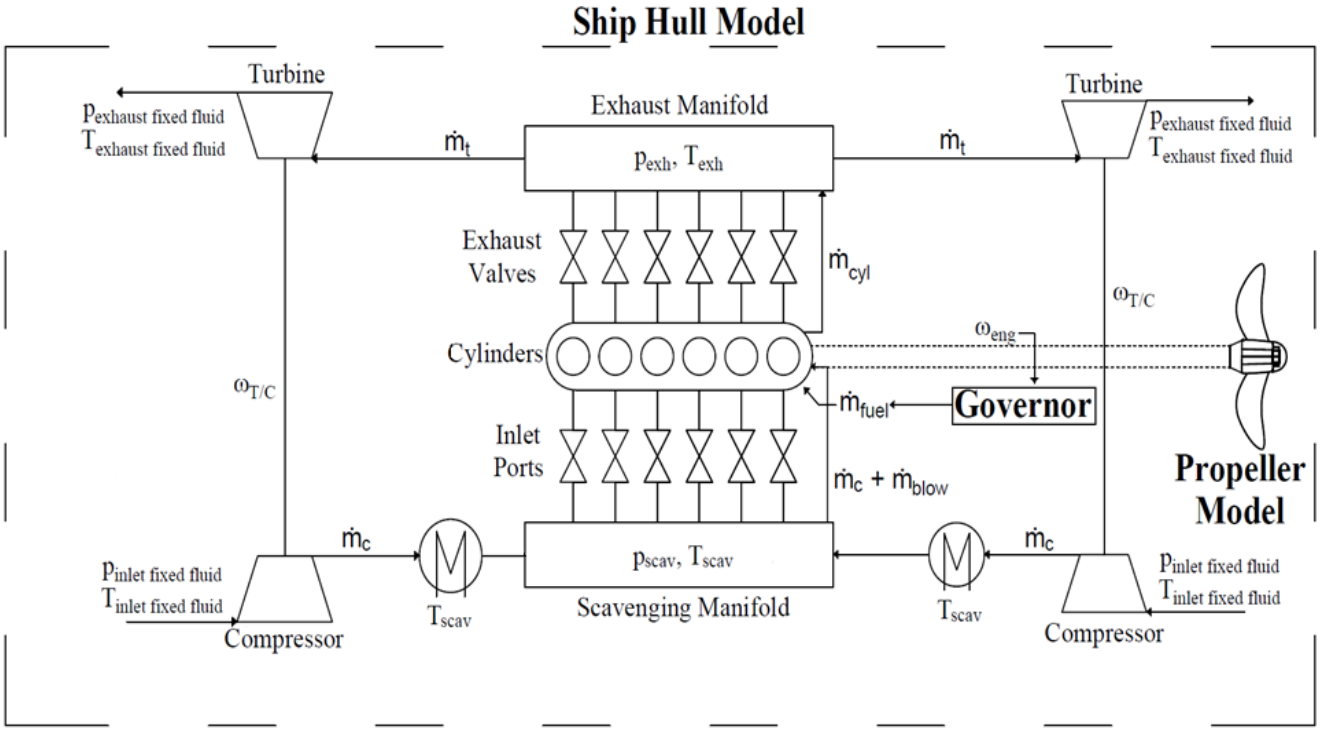

Figure 6.7: Engine components action together with speed governor and models

Chapter 7: Simulations

7.1 Simulation Specifics

In this section, the particulars of the engine, the propeller and the vessel are summarized. The models used and the simulation software MOTHER, in order to function properly, required some details on the components involved. The whole thesis revolves around the marine engine MAN B&W 6S70MC-C with the following specifications:

Table 7.1: Engine Characteristics

ENGINE CHARACTERISTICS	
Engine Model	6S70MC-C
No. of Cylinders	6
Bore	700 mm
Stroke	2800 mm
Compression Ratio (ε)	17.57
Power per Cylinder	3110 kW
Engine Speed (n_{max})	91 rpm
Firing Order	1-5-3-4-2-6
Engine Inertia	230600 kgm^2

The data required was acquired from the Project Guide of the engine. The total inertia of the engine was taken from the similar WIN-GD engine W6X72 using the program GTD [51]. Having specified the engine, a short survey was carried out in order to find a fitting vessel which could house it. The results produced a Tanker vessel whose sea trials possessed the following specifications:

Table 7.2: Vessel Characteristics

VESSEL CHARACTERISTICS	
Length Between Perpendiculars (L_{BP})	264.00 m
Breadth (B)	48.00 m
Mean Draught (T)	15.985 m
For Peak Draught (T_f)	15.871 m

Aft Peak Draught (T_a)	16.085 m
Depth (D)	23.10 m
Deadweight (DWT)	169797.50 t

Other specifications such as the hull coefficients (C_B, C_M, C_P and C_{WP}), the wetted surface (S) and longitudinal center of buoyancy (LCB) were calculated using equations derived from the bibliography [33, 34, 35, 36] and are summarized in the section "APPENDIX A': Equations Used". Others such as the immersed surface of transom (A_T) or the wetted appendages' surface (S_{APP}) were calculated in comparison with other vessels of similar size.

In addition, having specified the hull and the engine, a similar survey was conducted for an according propeller. Finally, the propeller which was used had the following particulars:

Table 7.3: Propeller Characteristics

PROPELLER CHARACTERISTICS	
Model	B4-70
Type	Wageningen B-Series
No. of Blades (Z)	4
Diameter (D_P)	8.15 m
Pitch (P)	6.00 m
Expanded Area Ratio (EAR)	0.70
Pitch – Diameter Ratio (P/D_P)	0.7362
Propeller Material Density (ρ_P)	7600 kg/m^3

Other specifications which were needed such as blade measurements and the hub's length were taken from the according propeller documents. The material of the propeller selected was estimated to be of a copper based alloy with nickel and aluminum [7].

All things considered, the ambient conditions which were taken into account were the following:

Table 7.4: Ambient Conditions

AMBIENT CONDITIONS	
Air Temperature	25 ^{o}C
Air Pressure	1 bar

Sea Water Temperature	9 ^{o}C
Sea Water Density	1025 kg/m^3
Gravitational Acceleration	9.80665 kg/sec^2

Finally the viscosity of the sea water in [m^2/sec] was estimated utilizing the ITTC Recommended Procedures 1978 [52] equation (7.1):

$$v = \left((0.659 \cdot 10^{-3} \cdot (T_{amb} - 1.0) - 0.05076) \cdot (T_{amb} - 1.0) + 1.7688\right) \cdot 10^{-6} \quad (7.1)$$

Where T_{amb} is the sea water temperature in [^{o}C].

Finally, the BSR of the engine was estimated to be around 20-30% of the engine's maximum load.

7.2 Simulation Runs

In the previous chapters, a passage explaining the basic theory behind marine engineering, the Barred Speed Range, its mechanisms and the systems which were used was presented. Moreover, the different models used were explained as well as the basics behind the engine simulation code MOTHER. Nonetheless, it is very important to also describe the procedure which was followed during the simulations and how the different systems were applied and adjusted for each trial.

For all of the trials the simulation procedure followed the same basic steps. First of all, the engine was tuned so that each scenario was represented by the correct adjustments of the engine parameters. For instance, a VCR trial would have the compression ratio for all the cylinders altered to its appropriate value while a VVT trial would have the exhaust valves' closing or opening timing adjusted.

In addition, since the BSR of the engine was estimated around 20-30% of the engine's maximum load, the simulations started with the engine operating at 20% of its maximum load where it remained for some time so that all of its parameters converged and stabilized. Once sufficient time had passed, the engine was ordered via the governor to accelerate at 50% of its maximum load. Once the engine had finished accelerated and started to decelerate and equilibrate, the simulation was ended since only the period of the acceleration was of importance for this thesis.

The period during which the acceleration took place was monitored and all useful engine data was collected and analyzed so that different conclusions could be made considering the effect of the different systems and methods applied during the trials.

7.2.1 Application of VIT

Regarding the Variable Injection Timing trials, MOTHER gives the option to alter a parameter called VIT Index. This parameter controls the start of the fuel injection, and more specifically the crank angle at which the injection takes place, via a specific control law. The VIT Index was controlled via the fuel index of the engine and in succession the VIT index controlled the crank angle where the fuel injection took place. A higher value of VIT Index is associated with an injection that takes place earlier while a lower VIT Index means a delayed injection. Since an advanced injection increases the in-cylinder pressures, the power and acceleration were expected to increase due to the increased produced work.

Following this mentality, the cases which were tested included advancing the start of injection (SOI) by:

- -2.0 degrees (SOI)
- -5.0 degrees (SOI)
- -10.0 degrees (SOI)
- -15.0 degrees (SOI)

In reality, both -10.0 degrees and -15.0 degrees cases are inapplicable but were nevertheless examined for research purposes.

7.2.2 Application of VCR

MOTHER also offers the option to change the compression ratio in each cylinder of the engine. The user may directly specify either the desired compression ratio or the desired clearance volume while MOTHER automatically computes the equivalent value of the remaining parameter.

According to the bibliography, the VCR system was used in a 6-cylindered two stroke marine engine [32] and it was observed that an increase to the piston's projection of up to 100mm was followed by an increase of up to 50% in the compression ratio. An increase of the compression ratio is associated with an increase of the pressures inside the cylinders which should affect the engine's acceleration and power. Moreover, an increase in the efficiency of the engine is expected. However, the VCR cannot be used uncontrollably to increase the compression ratio and the engine's acceleration capability due to the fact that there are specific pressure thresholds which must not be exceeded since they might damage the engine.

According to that research, in the scenarios tested, this thesis investigated the cases of:

- +10% compression ratio (ε)
- +20% compression ratio (ε)
- +30% compression ratio (ε)

7.2.3 Application of VVT

In MOTHER, for each cylinder configuration, the user is given the option to not only specify geometrical settings such as its bore, phase angle, connection rod length etc., but also its more advanced in-cylinder parameters such as friction and thermal coefficients, injection timings and combustion settings. This also includes, for each cylinder, the option to intervene to the exhaust valve timing.

The EVO (exhaust valve opening) and EVC (exhaust valve closing) of the engine's exhaust valve were alerted in order to assess the effect of advanced or delayed EVO and EVC on the engine's acceleration. The cases that were investigated are listed below:

- -2.5 degrees in Valve Closing / -5.0 degrees in Valve Closing / -7.5 degrees in Valve Closing / -10.0 degrees in Valve Closing
- +2.5 degrees in Valve Closing / +5.0 degrees in Valve Closing / +7.5 degrees in Valve Closing / +10.0 degrees in Valve Closing
- -2.5 degrees in Valve Opening / -5.0 degrees in Valve Opening / -7.5 degrees in Valve Opening / -10.0 degrees in Valve Opening
- +2.5 degrees in Valve Opening / +5.0 degrees in Valve Opening / +7.5 degrees in Valve Opening / +10.0 degrees in Valve Opening

In general, we expected an early EVO to produce hotter exhaust gas but fall short in terms of work while, on the opposite, a delayed EVO will produce increased work but also exhaust gas with a lower temperature. On the other hand, an early EVC should show improved compression and work accompanied by reduced scavenging while a delayed EVC should show improved scavenging and reduced compression and, thus, work.

7.2.4 Application of increased Fuel

The effect of increased fuel mass injection on the acceleration capabilities of the engine was also investigated. Therefore, a set of simulations was executed were the fuel injected was increased by 30% compared to the initial values. In MOTHER this can be achieved by altering the control law that links the mass of the fuel injected with the fuel index of the fuel pumps.

The combination of enhanced fuel with other methods referred above was examined. The simulations were one VIT scenario, one VCR scenario and one set of VVT scenarios picked from the above, with the difference that the control law which controlled the fuel injected was enhanced by 30%. The scenarios chosen were:

- -10 degrees in the start of injection (VIT scenario)
- +20% compression ratio (VCR scenario)
- -10 degrees in Valve Closing / +10 degrees in Valve Closing / -10 degrees in Valve Opening / +10 degrees in Valve Opening (VVT scenario)

7.2.5 Application of increased Air Mass Flow

Lastly, another option which was examined was the increase of the mass of the air flowing in the cylinders. This could be achieved via a plethora of ways.

The amount of air entering the cylinders is directly dependent to the Turbocharger. One option would be to modify the compressor performance maps in order to supply more air at the given conditions. However, it was decided to modify the turboshaft's polar moment of inertia. This would cause the Turbocharger to accelerate faster and thus increase the mass flow of the air inside each cylinder. For the purposes of this thesis, the Turbocharger's inertia was reduced by 20 times.

The simulations performed were the same as in the case of the "enhanced fuel": one VIT scenario, one VCR scenario and one set of VVT scenarios picked from the above, with the only difference that the Turbocharger's inertia was 20 times smaller. Thus, the scenarios chosen were:

- -10 degrees in the start of injection (VIT scenario)
- +20% compression ratio (VCR scenario)
- -10 degrees in Valve Closing / +10 degrees in Valve Closing / -10 degrees in Valve Opening / +10 degrees in Valve Opening (VVT scenario)

Chapter 8: Results

In this section, the results of the simulations are presented. As mentioned before, there were five groups of simulations (VIT, VVT, VCR, enhanced fuel and enhanced air mass flow scenarios) depending on the different systems and conditions that were applied at each run. Each one of these groups is characterized by changes at only one of the aforementioned systems at a time and is analyzed in its according passage, accompanied by its respectful figures.

We need to note that the Governor settings remained unchanged between each simulation. Obviously, altering the PID controller and making it more or less rigid would have a direct effect on the acceleration of the engine. However, this thesis concentrated on the effect that specific parameters had on the acceleration capabilities of the engine and did not strive to find different ways to improve it.

8.1 Variable Injection Timing Simulations (VIT)

For this group of simulations, the effect of the injection timing was investigated. The control parameter was the VIT Index which controlled the start of injection (SOI) timing. The control law between the VIT Index and SOI was altered by advancing the SOI by 2.0, 5.0, 10.0 and 15.0 degrees while the rest of the engine parameters remained unchanged.

Once again, we need to note that the 10.0 degrees and 15.0 degrees scenarios are not applicable in reality but nevertheless they were examined for the purposes of more complete simulations and research.

The changes were implemented on all cylinders simultaneously so that they operated in unison.

In the figures below, the rotational speed of the engine and the power produced are depicted for the four scenarios mentioned above and are compared to the respectful ones of the “initial” engine operation where no changes were made and the engine operated at its default settings.

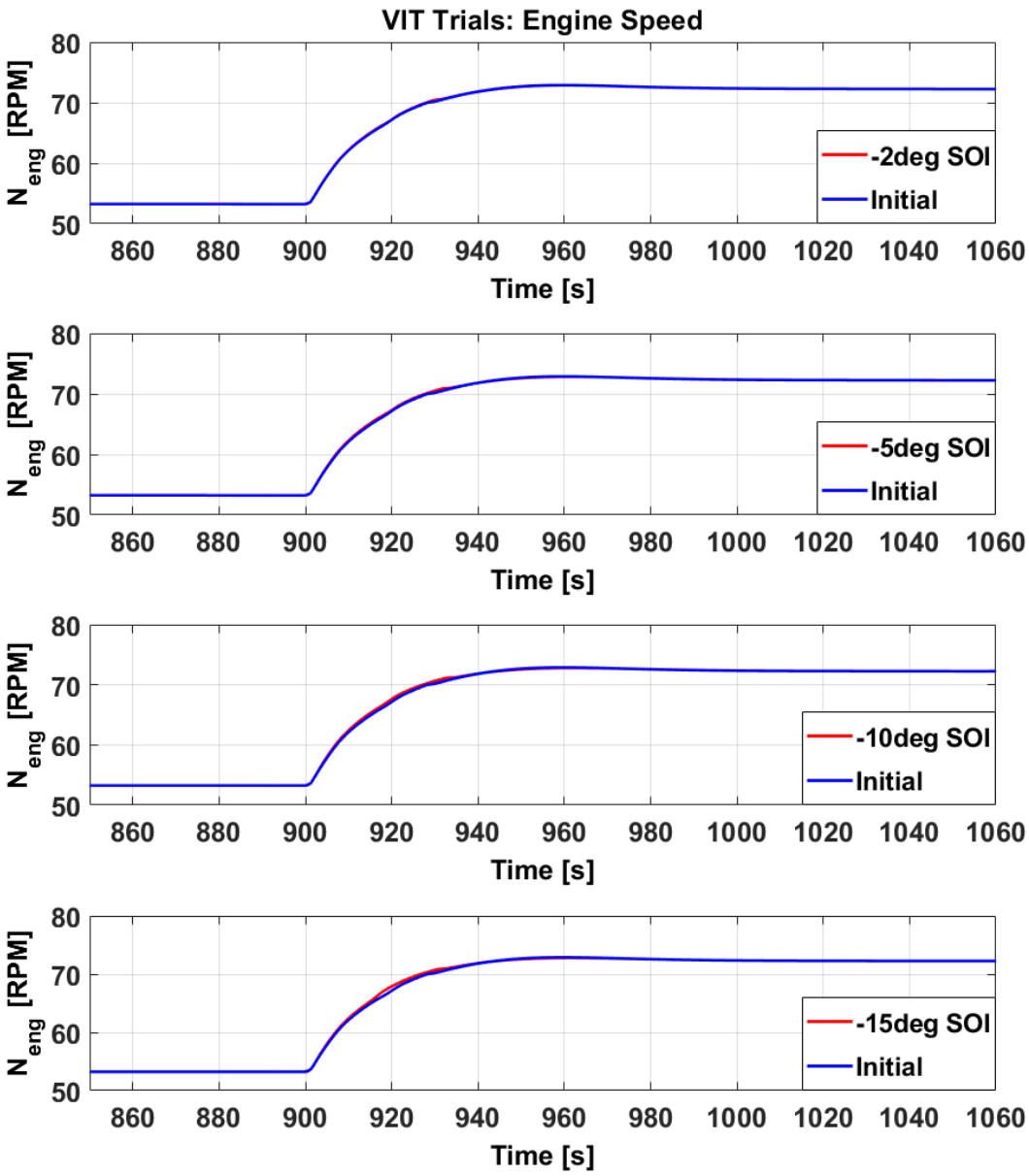

Figure 8.1: Engine Speed – Variable Injection Timing -2.0 / -5.0 / -10.0 / -15.0 degrees

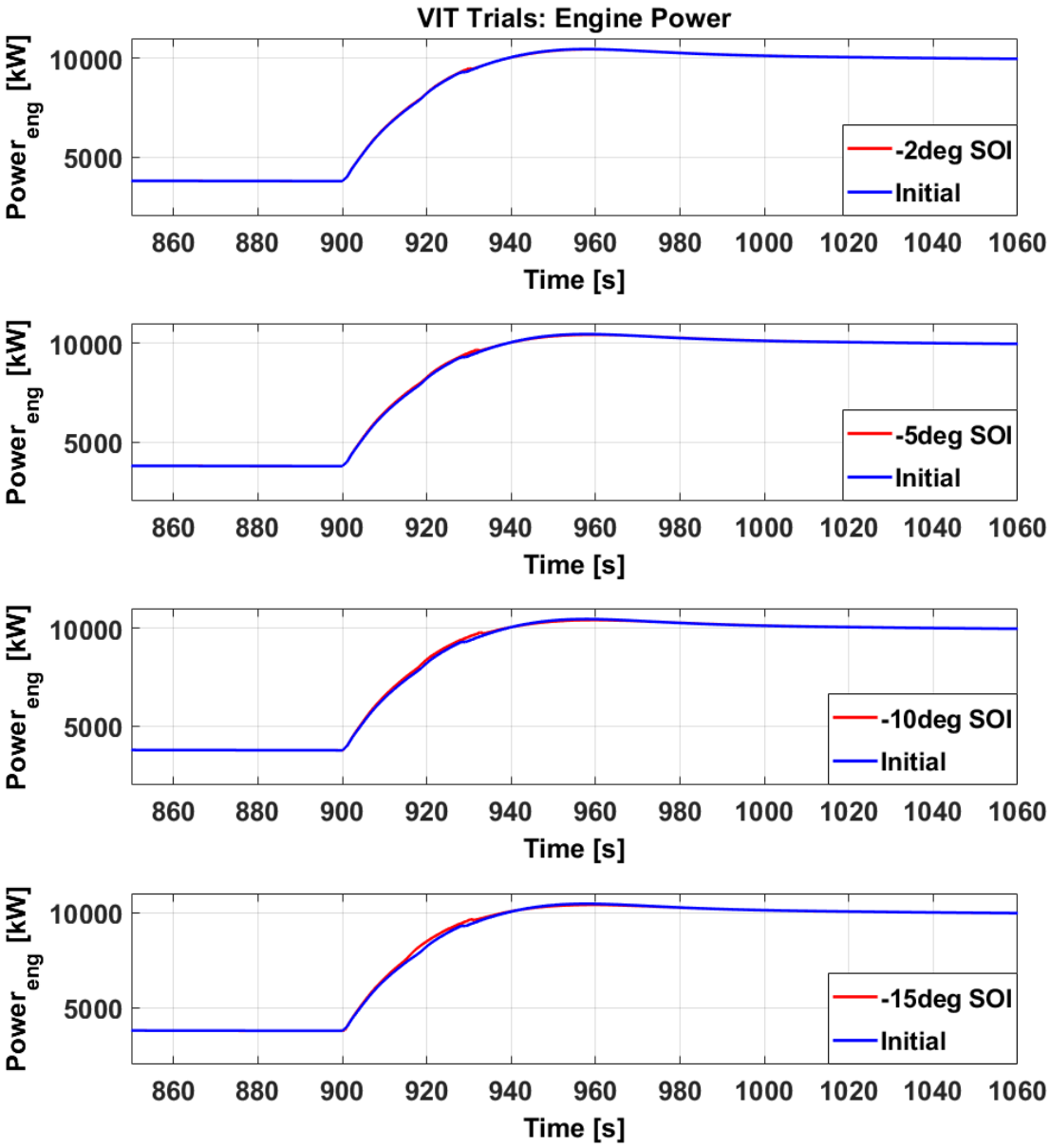

Figure 8.2: Engine Power – Variable Injection Timing -2.0 / -5.0 / -10.0 / -15.0 degrees

In the above figures it is evident that advancing the SOI has a little impact in the acceleration and power output of the engine on the specific load region. However, small changes can be observed between each scenario and it appears that both acceleration and power output of the engine have increased, even by a small fraction. The engine accelerates slightly faster while also producing slightly increased power.

Considering the in-cylinder pressures, by advancing the SOI it was observed that the maximum pressure was increased at each run, confirming the theory behind an advanced injection. Furthermore, the earlier the injection took place, the larger this increase was and, in succession, there was a larger impact on the engine's work and, hence, acceleration and power. The increased pressures led to increased work produced during these simulations. For low values it was moderately increased while for larger advancements the increase was significantly magnified. Nonetheless, the friction losses which are linked to the engine rotational speed and maximum pressure and the losses due to heat transfer were likewise increased. Furthermore, both the wasted power in the exhaust gas and the power lost due to air cooling showed a decrease for small values of fuel advancement while for values higher than 10.0 degrees these losses started to increase. This explains why, even though the engine produces more work and higher pressures, there is a small change in the acceleration of the engine since, despite the small increase in power, the major part of the extra work is expended in increased losses.

Consequently, this introduces a threshold on the degrees that the SOI can be advanced after which the engine accelerates faster but has significantly increased pressures and losses. Hence, while in the 2.0 degree scenario the effect of the VIT is barely visible compared to the initial operation, as the injection is advanced, its effects are intensified and tend to become clearer.

Nonetheless, we need to note that this method cannot be used unrestrictedly since the earlier the injection, the higher the increase in the maximum pressure which, after a specific threshold, may compromise the integrity of the engine. For instance, in the case of 10.0 degrees advance, the pressures have increased significantly compared to the 5.0 degrees scenario while in the 15.0 degrees scenario they have almost doubled compared to the initial state.

Moreover, it was observed that the Turbocharger speed gradually fell as the fuel advancement was increased. However, this reduction was gradually smaller while advancing the SOI and finally it was observed that in the 15.0 degrees scenario the Turbocharger speed had started to increase. This behavior can be attributed to the wasted power in the exhaust gas. Since for the smaller values of advancement the wasted power was lower, the Turbocharger faced weaker gasses which meant its speed reduction. On the contrary, as the fuel advancement was increased so did the wasted power in the exhaust gas and, thus, the Turbocharger started to accelerate.

A similar behavior was observed in the pressure and temperature of the scavenger and exhaust receivers which are linked to the Turbocharger's speed. An increase in its speed meant an increase in the exhaust and scavenger pressure, more air inserted and thus a decrease in the exhaust and scavenger temperature due to the additional air's cooling capabilities. Also, since the air mass flow was similarly affected, the behavior of the losses due to the air cooling is explained. Of course, the deceleration of the Turbocharger had the opposite effect.

Lastly, during the acceleration, the specific fuel consumption (SFOC) for the 2.0 and 5.0 degrees scenarios tended to decrease slightly as the fuel advancement was increased. In succession, for the 10.0 and 15.0 degrees scenarios, the SFOC started to significantly increase. This phenomenon can be explained by the sudden increase of the different losses observed in this angle range and mainly of the heat transfer losses. For small advancements the total losses were slightly dropping as a percentage of the total work produced which led to increased engine efficiency. On the other hand, for larger advancements the increasing total losses were also increasing percentagewise and thus the reduced engine's efficiency.

8.2 Variable Compression Ratio Simulations (VCR)

In this group of simulations the effect the compression ratio had on the acceleration capabilities and power output of the engine was examined. Consequently, the parameter that controlled these simulations was the compression ratio in each cylinder and more specifically their clearance volume. To be more precise, the clearance volume was reduced to different values in order to achieve an increase in the compression ratio (ε) by 10%, 20% and 30% while the rest of the engine parameters remained unchanged. This increase was applied to the default compression ratio given by the manufacturers.

The changes were implemented on all cylinders simultaneously so that they operated in unison.

In the figures below, the rotational speed of the engine and the power produced are depicted for the three scenarios mentioned above and are compared to the respectful ones of the "initial" engine operation where no changes were made and the engine operated at its default settings.

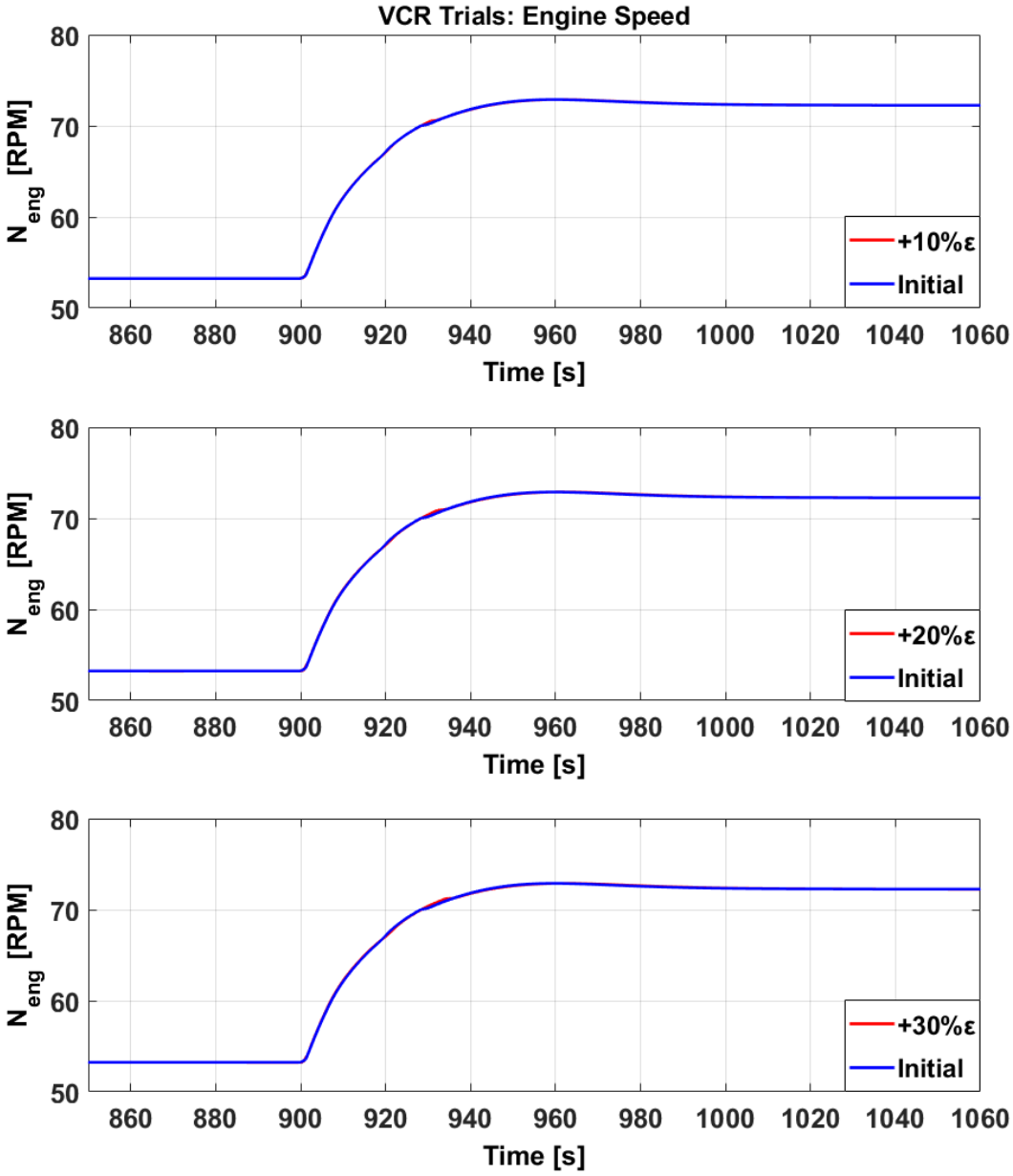

Figure 8.3: Engine Speed – Variable Compression Ratio +10% / +20% / +30% ε

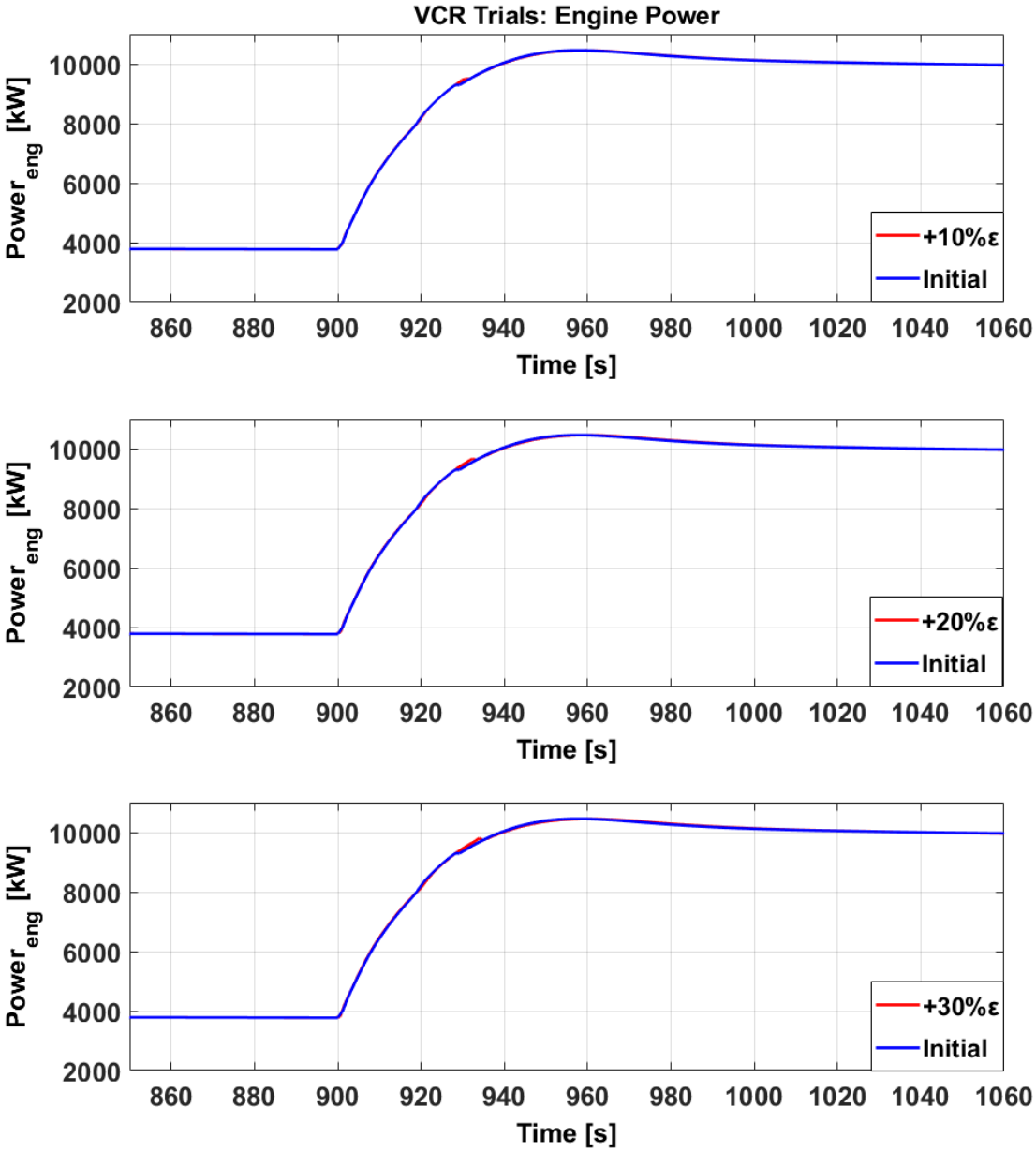

Figure 8.4: Engine Power – Variable Compression Ratio +10% / +20% / +30% ε

During these simulations, it can be observed that the increase of the compression ratio had a trivial effect on the acceleration capabilities and power output of the engine. Even though while increasing the compression ratio the speed and power curves tended to become a little clearer, still, they did not differentiate substantially as to the corresponding curves from the initial state of the engine. This means that the VCR affects little the acceleration capabilities and power output of the engine on the specific load region.

Nonetheless, as anticipated according to theory, while increasing the compression ratio there was a small but steady increase in both the compression pressure and the maximum pressure inside the cylinders. This was also accompanied by a steady but small increase in the total work produced which was also accompanied by slightly reduced total losses. In total, the work gained and the total losses came to leave some very little extra power for acceleration.

More specifically, with larger increases in the compression ratio it was observed that the wasted power in the exhaust gas was steadily decreasing while the power wasted on heat transfer was slightly increasing. The friction losses tended to slightly increase due to the small acceleration that took place and the increase in the in-cylinder pressures. What is more, the power lost due to air cooling was steadily decreasing due to the steady decrease in the air mass flow.

However, since the total losses were percentagewise reduced, this meant a steady decrease in the SFOC of the engine that confirmed that the VCR helps improve the engine's efficiency.

Lastly, the increase of the compression ratio was followed by a small, but steady, decrease in the Turbocharger speed which is attributed to the less energy contained in the exhaust gas. In succession, lower Turbocharger speed meant a decrease in both scavenger and the exhaust pressures while the more efficient combustion produced exhaust gas with slightly lower temperature.

8.3 Variable Valve Timing Simulations (VVT)

During these simulations, the effect of changing the timing of the valves was examined. Since the simulated engine was a two stroke marine diesel engine, this meant that there were inlet ports instead of inlet valves and thus only the control of the exhaust valves was examined.

The control parameter was the crank angle that controlled the exhaust valves. More specifically, the crank angles that determined the opening or closing of the exhaust valves were increased or reduced and in succession their effect on the engine's acceleration and power was observed.

For these increases and reductions, four values were tested: ± 2.5degrees, ± 5.0 degrees, ±7.5 degrees and ±10.0 degrees. Moreover, we need to note that each increase or decrease was investigated on both cases of opening and closing of the valve. However, never was a scenario implemented where a change was concomitantly applied on both the opening and the closing crank angles of the exhaust valves.

Consequently, there were the following four scenarios with four sub scenarios each:

- Closing Earlier the Exhaust Valve (-2.5 degrees in Valve Closing / -5.0 degrees in Valve Closing / -7.5 degrees in Valve Closing / -10.0 degrees in Valve Closing)
- Closing Later the Exhaust Valve (+2.5 degrees in Valve Closing / +5.0 degrees in Valve Closing / +7.5 degrees in Valve Closing / +10.0 degrees in Valve Closing)
- Opening Earlier the Exhaust Valve (-2.5 degrees in Valve Opening / -5.0 degrees in Valve Opening / -7.5 degrees in Valve Opening / -10.0 degrees in Valve Opening)
- Opening Later the Exhaust Valve (+2.5 degrees in Valve Opening / +5.0 degrees in Valve Opening / +7.5 degrees in Valve Opening / +10.0 degrees in Valve Opening)

The different values were applied to the default ones given by the manufacturers. The changes were implemented on all cylinder exhaust valves simultaneously so that they operated in unison.

In the figures below, the rotational speed of the engine and the power produced are depicted for the four scenarios mentioned above and are compared to the respectful ones of the “initial” engine operation where no changes were made and the engine operated at its default settings.

In the following figures, the abbreviations “VC” and “VO” stand for valve closing and valve opening respectively.

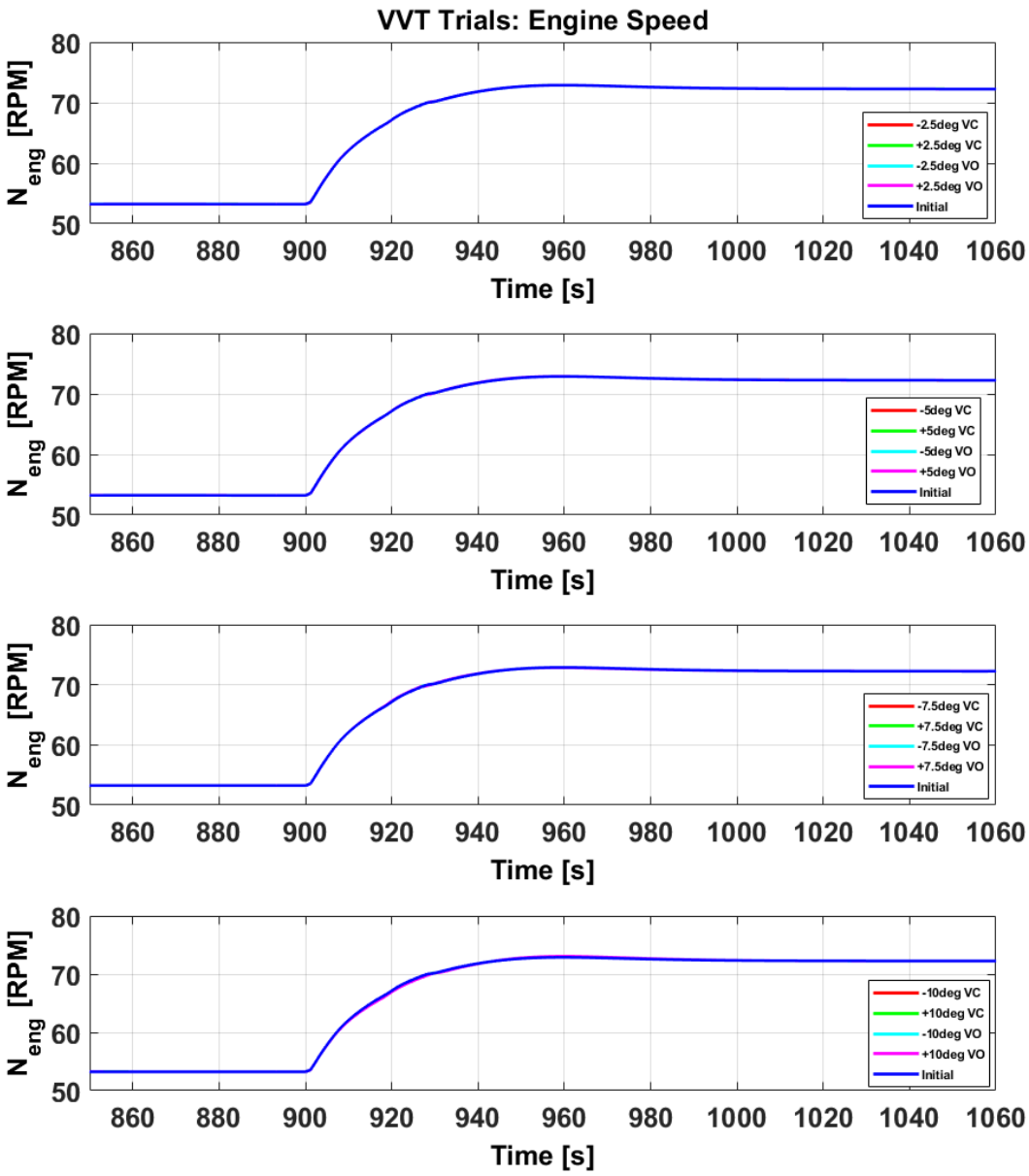

Figure 8.51: Engine Speed – Variable Valve Timing ±2.5 / ± 5.0 / ±7.5 / ±10.0 degrees

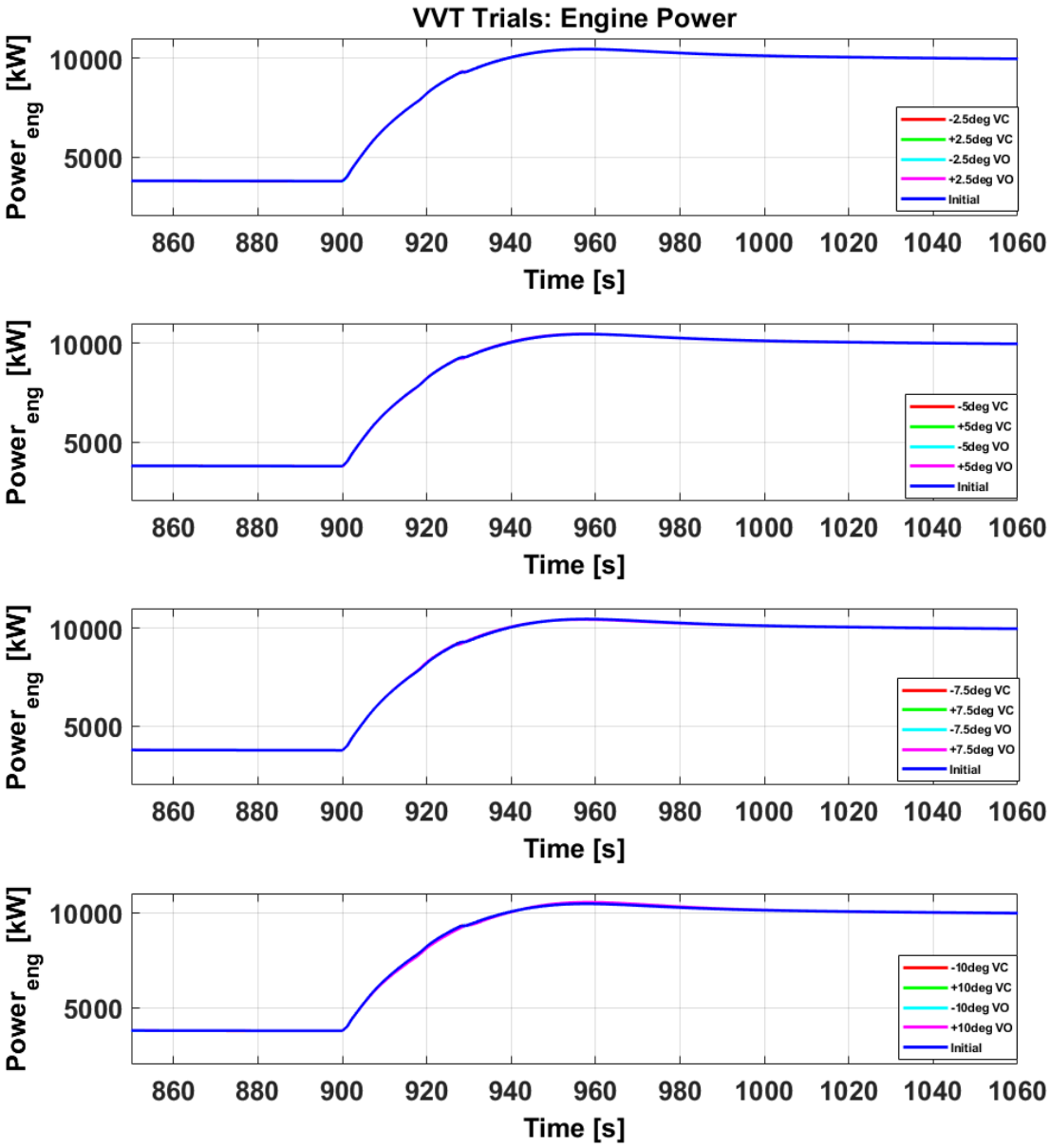

Figure 8.6: Engine Power – Variable Valve Timing ±2.5 / ±5.0 / ±7.5 / ±10.0 degrees

From the results of this group's simulations we can deduce that by changing the crank angle linked to the opening and closing of the exhaust valve, the engine's speed and power change is negligible. In the examined load region, none of the above cases seemed to increase or decrease the acceleration or power output of the engine substantially.

A closer look showed that, as the changes intensified, an earlier valve closing or opening produced trivially increased maximum and compression pressure. On the other hand, larger delays in the EVC or the EVO produced trivially reduced maximum and compression pressure. As a result there was an extremely small increase of the produced work for the earlier valve closing and opening and an extremely small reduction for the delayed valve closing and opening. Increased pressures were accompanied by increased total losses of the same intensity and, on the other hand, reduced pressures were followed by accordingly lower total losses. In total, this left almost no room for either acceleration or deceleration. Consequently, it seemed that advancing the EVO or the EVC had insignificant but positive effects on the acceleration and power output while on the contrary, delaying, had insignificant but negative effects. We need to note that the EVC gave slightly more intense results than the EVO.

More specifically, the friction losses depended on the in-cylinder pressures and, hence, followed their trend. Slight increase in the in-cylinder pressures led to slight increase of the friction losses and vice versa.

Moreover, an earlier valve closing or delayed valve opening was accompanied by a slight decrease in the Turbocharger speed while a delayed closing or advanced opening had the opposite effect. This can be justified due to the fact that the first two cases had slightly lower power wasted in the exhaust gas while in the other two cases the losses due to the wasted power in the exhaust gas were slightly higher.

Due to the slight acceleration of the Turbocharger during the advanced EVO, there was a slight increase in the scavenge pressures which lead to more air in the cylinder and a small drop in the scavenging temperatures. The opposite phenomenon was observed with the slight deceleration of the Turbocharger during the retarded EVO.

The scavenger temperature in the retarded EVO showed an interesting increase. This can be justified due to the fact that increased delays in the EVO increased the exhaust backflow which meant more exhaust gas entering in the scavenger plenums and, thus, increased the scavenger temperature.

Furthermore, in contrast to earlier EVC and delayed EVO, when the EVC was retarded or the EVO advanced, better scavenging was achieved which slightly lowered the exhaust gas temperature and increased the air cooling losses.

What is more, it was observed that in all cases there was an insignificant to minor rise in the SFOC except the advanced EVC where there was a minor drop. This is due to the fact that, from the four cases examined, only in the advanced valve closing was there a slight percentagewise decrease of the total losses compared to the work produced.

8.4 Enhanced Fuel Simulations

This group of simulations involved a series of runs where the fuel injected in each cylinder was altered. To be more precise, the control law connecting the fuel pump's fuel index with the mass of the fuel injected was modified so a 30% fuel increase was achieved. The increase in the fuel mass injected means that for the same governor's rack positions and, thus, the same fuel indexes, more fuel is injected.

The scenarios tested included one VIT scenario, one VCR scenario and a set of VVT scenarios which all had their fuel control law enhanced. In particular, the scenarios chosen were:

- -10 degrees in the start of injection (VIT scenario)
- +20% compression ratio (VCR scenario)
- -10 degrees in Valve Closing / +10 degrees in Valve Closing / -10 degrees in Valve Opening / +10 degrees in Valve Opening (VVT scenario)

The increase took place on all of the cylinders simultaneously so that they operated in unison.

In the figures below, the rotational speed of the engine and the power produced are depicted for the three "enhanced Fuel" scenarios mentioned above and are compared to the respectful ones of the "initial" engine's condition, where the engine operated at its default settings.

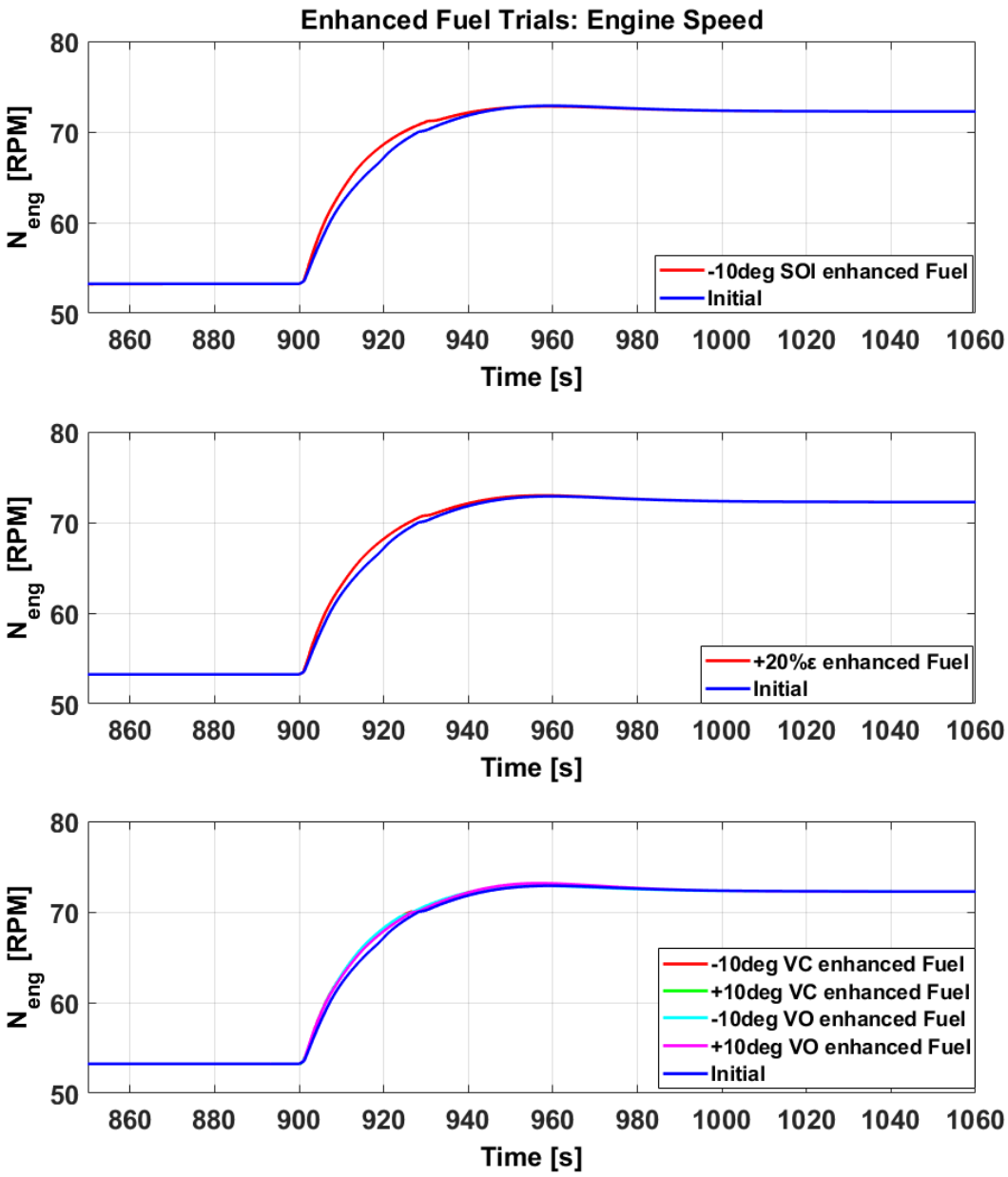

Figure 8.7: Engine Speed – Enhanced Fuel Simulations

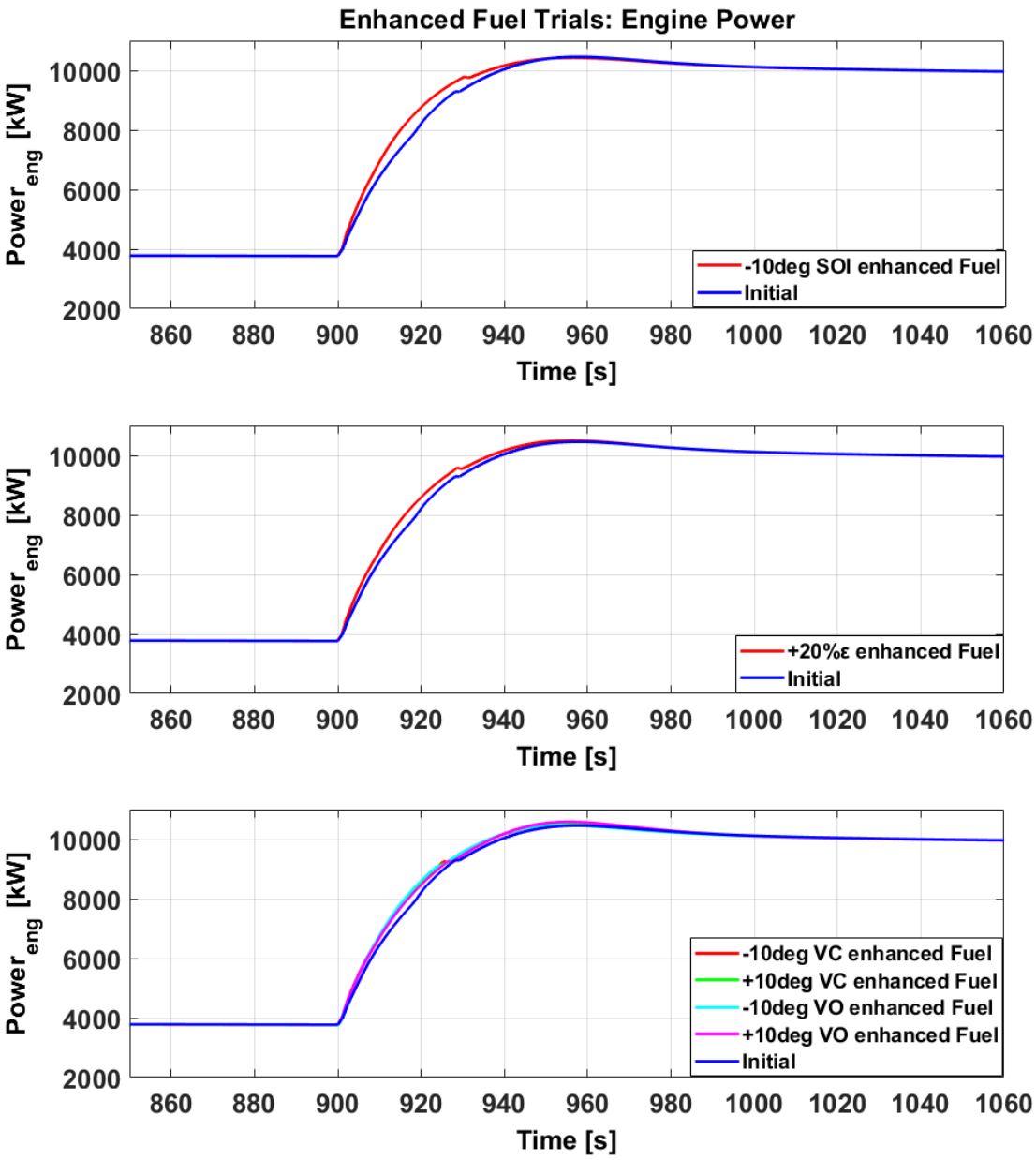

Figure 8.8: Engine Power – Enhanced Fuel Simulations

From the above results it is obvious that with the increase in the mass of fuel injected, there was a major change in how the engine operated for all the systems (VIT, VCR and VVT) applied. The curves in the specific load region were different compared to the "initial" condition with an evident acceleration in the engine's speed. In addition, the power produced was also significantly affected, with the engine building faster its power and reaching a slightly higher peak.

Between the scenarios with the systems combined with the increased fuel (enhanced fuel scenarios) and the ones where there was only the application of the systems, there were increases in the in-cylinder pressures which led to increased produced work.

What was also observed from a quick comparison between the above curves was that the simultaneous application of the enhanced fuel and one of the above systems did not differentiate substantially in terms of acceleration compared to solely increasing the fuel injected. In other words, the acceleration observed was mainly attributed to the enhanced fuel since the application of the VIT, VCR and VVT systems together with the enhanced fuel gave similar results with little differences.

However, each of the scenarios maintained some of their original characteristics from the previous simulations showing that the application of each system had some impact. For example, compared to simply injecting increased fuel, the "enhanced fuel – VIT" scenario showed a significant increase in the maximum and compression pressures while there was also a significant increase in the total losses. In addition, as also exhibited in the different VVT scenarios, likewise, it was revealed in the "enhanced fuel – VVT" scenarios that earlier valve closing and opening cases produced a minor increase in the maximum and compression pressures whereas delayed valve closing and opening cases showed a minor decrease.

Considering the SFOC, it was generally increased compared to its prior values because, even though there was an increase in the power available for acceleration, the losses were further increased. However, as shown in the original simulations, the SFOC was ultimately lower for the "enhanced fuel – VCR" compared to the initial state. This can be attributed to the improvement of the engine's thermal efficiency, despite the increase in the fuel injected.

Considering the losses, unavoidably, during the acceleration there was an increase in the power wasted in the exhaust gas from the extra fuel injected. Also, an increase in the heat transfer losses was observed since the difference between the gas and the cylinders walls' temperature was increased due to the richer combustion. The increase of the wasted power in the exhaust gas was followed by a slight acceleration of the Turbocharger while due to the richer combustion, ultimately, produced increased scavenger and exhaust temperatures and pressures.

All in all, the entire group of the engine's thermodynamic characteristics (such as the in-cylinder pressures, the exhaust and scavenger temperatures etc.) were observed to slightly accelerate during the beginning of the acceleration and then showed a deceleration towards its competition. Consequently, the scenarios with the increased mass of fuel injected, compared to their original scenarios, reached their peak values almost at the same time period.

Nevertheless, since the three systems (VIT, VCR and VVT) are very different in how they affect the total operation of the engine it is not safe to compare their "enhanced fuel" scenarios. Plus, there is

no specific correlation between the compression ratio, fuel injection timing and exhaust valve timing. What can be concluded though is that an increase in the amount of fuel injected had a positive effect on both the acceleration and power output of the engine even without the application of one of the examined systems.

8.5 Enhanced Mass of Air Simulations

The last group of simulations involved a series of runs where the mass of air flowing in each cylinder was altered. To be more specific, the moment of inertia of the Turbocharger was reduced by 20 times. This, in succession, increased the air mass flow in the cylinders sending more air in less time.

In practice, this could be achieved by attaching an electrical motor on the turboshaft. The motor's function would be to aid the rotation of the Turbocharger. As a result, the Turbocharger would have its polar moment of inertia reduced and would rotate faster. A faster rotation is related to an increased air mass flow.

This kind of Turbocharger has already been developed by Mitsubishi Heavy Industries Marine Machinery & Engine Co., Ltd. [53] where a compact electric motor is incorporated, limited to power functions that assist the driving of the Turbocharger.

The scenarios tested included the same scenarios as the "enhanced fuel" cases. Thus, there were one VIT scenario, one VCR scenario and a set of VVT scenarios which all had their Turbocharger's moment of inertia reduced by 20 times. Since the engine of the simulations possessed two Turbocharger units, this reduction was implemented simultaneously on both of them. In particular, the scenarios chosen were again:

- -10 degrees in the start of injection (VIT scenario)
- +20% compression ratio (VCR scenario)
- -10 degrees in Valve Closing / +10 degrees in Valve Closing / -10 degrees in Valve Opening / +10 degrees in Valve Opening (VVT scenario)

In the figures below, the rotational speed of the engine and the power produced are depicted for the three "enhanced Air" scenarios mentioned above and are compared to the respectful ones of the "initial" engine's condition, where the engine operated at its default settings.

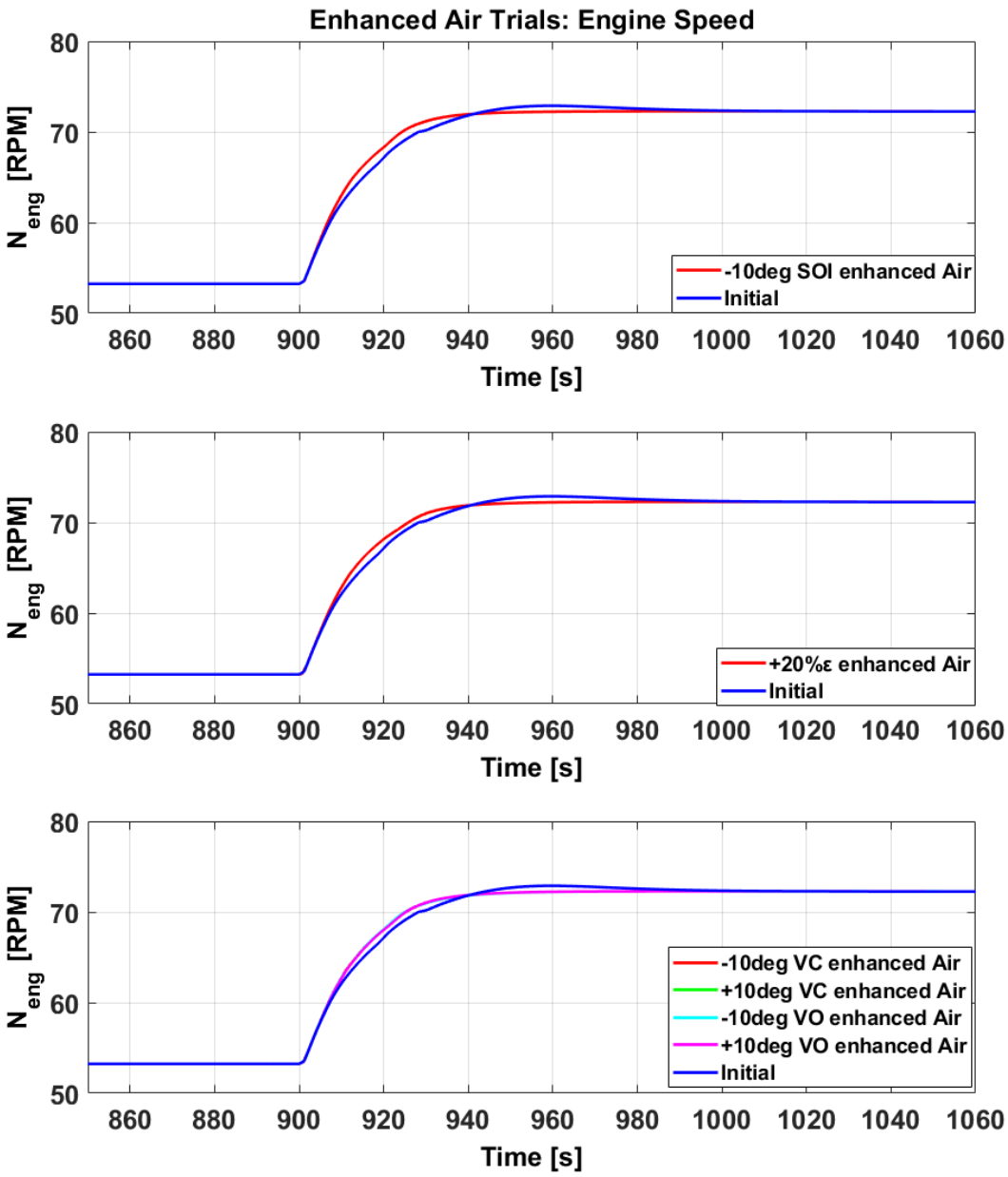

Figure 8.9: Engine Speed – Enhanced Air Mass Flow Simulations

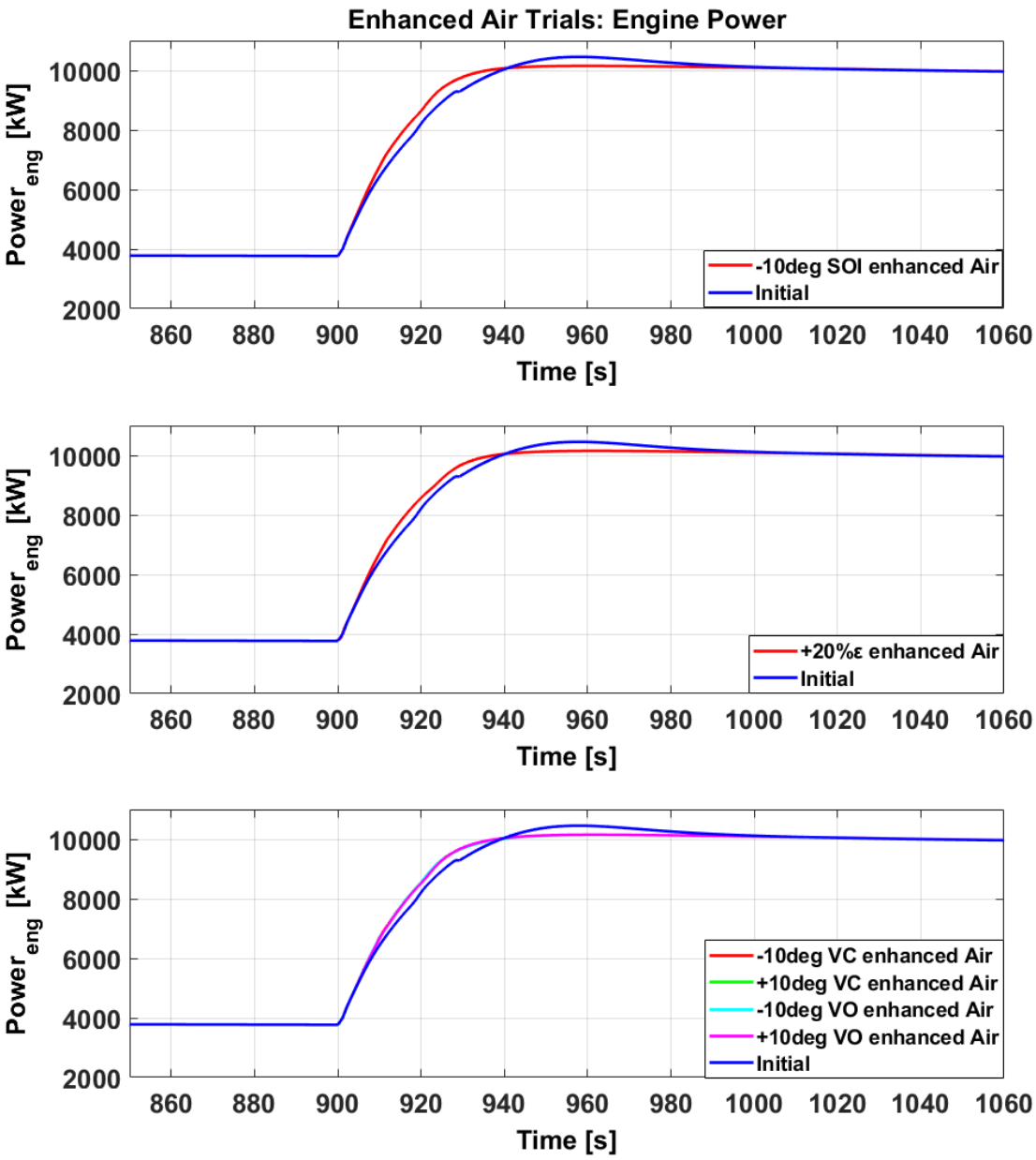

Figure 8.10: Engine Power – Enhanced Air Mass Flow Simulations

From this final group of simulations it is evident that by reducing the moment of inertia of the Turbocharger there is an important impact on the operation of the engine for the specific load region. For all three scenarios, its rotating speed is accelerated substantially while the power output is similarly accelerated and increased. As expected, the Turbocharger accelerated intensely converging in almost one third of the time that it would require compared to the initial cases. Also, it was confirmed that the air mass flow was accelerated and thus more air was flowing inside the cylinders and faster. However, this led to increased losses from air cooling.

What is more, in all cases, both the engine speed and power showed a smaller overshoot and converged faster. This was also the case for all of the parameters examined such as the maximum and compression pressures, the torque produced etc. For instance, the torque converged in almost one third of the time that it would require if its moment of inertia wasn't reduced while the maximum and compression pressures converged in almost half the time.

Considering the exhaust and scavenger pressures and temperatures they also built up and converged faster. However, the exhaust temperature for all the cases was greatly reduced during the acceleration period which can be attributed to the larger air mass flow which unavoidably works as a strong coolant, hence, reducing the temperatures of the exhaust gas.

Moreover, the acceleration of the engine's rotational speed and in-cylinder pressures was accompanied by acceleration in the friction losses. A significant reduction in the power wasted in the exhaust gas and the heat transfer was observed. In particular, the increased amount of air inserted lowered the in-cylinder temperatures which in succession reduced the difference between the temperatures of the cylinder walls and the air-fuel mixture. Consequently, the heat transfer was reduced.

This acceleration observed in all values can be explained by the combination of increased air mass flow and the significant reductions in the heat transfer losses. More air enters the cylinders increasing the air-fuel mixture and thus increasing the compression. Higher compression leads to elevated in-cylinder pressures which produce higher work values. However, since the heat transfer losses are significantly reduced the extra work is less expended and, hence, more work is directed towards the acceleration of the engine.

In general, the major difference in the behavior of the engine was attributed to reducing the Turbocharger's inertia and not by applying the different systems (VIT, VCR and VVT) since, once more, the combined scenarios gave similar results to the scenario of solely reducing the Turbocharger's inertia.

However, as in the case of the "enhanced fuel" simulations, similarly in these simulations the different scenarios maintained some of their original characteristics. For instance, once again increased pressures are observed in the "enhanced Air – VIT" scenario while reduced SFOC was observed for the "enhanced Air – VCR" scenario, compared to simply reducing the inertia of the Turbocharger. In particular, considering the SFOC for these simulations, even though it was increased during the acceleration phase, it converged in almost half the time compared to the "initial" scenario due to the faster acceleration of the engine. Consequently, due to the fact that the acceleration lasted less, the SFOC was increased for a smaller time period and dropped to lower

levels faster. Thus, compared to the “initial” operation of the engine, the total SFOC could be said to be ultimately reduced for all cases.

All things considered, once more, we cannot make conclusions as to which case was altogether more beneficial to the engine. The different cases had different effects on the engine’s operation and, what is more, there is no index correlating the compression ratio or the fuel and valve timing. What is certain though is that, despite the system used, in each case, the reduction of the Turbocharger’s moment of inertia had a positive impact on the performance of the engine. The air flow mass was enhanced and all of the engine functions were accelerated leading to an increased engine acceleration and power output, with faster convergence and smaller overshoots.

Chapter 9: Conclusions

9.1 Discussion

During this thesis, the swift passage of a large two-stroke marine diesel engine through the BSR was investigated. Firstly, variability in the fuel injection timing, the compression ratio and the exhaust valve timing was examined in order to determine whether the VIT, VCR and VVT systems could aid the acceleration capabilities and power output of the engine. The cases of -2.0, -5.0 and the extreme case of -10.0 and -15.0 degrees in fuel injection, 10%, 20% and 30% increase in the compression ratio and ±2.5, ± 5.0, ±7.5 and ±10.0 degrees in the EVC and EVO timing were examined.

In the end, all three cases had from small to negligible impact on the engine speed and power. In addition, the larger the change in each system's parameters, the more magnified was its effect on the engine's performance. In general, increased work was produced which aided the acceleration but was mostly expended in increased losses, justifying the weak acceleration results.

All in all, the VIT modifications seemed to have the most significant impact on the engine though restrictions apply due to the excessively high in-cylinder pressures. What was observed was that increased delay in the fuel injection aided the engine's acceleration and power and considerably increased the work produced. However, the total losses were increased accordingly. Moreover, there was a threshold after which the operation of the engine, in terms of SFOC, in-cylinder pressures and losses, was negatively affected. On the other hand, the VCR simulations showed that even with increased compression ratio there was little change in the acceleration and power of the engine. The small increase in the produced work and the slight reduction of the total losses were responsible for a minor improvement in the engine's acceleration and power output. Furthermore, it was observed that a higher compression ratio led to higher in-cylinder pressure increases and, thus, the improvement of the engine's efficiency and the reduction of its SFOC. Lastly, the VVT scenarios had the least effect even though significant changes on the valve timing were implemented. In general, little work was produced which was balanced by the total losses. Minor changes on all of the engine's operational characteristics were observed with an early valve closing and opening affecting positively and a delayed valve closing and opening affecting negatively the acceleration and power of the engine. The EVC cases were noted to have slightly more intense results then the EVO cases.

The final simulations included the implementation of the above methods combined with increased fuel or air mass flow in the cylinders. The first was achieved by increasing 30% the relation between the mass of fuel injected and the fuel index of the fuel pumps. The latter was achieved by reducing the polar moment of inertia of the turboshaft so that it would accelerate faster which, in reality, could be achieved by attaching a motor on the turboshaft. Both cases produced a significant increase in the engine's acceleration, power output and produced work due to the increased pressures. Moreover, it was found out that, in these combined cases, this improvement came mainly from the fuel or air increase while the systems (VIT, VCR and VVT) played a smaller role. Nevertheless, each system still had a small impact and maintained some of its own original characteristics from when it was tested alone. An example would be the highly increased pressures in the combined VIT scenarios and the decreased SFOC in the combined VCR scenarios.

Lastly, in the increased fuel scenarios, it was observed that most of the engine's operational and thermodynamic characteristics accelerated and reached their peak values in the same time period compared to the initial engine condition. On the other hand, in the increased air scenarios, it was observed that most of the engine's operational and thermodynamic characteristics accelerated more intensely and started to converge much faster compared to initial engine condition.

9.2 Recommendations for Future Research

Simulations and modelling of the transient behaviour of marine engines can prove quite challenging and constant research is always important. In this section, recommendations and ideas for future research are proposed. These are based on the conclusions of this thesis and would supplement and reinforce the current findings on the swift passage of the BSR.

- Investigation of the effect of the aforementioned systems with the combined application of the EGR and SCR systems. Due to the latest regulations considering the reduction of the NO_x and SO_x produced in the marine industry, there has been a great interest in applying the EGR and SCR systems on marine engines. These systems however affect the performance of the engine during transient conditions. Consequently, it would be useful to investigate the effect of the EGR and SCR systems on the passage of the BSR and how it could be aided.

- This thesis focused on the thermodynamical effects of the different methods tested. Nonetheless, the BSR is related to torsional vibration. Consequently, a dynamic investigation on the torsional stresses that are produced should also be made in order to see their behavior and whether loitering near the resonance point is averted

- This thesis investigated loads in the region between 20% and 50% of the maximum engine load. However, in lower loads and speed ranges there is a different margin for power increase until reaching the torque limiter. In the same context, a derated engine would have its BSR moved to higher loads which likewise has a lower power margin but higher efficiency. Consequently, a similar investigation of the effect of the examined methods should be carried in order to see their efficiency in different load regions.

- The use of a CPP propeller which can alter its pitch may also show alterations in the torque that it demands from the engine. An assessment on the effect that a CPP propeller could have in aiding the acceleration of the engine through the BSR could be examined.

- A variable geometry compressor (VGC) or a variable geometry turbine (VGT) could be implemented in order to affect the air mass flow in the cylinders which in succession affects the engine performance. Similarly, changing the compressor maps will alter the air mass flow.

- Simulations of a marine engine passing through the BSR where a combination of the aforementioned systems is applied. The simultaneous use of two or more of the VIT, VCR and VVT systems could produce interesting results on the acceleration capabilities and power output of the engine. In addition, the simultaneous use of increased fuel and air mass should be investigated.

References

[1] J. B. Woodward and R. G. Latorre, "Modeling of Diesel Engine Transient Behavior in Marine Propulsion Analysis," 1984.

[2] "Energy Efficiency Measures," [Online]. Available: http://www.imo.org/en/ourwork/environment/pollutionprevention/airpollution/pages/technical-and-operational-measures.aspx.

[3] Germanischer Lloyd, GL Rules & Guidelines, 2008.

[4] MAN Diesel & Turbo, *Dynamic Limiter Function.*

[5] J. R. Pérez Osses and R. W. G. Bucknall, "On the impact of marine engineering efficiency with de-rated engines: A study using VLCCs," in *Low Carbon Shipping Conference*, London, 2013.

[6] N. Kyrtatos, MOtor THERmodynamics Ver 2.1-USERS MANUAL, NTUA/LME, 2013.

[7] J. Carlton, Marine Propellers and Propulsion, 1994.

[8] J. Holtrop, "A Statistical Re-analysis Of Resistance And Propulsion Data," *International Shipbuilding Progress,* 1984.

[9] J. Holtrop and G. G. Mennen, "An Approximate Power Prediction Method," *International Shipbuilding Progress,* 1982.

[10] R. F. Roddy, D. E. Hess and W. Faller, "Neural Network Predictions of the 4-Quadrant Wageningen Propeller Series," Defense Technical Information Center, 2006.

[11] "The Basics The 2 Stroke Diesel Cycle," [Online]. Available: http://www.marinedieselsinfo/Basics/the_2_stroke_engine_explanation.htm. [Accessed May 2018].

[12] C. D. Rakopoulos and E. G. Giakoumis, Diesel Engine Transient Operation, Springer, 2009.

[13] MAN B&W Diesel A/S, *An Introduction to Vibration Aspects of Two-stroke Diesel Engines in Ships,* 1995.

[14] L. Bryndum and S. B. Jakobsen, Vibration Characteristics of Two-stroke Low Speed Diesel Engines, London: Man B&W Diesel A/S, 1988.

[15] D. Geir, J. Roaldsøy and E. Sandberg, "Det Norske Veritas' methodology for propulsion shaft design - A cost-saving and reliable supplement to the IACS simplified code," in *SNAME Symposium on Propellers / Shafting 2006*, Williamsburg VA, USA, 2006.

[16] Y. Kim, S. Hwang, K. Cho and U. Kim, "Characteristics of propulsion shafting system in ships with

engine acceleration problems in the barred speed range," *Ocean Engineering,* 2017.

[17] IACS, "Dimensions of propulsion shafts and their permissible torsional vibration stresses," in *Requirements concerning MACHINERY INSTALLATIONS*, 2005.

[18] "EEDI & SEEMP," [Online]. Available: https://www.marpol-annex-vi.com/eedi-seemp/.

[19] P. Zachariadis, "EEDI Explained," 15 December 2011. [Online]. Available: https://higherlogicdownload.s3.amazonaws.com/SNAME/e10ad46f-35fe-4b7d-a4cf-3da678bacc3f/UploadedImages/SNAME%20EEDI%20finalf.pdf.

[20] J. Babicz, Wärtsilä Encyclopedia of Ship Technology, Helsinki: Wärtsilä, 2015.

[21] MAN Diesel & Turbo, *Derating.*

[22] "What's the need to change Injection Timing? – Variable Injection Timing," [Online]. Available: https://shipfever.com/variable-injection-timing-vit/.

[23] "Operational Information The MAN B&W MC Engine VIT Fuel Pump," [Online]. Available: http://www.marinediesels.info/2_stroke_engine_parts/Other_info/MANBW_VIT_pump.htm.

[24] Wärtsilä, *Variable Injection Timing and Fuel Quality Setting.*

[25] N. P. Kyrtatos and I. Koumbarelis, "Performance prediction of next generation slow speed diesel engines during ship manoeuvres," 1994.

[26] D. T. Hountalas, S. Raptotasios, A. Antonopoulos, S. Daniolos, I. Dolaptzis and M. Tsobanoglou, "Two-Stroke Marine Diesel Engine Variable Injection Timing System Performance Evaluation And Optimum Setting For Minimum Fuel Consumption At Acceptable NOx Levels," in *ASME 2014 12th Biennial Conference on Engineering Systems Design and Analysis*, Copenhagen, 2014.

[27] N. P. Kyrtatos, Marine Diesel Engines, Athens: SIMMETRIA, 1993.

[28] "Operational Information The Two Stroke Crosshead Engine The Exhaust Valve," [Online]. Available: http://www.marinediesels.info/2_stroke_engine_parts/exhaust_valve.htm. [Accessed May 2018].

[29] "Operational Information Two Stroke Exhaust Valve Timing," [Online]. Available: http://www.marinediesels.info/2_stroke_engine_parts/Other_info/exhaust_valve_cam.htm. [Accessed May 2018].

[30] Mechadyne International, "The Impact of Valve Events Upon Engine Performance and Emissions," 2006.

[31] H. U. Basaran and O. A. Ozsoysal, "Effects of application of variable valve timing on the exhaust gas temperature improvement in a low-loaded diesel engine," 2017.

[32] Y. Masuda, T. Hirose, Y. Umemoto and T. Yamada, "Innovative Development of Variable Compression Ratio System for Crosshead Type Low Speed Two Stroke Engines," in *International Symposium on Marine Engineering (ISME) October 15-19*, Japan, 2017.

[33] H. Schneekluth and V. Bertram, Ship Design for Efficiency and Economy, 1998.

[34] V. Bertram, Practical Ship Hydrodynamics, 2000.

[35] A. Papanikolaou, Methodology of Ship Preliminary Study, 2009.

[36] M. Ventura, *Estimation Methods For Basic Ship Design.*

[37] S. Harvald, "Estimation of power of ships," *International Shipbuilding Progress,* 1978.

[38] G. Politis, Ship's Resistance and Propulsion, National Technical University of Athens.

[39] D. W. Taylor, The speed and power of ships : a manual of marine propulsion, Washington D.C: Press of Ransdell, Incorporated, 1933.

[40] S. A. L. Ayre, "Approximating EHP - Revision of data given in papers of 1927 and 1948".

[41] W. Auf'm Keller, "Extended diagrams for determining the resistance and required power for single-screw ships," *International Shipbuilding Progress,* 1973.

[42] A. Lap, "Diagrams for determining the resistance of single screw ships," *International Shipbuilding Progress,* 1954.

[43] ITTC, *Testing and Extrapolation Methods High Speed Marine Vehicles Resistance Test,* 2002.

[44] W. v. Lammeren, L. Troost and J. Koning, Weerstand en Voortstuwing van Schepen, 1942.

[45] K. Schoenherr, Propulsion and propellers, Society of Naval Architects, 1939.

[46] M. W. C. Oosterveld and P. Van Oossanen, "Further Computer-Analyzed Data of the Wageningen B-Scew Series," *Shipbuilding and Marine Engineering Monthly,* 1975.

[47] K. Mournianakis, "Modeling and simulation of the starting procedure of a large two-stroke marine diesel engine," 2015.

[48] W. P. A. Van Lammeren, J. D. Van Manen and M. W. C. Oosterveld, "The Wageningen B-Screw Series," p. Netherlands Ship Model Basin, 1969.

[49] D. M. MacPherson, V. R. Puleo and M. B. Packard, "Estimation of Entrained Water Added Mass Properties for Vibration Analysis," *SNAME New England Section,* 2007.

[50] R. Hope, "Marine Engines & Propulsion," 2015. [Online]. Available: http://www.splashmaritime.com.au/Marops/data/text/Med3tex/Engpropmed2.htm#_1.4_Timing_-.

[51] "WinGD," [Online]. Available: https://www.wingd.com/en/engines/general-technical-data-(gtd)/.

[52] ITTC, *Testing and Extrapolation Methods, General Density and Viscosity of Water,* 1999.

[53] Mitsubishi Heavy Industries Marine Machinery & Engine Co., Ltd., "Electro-assist MET Turbocharger to Achieve 30% Energy Saving, In Partnership with Calnetix Technologies," 2013.

APPENDIX A': Equations Used

In this section are included all the equations used in this thesis along with the passage they were referred-used at for the comfort of the reader.

The Barred Speed Range

1. $\tau_1 = \pm C_W \cdot C_K \cdot C_D \cdot (3 - 2 \cdot \lambda^2)$ for speed ratio values $\lambda < 0.9$
2. $\tau_1 = \pm C_W \cdot C_K \cdot C_D \cdot 1.38$ for speed ratio values $0.9 \leq \lambda \leq 1.05$
3. $\tau_2 = \pm 1.7 \cdot 6.0 \cdot \frac{\tau_1}{\sqrt{C_K \cdot C_W}}$ depending on the material and design
4. $C_W = \frac{R_m + 160}{18}$
5. $\frac{16 \cdot n_c}{18 - \lambda_c} \leq n \leq \frac{(18 - \lambda_c) \cdot n_c}{16}$

Energy Efficiency Design Index (EEDI)

1. $EEDI = \frac{P_{ME} \cdot CF_{ME} \cdot SFC_{ME}}{Capacity \cdot V_{ref}}$

The Dynamic Limiter Function & the BSR Power Margin Index

1. $BSR_{PM} = \frac{P_L - P_P}{P_P} \cdot 100\%$

Variable Compression Ratio (VCR)

1. $\varepsilon = \frac{V_d + V_c}{V_c}$

MOTHER

1. $\dot{T} = f(\dot{U}, \dot{H}, \dot{\varphi}, \dot{Q}, \dot{W})$
2. $\dot{m} = f(P, T, g, R, A_{flow}, C_d)$
3. $\dot{m} = \sum \dot{m}_j$
4. $P = f(m, R, T, V)$

In-Cylinder Models

1. $x_b = \frac{m_b}{m_{tot}} = 1 - e^{-a\cdot\left(\frac{\theta-\theta_0}{\Delta\theta_b}\right)^{m+1}}$
2. $fmep = k_1 + k_2 \cdot P_{max} + k_3 \cdot V_P$
3. $q = h \cdot A \cdot \left(T_{gas} - T_{wall}\right)$
4. $h = 0.00326 \cdot B^{-0.2} \cdot P^{0.8} \cdot T_{gas}^{-0.55} \cdot w^{0.8}$

Ship Model

1. $\sum F = M \times a$
2. $\dot{V}_{SHIP} \cdot (M_{SHIP} + M_{ADDED}) = T_{pr} - R_{tot}/(1-t)$
3. $V_{SHIP\_NEW} = V_{SHIP\_OLD} + dt \cdot \dot{V}_{SHIP}$
4. $R_{tot} = (1+k_1) \cdot R_F + R_{APP} + R_W + R_B + R_{TR} + R_A$
5. $(1+k_1) = C_{13} \cdot \left\{0.93 + C_{12} \cdot \left(\frac{B}{L_R}\right)^{0.92497} \cdot (0.95 - C_P)^{-0.521448} \cdot (1 - C_P + 0.0225 \cdot lcb)^{0.6906}\right\}$
6. $R_F = \frac{1}{2} \cdot \rho \cdot C_F \cdot S \cdot {V_{SHIP}}^2$
7. $C_F = \frac{0.075}{(log_{10}Re-2)^2}$
8. $R_{APP} = \frac{1}{2} \cdot \rho \cdot {V_{SHIP}}^2 \cdot C_F \cdot (1+k_2)_{eq} \cdot S_{APP} + R_{BT}$
9. $(1+k_2)_{eq} = \frac{\sum_j (1+k_2)_j S_{APPj}}{S_{APP}}$
10. $R_{W-B} = C_{17} \cdot C_2 \cdot C_5 \cdot \nabla \cdot \rho \cdot g \cdot \exp\{m_3 \cdot {F_n}^d + m_4 \cdot cos(\lambda \cdot {F_n}^{-2})\}$
11. $R_{W-A} = C_1 \cdot C_2 \cdot C_5 \cdot \nabla \cdot \rho \cdot g \cdot \exp\{m_1 \cdot {F_n}^d + m_4 \cdot cos(\lambda \cdot {F_n}^{-2})\}$
12. $R_W = R_{W-A\,0.4} + (10 \cdot F_n - 4) \cdot \frac{(R_{W-B\,0.55} - R_{W-A\,0.4})}{1.5}$
13. $R_B = 0.11 \cdot \exp(-3 \cdot {P_B}^{-2}) \cdot {F_{ni}}^3 \cdot {A_{BT}}^{1.5} \cdot \rho \cdot \frac{g}{(1+{F_{ni}}^2)}$
14. $R_{TR} = \frac{1}{2} \cdot \rho \cdot {V_{SHIP}}^2 \cdot A_T \cdot C_6$
15. $R_A = \frac{1}{2} \cdot \rho \cdot C_A \cdot S \cdot {V_{SHIP}}^2$
16. $C_A = 0.006 \cdot (L_{WL} + 100)^{-0.16} - 0.00205 + 0.003 \cdot \sqrt{L_{WL}/7.5} \cdot C_B^4 \cdot C_2 \cdot (0.04 - C_4)$
17. $t = \frac{0.25014 \cdot (B/L_{WL})^{0.28956} \cdot (\sqrt{B \cdot T}/D)^{0.2624}}{(1-c_P+0.0225 \cdot lcb)^{0.01762}} + 0.0015 \cdot C_{STERN}$
18. $L_R = (1 - C_P + \frac{0.06 \cdot C_P \cdot lcb}{4 \cdot C_P - 1}) \cdot L_{WL}$
19. $i_E = 1 + 89 \cdot \exp\{-\left(\frac{L_{WL}}{B}\right)^{0.80856} \cdot (1 - C_{WP})^{0.30484} \cdot (1 - C_P - 0.0225 \cdot lcb)^{0.6367} \cdot \left(\frac{L_R}{B}\right)^{0.34574} \cdot \left(100 \cdot \frac{\nabla}{{L_{WL}}^3}\right)^{0.16302}\}$
20. $P_B = \frac{0.56 \cdot \sqrt{A_{BT}}}{T_F - 1.5 \cdot h_B}$

21. $F_{ni} = \frac{V_{SHIP}}{\sqrt{g \cdot (T_F - h_B - 0.25 \cdot \sqrt{A_{BT}}) + 0.15 \cdot {V_{SHIP}}^2}}$
22. $F_{nT} = \frac{V_{SHIP}}{\sqrt{\frac{2 \cdot g \cdot A_T}{B + B \cdot C_{WP}}}}$

General Ship Particulars and other units

1. $L_{wl} = 1.01 * L_{BP}$
2. $S1 = L_{WL} \cdot (2 \cdot T + B) \cdot \sqrt{C_M} \cdot \left(0.453 + 0.4425 \cdot C_B - 0.2862 \cdot C_M - 0.003467 \cdot \frac{B}{T} + 0.3696 \cdot C_{WP}\right) + 2.38 \cdot \frac{A_{BT}}{C_B}$
3. $S2 = 3.4 \cdot (\nabla^{\frac{1}{3}} + 0.5 \cdot L_{WL}) \cdot \nabla^{\frac{1}{3}}$
4. $S = \frac{S1 + S2}{2}$
5. $lcb1 = (-0.135 + 0.194 \cdot C_P) \cdot 100$
6. $lcb2 = 8.8 - 38.9 \cdot F_n$
7. $lcb = \frac{lcb1 + lcb2}{2}$
8. $R_n = \frac{V_{SHIP} \cdot L_{WL}}{v}$
9. $F_n = \frac{V_{SHIP}}{\sqrt{(g \cdot L_{WL})}}$

Hull Coefficients

1. $C_B = \frac{\nabla}{B * L_{BP} * T}$
2. $C_{M1} = 1.006 - 0.0056 * {C_B}^{-3.56}$
3. $C_{M2} = \frac{1}{1 + (1 - C_B)^{3.5}}$
4. $C_M = \frac{C_{M1} + C_{M2}}{2}$
5. $C_P = \frac{C_B}{C_M}$
6. $C_{WP} = \frac{C_B}{0.471 + 0.551 \cdot C_B}$

Coefficients

1. $C_1 = 2223105 \cdot C_7^{3.78613} \cdot \left(\frac{T}{B}\right)^{1.07961} \cdot (90 - i_E)^{-1.37565}$
2. $C_2 = \exp\left(-1.89 \cdot \sqrt{C_3}\right)$
3. $C_3 = 0.56 \cdot \frac{{A_{BT}}^{1.5}}{B \cdot T \cdot (0.31 \cdot \sqrt{A_{BT}} + T_F - h_B)}$
4. $C_4 = {T_F}/{L_{WL}} \ \ when \ {T_F}/{L_{WL}} \leq 0.04$
   $C_4 = 0.04 \ when \ {T_F}/{L_{WL}} > 0.04$

5. $C_5 = 1 - 0.8 \cdot \frac{A_T}{B \cdot T \cdot C_M}$
6. $C_6 = 0.2 \cdot (1 - 0.2F_{nT})$ $when\ F_{nT} < 5$
   $C_6 = 0$ $when\ F_{nT} \geq 5$
7. $C_7 = 0.229577 \cdot \left(\frac{B}{L_{WL}}\right)^{0.33333}$ $when\ {}^{B}/_{L_{WL}} < 0.11$
   $C_7 = {}^{B}/_{L_{WL}}$ $when\ 0.11 < {}^{B}/_{L_{WL}} < 0.25$
   $C_7 = 0.5 - 0.0625 \cdot {}^{L_{WL}}/_{B}$ $when\ {}^{B}/_{L_{WL}} > 0.25$
8. $C_8 = \frac{B \cdot S}{L_{WL} \cdot D \cdot T_A}$ $when\ {}^{B}/_{T_A} < 5$
   $C_8 = S \cdot \frac{\left(7 \cdot \frac{B}{T_A} - 25\right)}{L_{WL} \cdot D \cdot \left(\frac{B}{T_A} - 3\right)}$ $when\ {}^{B}/_{T_A} > 5$
9. $C_9 = C_8$ $when\ C_8 < 28$
   $C_9 = 32 - \frac{16}{C_B - 24}$ $when\ C_8 > 28$
10. $C_{10} = \frac{B}{L_{WL}}$ $when\ {}^{L_{WL}}/_{B} > 5.2$
    $C_{10} = 0.25 - \frac{0.003328402}{\frac{B}{L_{WL}} - 0.134615385}$ $when\ {}^{L_{WL}}/_{B} < 5.2$
11. $C_{11} = {}^{T_A}/_{D}$ $when\ {}^{T_A}/_{D} < 2$
    $C_{11} = 0.0833333 \cdot \left({}^{T_A}/_{D}\right)^3 + 1.33333$ $when\ {}^{T_A}/_{D} > 2$
12. $C_{12} = \left(\frac{T}{L_{WL}}\right)^{0.2228446}$ $when\ {}^{T}/_{L_{WL}} > 0.05$
    $C_{12} = 48.20 \cdot \left(\frac{T}{L_{WL}} - 0.02\right)^{2.078} + 0.479948$ $when\ 0.02 < {}^{T}/_{L_{WL}} < 0.05$
    $C_{12} = 0.479948$ $when\ {}^{T}/_{L_{WL}} < 0.02$
13. $C_{13} = 1 + 0.003 \cdot C_{STERN}$
14. $C_{14} = 1 + 0.011 \cdot C_{STERN}$
15. $C_{15} = -1.69385$ $when\ {}^{{L_{WL}}^3}/_{\nabla} < 512$

    $C_{15} = -1.69385 + \frac{\left(\frac{L_{WL}}{\frac{1}{\nabla^3}} - 8\right)}{2.36}$ $when\ 512 < {}^{{L_{WL}}^3}/_{\nabla} < 1726.91$

    $C_{15} = 0$ $when\ {}^{{L_{WL}}^3}/_{\nabla} > 1726.91$

16. $C_{16} = 8.07981 \cdot C_P - 13.8673 \cdot {C_P}^2 + 6.984388 \cdot {C_P}^3$ $when\ C_P < 0.80$
    $C_{16} = 1.73014 - 0.7067 \cdot C_P$ $when\ C_P > 0.80$
17. $C_{17} = 6919.3 \cdot {C_M}^{-1.3346} \cdot \left(\frac{\nabla}{L^3}\right)^{2.00977} \cdot \left(\frac{L_{WL}}{B} - 2\right)^{1.40692}$
18. $C_{19} = \frac{0.12997}{0.95 - C_B} - \frac{0.11056}{0.95 - C_P}$ $when\ C_P < 0.70$
    $C_{19} = \frac{0.18567}{1.3571 - C_M} - 0.71276 + 0.38648 \cdot C_P$ $when\ C_P > 0.70$
19. $m_1 = 0.0140407 \cdot \frac{L_{WL}}{T} - 1.75254 \cdot \frac{\nabla^{1/3}}{L_{WL}} - 4.79323 \cdot \frac{B}{L_{WL}} - C_{16}$
20. $m_3 = -7.2035 \cdot \left(\frac{B}{L_{WL}}\right)^{0.326869} \cdot \left(\frac{T}{B}\right)^{0.605375}$
21. $m_4 = C_{15} \cdot 0.4 \cdot \exp\left(-0.034 \cdot {F_n}^{-3.29}\right)$

22. $d = -0.9$
23. $\lambda = 1.446 \cdot C_P - 0.03 \cdot \frac{L_{WL}}{B}$ $when$ ${L_{WL}}/{B} < 12$

    $\lambda = 1.446 \cdot C_P - 0.36$ $when$ ${L_{WL}}/{B} > 12$

Propeller Model

1. $V_A = (1 - w) \cdot V_{SHIP}$
2. $w = C_9 \cdot (1 + 0.015 \cdot C_{STERN}) \cdot [(1 + k) \cdot C_F + C_A] \cdot \frac{L_{WL}}{T_A} \cdot \left\{0.050776 + 0.93405 \cdot C_{11} \cdot \frac{(1+k) \cdot C_F + C_A}{1.315 - 1.45 \cdot C_P + 0.0225 \cdot lcb}\right\} + 0.27915 \cdot (1 + 0.015 \cdot C_{STERN}) \cdot \sqrt{\frac{B}{L_{WL} \cdot (1.315 - 1.45 \cdot C_P + 0.0225 \cdot lcb)}} + C_{19} \cdot (1 + 0.015 \cdot C_{STERN})$
3. $\beta = \arctan\left(\frac{V_A}{0.7 \cdot \pi \cdot n \cdot D_P}\right)$
4. $J = \frac{V_A}{n \cdot D_P}$
5. $T_{pr} = \frac{1}{2} \cdot \rho \cdot C_T^* \cdot {V_r}^2 \cdot A_0$
6. $Q_{pr} = \frac{1}{2} \cdot \rho \cdot C_Q^* \cdot {V_r}^2 \cdot A_0 \cdot D_P$
7. ${V_r}^2 = {V_A}^2 + (0.7 \cdot \pi \cdot n \cdot D_P)^2$
8. $A_0 = \frac{\pi}{4} \cdot {D_P}^2$
9. $T_{pr} = \frac{\pi}{8} \cdot \rho \cdot C_T^* \cdot ({V_A}^2 + (0.7 \cdot \pi \cdot n \cdot D_P)^2) \cdot {D_P}^2$
10. $Q_{pr} = \frac{\pi}{8} \cdot \rho \cdot C_Q^* \cdot ({V_A}^2 + (0.7 \cdot \pi \cdot n \cdot D_P)^2) \cdot {D_P}^3$
11. $C_T^* = \frac{1}{100} \cdot \sum_{k=1}^{N} \{A_k \cdot \cos(k \cdot \beta) + B_k \cdot \sin(k \cdot \beta)\}$
12. $C_Q^* = -\frac{1}{1000} \cdot \sum_{k=1}^{N} \{A_k \cdot \cos(k \cdot \beta) + B_k \cdot \sin(k \cdot \beta)\}$

Propeller Inertia

1. $A_x = \frac{0.2 \cdot c \cdot \Sigma_0}{3}$
2. $l_{ct_{tip}} = \frac{\Sigma_2}{\Sigma_1} \cdot \frac{{D_P}/{2} - r_h}{8}$
3. $l_{ct_{shaft}} = {D_P}/{2} - l_{ct_{tip}}$
4. $I_{tip} = \frac{2}{3} \cdot \left(\frac{{D_P}/{2} - r_h}{8}\right)^3 \cdot \Sigma_3$
5. $I_{blade} = \rho_P \cdot \left\{I_{tip} - {l_{ct_{tip}}}^2 \cdot \left(\frac{{D_P}/{2} - r_h}{8} \cdot \frac{2}{3} \cdot \Sigma_1\right) + {l_{ct_{shaft}}}^2 \cdot \left(\frac{{D_P}/{2} - r_h}{8} \cdot \frac{2}{3} \cdot \Sigma_1\right)\right\}$
6. $I_{blade} = \rho_P \cdot \left\{I_{tip} - \left(\frac{{D_P}/{2} - r_h}{8} \cdot \frac{2}{3} \cdot \Sigma_1\right) \cdot \left({l_{ct_{tip}}}^2 - {l_{ct_{shaft}}}^2\right)\right\}$
7. $I_{hub} = \frac{3}{10} \cdot \frac{{r_{h1}}^5 - {r_{h2}}^5}{{r_{h1}}^3 - {r_{h2}}^3} \cdot V_{hub} \cdot \rho_P$
8. $V_{hub} = \frac{\pi}{3} \cdot ({r_{h1}}^2 + {r_{h2}}^2 + r_{h1} \cdot r_{h2}) \cdot l_{hub}$

9. $I_{dry} = I_{hub} + Z \cdot I_{blade}$
10. $I_E = C_{IE} \cdot \rho \cdot {D_P}^5$
11. $C_{IE} = \frac{0.0703 \cdot \left({}^{P}/_{D_P}\right) \cdot EAR^2}{\pi \cdot Z}$
12. $I_{propeller} = I_{dry} + I_E$

Shaft-Propeller Dynamics

1. $\frac{d\omega}{dt} = \frac{\sum Q_i}{I_{total}}$
2. $\omega = 2 \cdot \pi \cdot \frac{n}{60}$
3. $\frac{dn}{dt} = \frac{30 \cdot \sum Q_i}{\pi \cdot I_{total}}$
4. $n_{new} = n_{old} + \dot{n} \cdot dt$

Speed Governor

1. $x(s) = K \cdot \{K_P \cdot e(s) + {K_I}/{s} \cdot e(s) + K_D \cdot s \cdot e(s)\}$
2. $x(t) = K \cdot \{K_P \cdot e(t) + K_I \cdot \int_{t_0}^{t} e(\chi) \cdot d\chi + K_D \cdot \frac{d}{dt} e(t)\}$
3. $e(t) = N_{ord}(t) - N(t)$

Synergy of Models

1. $dt = \frac{CAS \cdot 60}{n \cdot 360}$
2. $distance = distance_{last} + dt \cdot \frac{(V_{new} + V_{old})}{2}$
3. $P = k1 \cdot n^3$
4. $V = k2 \cdot n$

Simulation Specifics

1. $v = \left((0.659 \cdot 10^{-3} \cdot (T_{amb} - 1.0) - 0.05076) \cdot (T_{amb} - 1.0) + 1.7688\right) \cdot 10^{-6}$